# SOME PROBLEMS IN THE MOTION OF GAS BUBBLES

by

Mohamed El Sawi

A thesis submitted for the degree of Doctor of Philosophy of the University of London

Department of Mathematics,
Imperial College of Science
and Technology

November, 1970.

## ABSTRACT

The work described herein is primarily concerned with the distortion and shape of a gas bubble, of prescribed volume, rising steadily in an inviscid incompressible irrotational flow, under the action of surface tension forces. This is a well-posed non-linear free boundary value problem. However, the fact that the bubble shape is unknown, makes it an extremely difficult problem. The exact shape has not yet been found by any worker in this field except when the distortion is small, then the bubble is an oblate spheroid, Moore (1959).

In Chapter I, a general survey of previous theoretical and experimental results is given. Some approximations and idealized models which might be amenable to theoretical treatment are considered.

A perturbation series solution, for the bubble shape, is derived in Chapter II. A method of accelerating convergence is used to improve the results. Although the range of validity of this theory is small, within this range, the bubble shape is exact. The drag coefficient corresponding to this surface is also found.

The aim of Chapter III is to find an appropriate extension to the tensor virial theorem of the second order, relevant to the gas bubble problem. In consistency with experimental evidence and previous theoretical models, Siemes (1954), Saffman (1956), Hartunian and Sears (1957), Moore (1965), a trial shape for the bubble in the form of an oblate spheroid is used. It is shown that for small

deformations from the spherical shape, the results are exact. Comparison of the results with those of Moore's (1965) approximate theory revealed similar features and reasonable agreement. Direct assessment of the virial method showed considerable improvement on previous theories, particularly for highly distorted bubbles.

In Chapter IV an approximate method is developed for the study of slightly distorted spheroidal bubbles. The boundary value problem is solved, numerically, using an initial value technique. The shapes of the bubbles are then traced in comparison with the unperturbed spheroids. The theory is then extended to include gravity, as well as retaining surface tension forces. The dual effect of gravitational as well as surface tension forces on bubble shape has not appeared in earlier theories. These bubbles are then traced and it is observed that they are characterized by a dent at the rear stagnation point.

Finally comparisons for the velocity of rise, and other physical parameters, are made between the present predictions and experimental results. In particular the results are compared with some experimental data for the motion of gas bubbles in liquid metals, something which has not received much attention in earlier theories.

## ACKNOWLEDGEMENTS

I would like to express my sincere gratitude to Dr. D.W. Moore for his continued guidance and invaluable assistance throughout the past three years. I am also indebted to the Sudan Government for their financial support during that time.

CONTENTS

# CHAPTER I

## INTRODUCTION

Interest in the motion of gas bubbles in a fluid medium has existed for many years and has resulted in a number of experimental and theoretical investigations. Some of the features of the mechanics of bubbles are discussed in Batchelor and Davies (1956), and Levich (1962). The problem of the motion of gas bubbles in liquids is of considerable importance in several engineering processes. In particular, the shape of a bubble is found to play a leading role in these processes. This is because of the influence it exerts on the dynamics of a bubble.

It is well known, partly as a matter of observation and partly from mathematical analysis, that small gas bubbles are always spherical. However, it has been observed experimentally, Peebles and Garber (1953) and Haberman and Morton (1953), that as a bubble size increases it undergoes changes in its shape from spherical to ellipsoidal to a spherical cap. This is also accompanied by corresponding effects in other physical properties such as its velocity of rise and the drag. It is therefore necessary to examine the factors that govern the deformation of bubbles and the resulting influence of deformation on the flow parameters.

The motion of a bubble, of prescribed volume, rising steadily in an infinite incompressible pure liquid under the action of gravity, is determined by the viscosity, $\mu_o$, of the liquid, and the interfacial tension $\sigma$. In this study it is assumed that the liquid contains no surfactants. In addition the thermally induced surface tension gradients are negligible, (see Harper, Moore and Pearson, 1967). It is further assumed that the volume of the bubble is invariant, and that the motion of the enclosed gas has a negligible effect on the flow.

It is customary to use, as a length scale, the "equivalent spherical radius" $r_e$ defined by

$$\frac{4}{3}\pi r_e^3 = V, \tag{1.1}$$

where V is the volume of the bubble.

The dimensionless parameters which are of direct dynamical significance are the Rynolds number R, and the Weber number W, defined by

$$R = \frac{2r_e\rho U}{\mu_o}, \tag{1.2}$$

and

$$W = \frac{2r_e\rho U^2}{\sigma}, \tag{1.3}$$

respectively. Here U is the steady upward velocity of the bubble and $\rho$ is the density of the surrounding liquid. The Weber number, in particular, measures the ratio of inertia forces to surface tension forces which are maintaining the bubble shape. Finally we give the M number, defined by

$$M = \frac{g\mu_o^4}{\rho\sigma^3}, \tag{1.4}$$

where g is the acceleration due to gravity. Thus the parameter M is a sole property of the liquid.

The work described herein concerns the distortion and shape of a gas bubble rising steadily, at Reynolds number large enough such that boundary-layer ideas are applicable. It is clear that the surface of the bubble must be stress-free so that the tangential viscous stress component must be continuous across its surface. As this condition is not satisfied by the ideal flow, a thin boundary-layer forms at the bubble surface. Moore (1963) discussed the structure of the boundary layer on a spherical gas bubble. It was shown that the boundary-layer separated at the rear stagnation point to form a wake of breadth $O(R^{-1/4})$, and that the perturbation of the irrotational flow was $O(R^{-1/2})$ in the wake and viscous forces produced no significant modification to the velocity profile. In his (1965) paper he extended this theory to the case of ellipsoidal bubbles. Winnikow and Chao (1966) demonstrated the thinness of the wake in the case of droplet motion. In the present work we shall assume that the boundary-layer does not separate from the bubble surface.

Consider now Laplace's equation, for the pressure drop across the liquid-gas interface, which is to be applied to the solution of the profile of a bubble;

$$-P_{nn} + \sigma\left(\frac{1}{R_1} + \frac{1}{R_2}\right) = P_g, \tag{1.5}$$

where $P_{nn}$ is the normal stress, $R_1$ and $R_2$ are the principal radii of curvature and $P_g$ is the gas pressure inside the bubble and which is assumed to be constant. Equation (1.5) which is to be satisfied at every point of the bubble surface, expresses the constancy of the internal gas pressure. $-P_{nn}$ is equal to the pressure P in the irrotational flow plus the viscous normal stress which is smaller by a factor of $O(R^{-1})$ and its contribution is therefore neglected and the shape of the bubble calculated as if the flow were inviscid. Equation (1.5) then reduces to

$$P + \sigma\left(\frac{1}{R_1} + \frac{1}{R_2}\right) = P_g. \tag{1.6}$$

Viscosity still plays a role in the problem, since the velocity U depends on it. However, the shape of the bubble is now independent of viscous mechanics. Even then the resulting inviscid free-boundary problem is still exceedingly difficult, in view of the fact that the shape of the bubble is unknown. This emphasizes the need for some simplifying assumptions in order to render it tractable.

The problem posed here is to predict the shape of a bubble, of prescribed volume V, placed in a uniform stream, U, of an infinite incompressible fluid which is moving irrotationally. The work will be confined to axisymmetric bubbles so that the shape of the bubble may be represented, in spherical polar coordinates, by the surface

$$r = f(\mu, W), \tag{1.7}$$

where

$$\mu = \cos\theta, \tag{1.8}$$

and $\theta$ is the angle between the radial distance and the direction of translation of the bubble.

Several authors have investigated this problem in the experimental and theoretical fields.

Saffman (1956) investigated the motion of air bubbles in water, in a regime prior to that of the spherical cap formation. He gave a theoretical and experimental account of the spiralling and zig-zag motion of the bubble. Faced with the complication that the bubble shape is unknown, he made a simplifying assumption that the bubble is an oblate spheroid. This assumption has been justified in view of its consistency with experimental observation, where these bubbles are found to be approximately oblate spheroids. In his analysis, Saffman adopted assumptions about the pressure which are basically the same as those made by Davies and Taylor (1950) in their study of spherical cap bubbles. He assumed that the flow near the front of the bubble is inviscid and considered the distribution of the pressure in the vicinity of the front stagnation point. This led him to an equation relating the geometrical parameters of the spiral, the bubble shape, and the velocity of rise. In a similar way, he treated the zig-zag motion of the bubble and arrived at an equation which determines the stability of its rectilinear motion. Although Davies and Taylor (1950) by assuming inviscid flow only near the front of the spherical cap bubble, obtained excellent agreement between theory and experiment, one should bear in mind that, in this case, the drag coefficient is of $O(1)$ and there is flow separation at the rear of the bubble. In view of this, Saffman theory is likely to be inconsistent with non-separated flows. Also, since he used water in his experiments, his results are likely to be valid for impure liquids since water is often characterized by the presence of small impurities.

Hartunian and Sears (1957) analysis was concerned with the instability of bubbles due to hydrodynamical pressure and surface tension effects. In particular, they have shown that what decides the stability, or otherwise, for bubbles moving in pure relatively inviscid liquids is the Weber number. Thus for stability to occur, $W$ must exceed a certain critical value $W_c$. They assumed a bubble shape in the form of a deformable sphere and obtained a critical Weber number of 3.18 for the onset of instability. They further approximated the bubble shape by an oblate spheroid of revolution for all $W$. It was not then possible for them to satisfy the surface pressure condition (1.6) properly. They only satisfied it at the equator and the pole but their analysis was in error. This technique was also adopted by Siemes (1954), who studied gas bubbles, and their growth, in liquids.

Moore's papers (1959) and (1965) deal with both linear and non-linear theories for the distortion of spherical bubbles at large Reynolds number. He first examined the case of the nearly spherical bubble and proved that for small Weber numbers ($W < 0.1$), the bubble is oblate spheroidal. However for Weber numbers of $O(1)$, the shape of the bubble is unknown. Following Hartunian and Sears (1957), he assumed that bubbles whose Weber number is of order unity are still oblate spheroidal. In view of an algebraic error in their work, he found it necessary to reinvestigate this problem. We shall refer to this method as the "Two-point Theory". Moore satisfied the dynamic boundary condition (1.6) at the pole and the equator, being the points of minimum and maximum curvature respectively. It is instructive to mention that G.I. Taylor (1964), using the same approach for a problem in electrostatics, obtained good results on satisfying the respective condition at the same pair of points. Moore's analysis led him to the expression

$$W = \frac{4(x^3 + x - 2)[x^2 \sec^{-1} x - (x^2 - 1)^{1/2}]^2}{x^{4/3}(x^2 - 1)^3} \qquad (1.9)$$

which gives the Weber number in terms of the axis-ratio x which is a measure of the ratio of the transverse and longitudinal axes of the bubble. It is a very convenient parameter for characterizing the shape of the bubble. Moore has shown that the maximum error in the "Two-point Theory" should not exceed 10%, from the exact one, up to $x = 2$.

The experimental paper by Haberman and Morton (1953) includes a vast literature search on the problem. Their results regarding the velocity of rise, the bubble shape and the bubble trajectory for each liquid, depend on the parameter M which is solely a property of the liquid. In particular, for low M liquids ($M < 10^{-8}$), which are the subject of study in this thesis, they observed that as $r_e$ increases, the bubble changes shape from spherical to oblate spheroidal while U increases rapidly to a maximum, with the bubble rising steadily in a vertical straight line. Beyond this maximum, with further increase in $r_e$, the bubble motion is no longer rectilinear but may rise along a zig-zag path or in a uniform spiral. Also the bubble fluctuates and U decreases steadily to a minimum before rising again. For very large $r_e$, the bubble ultimately attains the shape of a spherical cap with fluctuations at the rear.

Jones (1965) studied bubble behaviour in liquids and fluidized beds. Although the results given in his thesis are primarily concerned with bubbles in liquids of high viscosity ($\mu_o > 1$ poise), the range of viscosities used covers some liquids of small viscosity. Of particular interest, he examined the shape of air bubbles rising through water. Photographs of these shapes are also to be found in Batchelor (1967) Plate 14.

More recently Schwerdtfeger (1968) investigated the rise of argon bubbles in mercury. As liquid metals are characterized by very high surface tension, compared to ordinary liquids, they are likely to differ from them in their hydrodynamic behaviour. In particular the M number (1.4) is relatively smaller for liquid metals. Schwerdtfeger doubted that the correlations for the velocity of rise of gas bubbles in ordinary liquids may not be applicable to those in liquid metals. However, he compared his experimental results with those of Haberman and Morton (1953) for the rise of air bubbles in water. In the case of argon bubbles in distilled water, the results compared favourably. On the other hand the velocity of rise of argon bubbles in mercury seemed to be lower than that of a gas bubble in distilled water, having the same volume.

Having now surveyed some of the experimental and theoretical background to the problem, we proceed to give a brief account of the work in the remaining chapters of this thesis.

The aim of Chapter II is to extend Moore's theory (1959), for small W, which gives the shape of the bubble in the form

$$r = a[1 - \frac{3W}{32} P_2(\mu)] + O(W^2), \tag{1.10}$$

where a is a length scale specified by the volume of the bubble and $P_2(\mu)$ is Legendre function of order 2. It is therefore plausible to proceed by expanding the departure of the shape, from the spherical, in powers of W. The analysis is confined to the calculation of second and third order surface deformation in powers of W, since the algebraic manipulations quickly become unwieldly. The surface (1.7) for the shape is assumed to have fore and aft symmetry, so that an expansion in Legendre functions of even order is used. The results are compared with those of the "Two-point Theory" which, as pointed out earlier, is reliable up to x = 2. It is found that the convergence is poor unless x < 1.4. Thus one cannot claim that the perturbation method is a suitable one for solving the problem. The range of validity is too small for that. In spite of this, we believe, the results are not without interest. First, to within the range of convergence the theory and consequently the shape are exact. Secondly, the features of the theory are interesting enough to record on their own merit. Thirdly, by appealing to Shank's method for accelerating convergence Van Dyke (1964), the results are considerably improved and they are found to be reliable up to W = 3.

In the remainder of this chapter, the drag for the perturbed surface, to $O(W^3)$, is calculated from the dissipation in the potential flow using the expression given by Lamb (1959). An expression for the drag coefficient has been obtained after tedious calculations. These computations could have been considerably reduced if one uses the brief elegant version of this expression developed by Harper (1970) in which velocity derivatives are not required. One needs to know only a coordinate system appropriate to the body and the value of the velocity potential over its surface. Unfortunately this paper appeared after the present calculations were made.

To the first order in W, the drag coefficient is found to agree exactly with Moore (1965) expression for the drag coefficient of a spheroid with flow parallel to its axis of symmetry. However, for higher orders in W, the theory gives higher values for the drag than those predicted by Moore's theory. These results are of small theoretical range of validity in view of the fact that corrections resulting from the boundary-layer are not computed.

Chapter III is devoted to the solution of the present problem using the virial method. An appropriate extension to the tensor virial theorem of the second order is established. A trial shape in the form of an oblate spheroid is used and the resulting tensors calculated. An expression for the Weber number in terms of the axis-ratio is finally obtained. To the first order in W, this expression reduces to Moore's (1959) result for linear theory. On comparing the theory with the "Two-point Theory" excellent agreement has been found up to $x = 2$. Again, on comparing it with the method of accelerating convergence, good agreement has been obtained up to $x = 3$. An important feature of the theory is the existence of a maximum Weber number of 3.271 at $x = 3.72$, and thus exhibiting the same sort of behaviour predicted by Moore's "Two-point Theory", though at a smaller axis-ratio. This supports Moore's (1965) conjecture that there is a maximum Weber number above which the symmetric shape is impossible. Finally direct assessment of the virial result using Moore's (1965) technique for calculating the percentage error in the curvature in equation (1.6), so that it may be satisfied exactly at a general point on the bubble surface, shows considerable improvement on the "Two-point Theory".

In Chapter IV an approximate method is developed for the study of slightly distorted spheroidal bubbles. The convenient system of oblate spheroidal coordinates is used. The fact that the bubble is an oblate spheroid for small W, suggests that the bubble might not be too different in shape from an oblate spheroid of the same axis-ratio even for W of O(1). In view of this we shall take an oblate spheroid as our starting point. Unfortunately, it is not possible to adopt the method of Chapter II in this section, since the perturbed first curvature for an ellipsoidal surface is an irrational function of one of the coordinates. Two main problems are investigated in this chapter. Also reasons are given for the failure of the perturbation scheme of Chapter II. It is illuminating to find that similar features exist in solving the problem of two dimensional motion of an ellipse. In particular it is shown that both theories break down at an axis-ratio $x = \sqrt{2}$, due to an improper representation of the velocity field at this value.

Now in the first problem an approximate method is developed, based on the hypothesis that the true shape of the bubble will differ little from an ellipsoid having the same volume. In view of this assumption, it is plausible to use the flow field about this ellipsoid to determine the dynamic pressure on the surface of the true shape. The shape is determined using the expression for the Weber number in terms of the axis-ratio, first for the "Two-point Theory" and then for the virial theory. The shapes are traced for different values of W and compared with those of the unperturbed ellipsoids. This method also provides an alternative way of comparing the "Two-point Theory" with the virial theory.

The second problem is the same as the first, apart from the inclusion of gravity. As far as I know, the problem of studying the simultaneous effect of surface tension and gravitational forces on the shape of the bubble, has not appeared before in the theoretical literature. Gravitational force is introduced through the known expression of the drag on the ellipsoid in terms of the Froude number. The resulting differential equation is solved using the same numerical method for the symmetric shapes. Results are obtained for different values of the M number, using the Weber number given by the virial theory, since it is more trustworthy. The predicted drag coefficient is plotted against the Reynolds number for a range of values of M. The shapes of the bubbles are traced in comparison with the unperturbed ellipsoids. They are found to be characterized by a dent at the rear stagnation point. Walters and Davidson (1962, 3) obtained similar shapes in their experimental and theoretical studies of accelerating bubbles under the action of gravitational forces alone. They observed a tongue of liquid forming at the back of an accelerating three-dimensional bubble. The bubble distorts into the form of a mushroom and ultimately into a spherical cap. Although this is mere coincidence with the present theory, it may indicate the natural development of a bubble shape from spherical to spheroidal to a spherical cap.

It has also been observed that as a bubble is deformed from the spherical shape, the appearance of a dent at its rear is delayed, in liquids of smaller M numbers, until larger axis-ratios are attained. This seems to be consistent with experiment in the sense that the effect of gravity is more profound, as M increases, so that a bubble may change from spherical into a spherical cap shape without having to go through the intermediate spheroidal shape.

Finally, the predicted velocity of rise of gas bubbles is tested with some experimental data. Three diverse cases are examined. The rise of air bubbles in water ($M = 2.4 \times 10^{-11}$) has often produced discrepancies in experimental results. This is attributed to the fact that water, however pure, is known to contain a small quantity of an unknown surface-active contaminant. The present data is taken from the classical results of Haberman and Morton (1953). Another data taken from this reference is that for the rise of air bubbles in methyl alcohol ($M = 8.9 \times 10^{-11}$). This provides a chance for comparing the present theory with Moore's (1965) earlier theoretical predictions, as well as with experiment. Finally, the theory is compared with the experimental results for the rise of argon bubbles in mercury ($M = 3.7 \times 10^{-14}$), Schwerdtfeger (1968). These results have not been compared with any relevant theoretical results. This provides a good opportunity for comparison with the present theory. The outcome of the above comparisons showed good agreement between theory and experiment.

# CHAPTER II

# NON-LINEAR PERTURBATIONS OF A SPHERICAL BUBBLE

## 1. Introduction

The aim of this chapter is to predict the shape of a bubble, of prescribed volume V, placed in a uniform stream U. The bubble is surrounded by an infinite inviscid incompressible fluid which is moving irrotationally. In the absence of gravity, thus, the shape of the bubble is maintained by the interaction of hydrodynamic pressure forces and surface tension forces. The physical parameter which measures the ratio of these forces is the Weber number W given by

$$W = \frac{2r_e \rho U^2}{\sigma}, \tag{2.1}$$

where $\rho$ is the fluid density, $\sigma$ is the interfacial stress and $r_e$ is the "equivalent spherical radius", (e.s.r.), defined by

$$\frac{4}{3}\pi r_e^3 = V. \tag{2.2}$$

If W is zero, the dynamic pressure has no effect and the bubble is spherical. This suggests we might proceed by expanding the departure of the shape from the spherical in powers of W and the first term of such an expansion has been found by Moore (1959). However, in practice, the algebraic manipulations quickly become unwieldy. We therefore limit ourselves to calculating only the second and third-order corrections to the surface deformation. We start by assembling some expressions needed in the solution.

## 2. Equations of axisymmetric irrotational flow

For flow with axial symmetry using the Stokes stream function $\psi$ as the dependent variable, the velocity components in the directions of increase of the spherical polar coordinates r and $\theta$ are given by

$$q_r = \frac{1}{r^2 \sin\theta} \frac{\partial\psi}{\partial\theta}, \qquad q_\theta = -\frac{1}{r\sin\theta}\frac{\partial\psi}{\partial r}. \tag{2.3}$$

The condition that the flow be irrotational is

$$\frac{\partial q_r}{\partial\theta} - \frac{\partial(rq_\theta)}{\partial r} = 0 \tag{2.4}$$

This leads to the differential equation for $\psi$ by substitution from (2.3)

$$\frac{\partial^2\psi}{\partial r^2} + \frac{(1-\mu^2)}{r^2}\frac{\partial^2\psi}{\partial\mu^2} = 0 \tag{2.5}$$

where

$$\mu = \cos\theta. \tag{2.6}$$

Two fundamental solutions of this equation are

$$\psi = \frac{1}{n+1} r^{n+1}(1-\mu^2)\frac{dP_n}{d\mu}, \quad -\frac{1}{n} r^{-n}(1-\mu^2)\frac{dP_n}{d\mu} \tag{2.7}$$

where $P_n$, which is understood to mean $P_n(\mu)$, is Legendre function which satisfies Legendre's differential equation of integral order n,

$$\frac{d}{d\mu}\left[(1-\mu^2)\frac{dP_n}{d\mu}\right] + n(n+1)P_n = 0. \tag{2.8}$$

Thus a general solution for the stream function in spherical coordinates is of the form

$$\psi = \sum_{n=1}^{\infty} (c_n r^{n+1} + D_n r^{-n})(1-\mu^2)\frac{dP_n}{d\mu} \tag{2.9}$$

where $c_n$, $D_n$ are constants to be determined by the boundary conditions. This will ultimately lead to the particular streamline generating the bubble's surface, on imposing the appropriate conditions of the problem.

## 3. Slip velocity

The pressure P is determined from Bernoulli's equation

$$P + \frac{1}{2}\rho(q_n^2 + q_t^2) = P_s, \tag{2.10}$$

where $P_s$ is the stagnation pressure, $q_n$ and $q_t$ are the normal and tangential components of velocity at a point $P(r,\theta)$ on a meridian section AB of the surface

$$r = r(\mu). \tag{2.11}$$

Now with this surface being a streamline, there is no flow normal to it so that

$$q_n = 0. \tag{2.12}$$

Equation (2.10) therefore reduces to

$$P + \frac{1}{2}\rho q_t^2 = P_s. \tag{2.13}$$

Now with the help of Figure 2.1 and the geometric relation

$$\tan\beta = -r/(\dot{r}\sqrt{\alpha}), \tag{2.14}$$

where dots designate differentiation with respect to $\mu$, it will be a straightforward matter to show that

$$q_t^2 = \frac{\alpha}{r^2 + \alpha\dot{r}^2}\left\{\frac{1}{\alpha}\frac{\partial\psi}{\partial r} - \frac{\dot{r}}{r^2}\frac{\partial\psi}{\partial\mu}\right\}^2. \tag{2.15}$$

This gives the square of slip velocity at a point P, on the surface r, where

$$\alpha = 1 - \mu^2. \tag{2.16}$$

4. First curvature

The first curvature J of a surface is defined by

$$J = \frac{1}{R_1} + \frac{1}{R_2}, \tag{2.17}$$

with $R_1$ and $R_2$ the principal radii of curvature. The derivation of J for a surface with axial symmetry, using orthogonal curvilinear coordinates, is described in appendix (2A). In this section, the expression is derived using the spherical polar coordinates $(r,\theta)$. The surface of revolution is taken to be

$$G = r - a - ag(\theta) = 0, \tag{2.18}$$

where a is a length parameter to be specified later. It is more convenient to work in the coordinates $(r,\mu)$, where $\mu$ is given by (2.6), so that (2.18) becomes

$$G = r - a - ag(\mu) = 0. \tag{2.19}$$

Now by straightforward calculations and substitution into equation (5) in appendix (2A), the expression for J, for a surface of revolution, in spherical coordinates is found to be

$$J = \frac{a(2r^3 + 3\alpha r\dot{g}^2 + 2\mu r^2\dot{g} + \alpha\mu\dot{g}^3 - \alpha r\ddot{g})}{r(r^2 + \alpha\dot{g}^2)^{3/2}}, \tag{2.20}$$

This expression may also be written in the form

$$J = \frac{a[2\alpha^2 r^3 - \alpha^2 r^2 \frac{d}{d\mu}(\alpha\dot{g}) + 3\alpha r(\alpha\dot{g})^2 + \mu(\alpha\dot{g})^3]}{\alpha^{1/2} r[\alpha r^2 + (\alpha\dot{g})^2]^{3/2}} \tag{2.21}$$

This is more suitable when g is given as a series expansion in terms of Legendre polynomials.

## 5. Formulation of the problem

We are now ready to state the problem formally. We seek a Stokes stream function $\psi$, a bubble shape $r = r(\mu)$ and a bubble gas pressure $P_g$ such (Figure 2.2)

(i) $\dfrac{\partial^2\psi}{\partial r^2} + \dfrac{\alpha}{r^2}\dfrac{\partial^2\psi}{\partial\mu^2} = 0$

(ii) $\psi \sim -\frac{1}{2}Ur^2\alpha$ as $r \to \infty$

(iii) $\psi = 0$ on $r = r(\mu)$

(iv) $P_s - \frac{1}{2}\rho q_t^2 + \sigma J = P_g$ on $r = r(\mu)$

(v) Volume $(r = r(\mu)) = V$.

By assuming the bubble to depart very little from a sphere, Moore (1959) has shown that to a first order in $\varepsilon(|\varepsilon|<<1)$ the bubble is deformed into an oblate spheroid. He represented its shape by the equation

$$r = a(1 + \varepsilon P_2) + O(\varepsilon^2) \tag{2.22}$$

where a is a length scale determined by the prescribed volume and

$$\varepsilon = -\frac{3W}{32} + O(W^2). \tag{2.23}$$

To the order of this approximation, it can easily be shown that a is equal to the e.s.r., $r_e$, so that it does not matter whether W is based on a or $r_e$.

Our purpose here is to calculate second and third order deformations as the Weber number increases. Consider now the surface

$$r = r_1 = a(1 + \varepsilon P_2 + \varepsilon' P_4 + \varepsilon'' P_6), \tag{2.24}$$

where, again, a is fixed by the condition (V).

We know that

$$\varepsilon = O(W)$$

and that

$$\varepsilon' = o(W)$$

so suppose, subject to a posteriori justification

$$\varepsilon' = O(W^2) = O(\varepsilon^2)$$

and similarly

$$\varepsilon'' = O(W^3) = O(\varepsilon^3),$$

so that equation (2.24) becomes

$$r = r_1 = a\{1 + \varepsilon P_2 + (\lambda_1\varepsilon^2 + \lambda_2\varepsilon^3)P_4 + \lambda_3\varepsilon^3 P_6\} + O(\varepsilon^4) \qquad (2.25)$$

where $\varepsilon$ has the form

$$\varepsilon = c_1 W + c_2 W^2 + c_3 W^3 + O(W^4). \qquad (2.26)$$

The $\lambda$'s and c's are constants of O(1) and are to be determined later. It should be pointed here that the use of $\varepsilon$ as a small parameter is only dictated by algebraic convenience. The choice of $P_n$'s with even order in (2.24) takes care of the assumption that the bubble has fore and aft symmetry.

Now bearing in mind that in the limit $W \rightarrow 0$ the bubble is a sphere and since $a \rightarrow r_e$ as $W \rightarrow 0$, we try an expansion

$$\psi = -U\alpha\{\frac{1}{2}(r^2 - \frac{a^3}{r})\dot{P}_1 + \sum_{m=0}^{\infty} \frac{B_m}{r^{2m+1}} a^{2m+3}\dot{P}_{2m+1}\}, \qquad (2.27)$$

for the stream function. The coefficients $B_m$ in (2.27) are dimensionless constants and $B_m \rightarrow 0$ as $W \rightarrow 0$. In the present case, only four terms of the above series are taken. Further we shall assume that

$$\left.\begin{aligned} B_0 &= O(\varepsilon) \\ B_1 &= O(\varepsilon) \\ B_2 &= O(\varepsilon^2) \\ B_3 &= O(\varepsilon^3), \end{aligned}\right) \qquad (2.28)$$

so that

$$\left.\begin{aligned} B_0 &= \varepsilon b_1^{(0)} + \varepsilon^2\, b_2^{(0)} + \varepsilon^3\, b_3^{(0)} \\ B_1 &= \varepsilon b_1^{(1)} + \varepsilon^2\, b_2^{(1)} + \varepsilon^3\, b_3^{(1)} \\ B_2 &= \varepsilon^2\, b_2^{(2)} + \varepsilon^3\, b_3^{(2)} \\ B_3 &= \varepsilon^3\, b_3^{(3)}, \end{aligned}\right\} \tag{2.29}$$

where the b's are constants of O(1) and are subject to later determination. This assumption will be justified a posteriori. It is not strictly necessary to make any assumption at this stage, but a commitment to this ordering greatly reduces the algebra.

Dimensionless form

It is convenient to non-dimensionalize the above equations. To do so, we divide all distances by a, all velocities by U, all pressures by $\rho U^2$ and stream functions by $Ua^2$. Then, on using the same notation one gets

$$r = r_1 = 1 + g(\mu) + O(g^4) \tag{2.30}$$

where

$$g = \varepsilon P_2 + (\lambda_1\varepsilon^2 + \lambda_2\varepsilon^3)P_4 + \lambda_3\varepsilon^3 P_6 + O(\varepsilon^4),$$

as the surface of the bubble. This notation will help to suppress some of the algebraic calculations. The dimensionless stream function obtained from (2.27) is

$$\psi = -\alpha\left\{\frac{1}{2}\left(r^2 - \frac{1}{r}\right)\dot{P}_1 + \sum_{m=0}^{\infty} \frac{B_m}{r^{2m+1}}\,\dot{P}_{2m+1}\right\}. \tag{2.31}$$

The boundary conditions are rearranged to give

$$\psi = 0 \text{ on } r_1, \tag{2.32}$$

and

$$2W_a \Delta P + 4J = W_a q_t^2 \quad \text{on } r_1, \tag{2.33}$$

where

$$\Delta P = P_s - P_g, \tag{2.34}$$

and

$$W_a = \frac{2a\rho U^2}{\sigma} \tag{2.35}$$

is the Weber number based on the length scale a. One remark that can be made at this stage, in anticipation of the analysis, is that the velocity perturbation "lags" behind that of the surface. This is revealed by equation (2.33) and considerations of earlier assumptions regarding the order of perturbations and that $\varepsilon$ is $O(W)$. Therefore in order to attain the order balance in (2.33) one only requires terms of $O(\varepsilon^2)$ in $q_t^2$ while in the first curvature needs terms of $O(\varepsilon^3)$.

## 6. Method of Solution

Having obtained the necessary equations with the appropriate boundary conditions, we now proceed to solve the problem. The kinematic boundary condition (2.32) is used for the determination of the b's in equation (2.29). On substituting for $r_1$ from (2.30) into (2.31) and applying condition (2.32), one gets an expression in terms of products and derivatives of Legendre polynomials. This has to be transformed into an expression which is linear in $P_2$, $P_4$ and $P_6$ and having no derivatives. The limitation to $P_6$ is, of course, dictated by the order of the B's. To achieve this form, one has to go through lengthy algebraic manipulations. Besides using Legendre identities, given in appendix (4A), one requires repeated use of the identity

$$P_2P_n = \frac{3(n+1)(n+2)}{2(2n+1)(2n+3)}P_{n+2} + \frac{n(n+1)}{(2n-1)(2n+3)}P_n + \frac{3n(n-1)}{2(4n^2-1)}P_{n-2} \qquad (2.36)$$

which may be derived by straightforward manipulations with Legendre identities.

Now equating the coefficients of $P_0$, $P_2$, $P_4$ and $P_6$ to zero, by virtue of the linear independence of Legendre polynomials, one gets a system of four equations in the B's and $\varepsilon$. The expressions (2.29) for the B's are then substituted into these equations, neglecting terms of $O(\varepsilon^4)$ or higher. Rearranging the terms, grouping coefficients of each power of $\varepsilon$ together and equating them to zero by the property of their linear independence one gets a set of ten equations in terms of the unknown b's and $\lambda$'s. Finally solving these simultaneous equations for the b's in terms of the $\lambda$'s and substituting their values into (2.29) gives

$$\left.\begin{aligned}
B_0 &= \frac{3}{10}\varepsilon - \frac{183}{350}\varepsilon^2 - \frac{1}{35}\left(\frac{191}{50} - 18\lambda_1\right)\varepsilon^3 \\
B_1 &= -\frac{3}{10}\varepsilon - \frac{1}{5}\left(\frac{3}{5} - \frac{5}{6}\lambda_1\right)\varepsilon^2 - \frac{1}{55}\left(\frac{2862}{175} + \frac{56}{3}\lambda_1 - \frac{55}{6}\lambda_2\right)\varepsilon^3 \\
B_2 &= -\frac{1}{3}\left(\frac{1}{2}\lambda_1 + \frac{27}{35}\right)\varepsilon^2 - \frac{1}{39}\left(\frac{1377}{175} + \frac{121}{35}\lambda_1 + \frac{13}{2}\lambda_2 - \frac{9}{2}\lambda_3\right)\varepsilon^3 \\
B_3 &= -\frac{1}{13}\left(\frac{36}{11} + \frac{60}{11}\lambda_1 + \frac{3}{2}\lambda_3\right)\varepsilon^3.
\end{aligned}\right\} \qquad (2.37)$$

Having found the B's in terms of $\varepsilon$ and the unknown $\lambda$'s, the stream function (2.31) is easily obtained by direct substitution. Our final task is to obtain an expression for the square of the slip velocity from equations (2.15), (2.31) and (2.37). Again one has to go through lengthy calculations in order to express $q_t^2$ as a linear combination of $P_2$, $P_4$ and $P_6$. Furthermore recalling that $q_t^2$ is only required to $O(\varepsilon^2)$, one finally gets

$$\begin{aligned} q_t^2 = &(\tfrac{3}{2} - \tfrac{162}{175}\varepsilon^2)P_0 + \\ &(-\tfrac{3}{2} + \tfrac{108}{35}\varepsilon + \tfrac{324}{175}\varepsilon^2 - \tfrac{12}{7}\lambda_1\varepsilon^2)P_2 + \\ &(-\tfrac{108}{35}\varepsilon + \tfrac{918}{1925}\varepsilon^2 + \tfrac{552}{77}\lambda_1\varepsilon^2)P_4 + \\ &(-\tfrac{108}{77}\varepsilon^2 - \tfrac{60}{11}\lambda_1\varepsilon^2)P_6 + \\ &O(\varepsilon^3). = \overline{q}_t^2, \text{ say.} \end{aligned} \tag{2.38}$$

Consider next the expression (2.21) for the first curvature. Expanding this to the third order in g and non-dimensionalizing w.r.t. a, one gets

$$\begin{aligned} J = &2(1 - g + g^2 - g^3) - (1 - 2g + 3g^2)\frac{d}{d\mu}(\alpha\dot{g}) \\ &+ \frac{1}{2}\frac{d}{d\mu}(\alpha^2\dot{g}^3) + O(g^4) \\ &= \overline{J}, \text{ say.} \end{aligned} \tag{2.39}$$

Upon substituting for g from (2.30) and carrying manipulations similar to the above in order to represent $\overline{J}$ as a linear expression in the P's, one gets

$$\bar{J} = (2 - 2\varepsilon^2 + \frac{32}{35}\varepsilon^3)P_0 +$$

$$(4\varepsilon - \frac{20}{7}\varepsilon^2 + \frac{12}{7}\varepsilon^3 - \frac{96}{7}\lambda_1\varepsilon^3)P_2 +$$

$$(-\frac{36}{7}\varepsilon^2 + 18\lambda_1\varepsilon^2 + 18\lambda_2\varepsilon^3 - \frac{960}{77}\lambda_1\varepsilon^3 + \frac{108}{35}\varepsilon^3)P_4$$

$$+ (40\lambda_3\varepsilon^3 - \frac{240}{11}\lambda_1\varepsilon^3 + \frac{72}{7}\varepsilon^3)P_6$$

$$+ O(\varepsilon^4). \tag{2.40}$$

Now upon neglecting terms of $O(\varepsilon^4)$, equation (2.33) becomes

$$2W_a\Delta P + 4\bar{J} = W_a\bar{q}_t^2 + O(\varepsilon^4), \text{ on } r = r_1. \tag{2.41}$$

Substituting for $\bar{J}$ from (2.40) and $\bar{q}_t^2$ from (2.38), equation (2.41) gives a linear expression in the $P_n$'s. Equating the coefficients of $P_n$ to zero, one gets a system of simultaneous equations leading to the evaluation of the $\lambda$'s in the form

$$\lambda_1 = \frac{26}{35}, \quad \lambda_2 = \frac{11842}{14553}, \quad \text{and} \quad \lambda_3 = \frac{197}{385}. \tag{2.42}$$

One also obtains

$$\varepsilon = -\Gamma W_a - \frac{47}{35}(\Gamma W_a)^2 - \frac{451}{175}(\Gamma W_a)^3 + O(W_a^4) \tag{2.43}$$

and

$$W_a\Delta P = 4[-1 + 2\Gamma W_a + (\Gamma W_a)^2 + \frac{334}{175}(\Gamma W_a)^3 + O(W_a^4)], \tag{2.44}$$

where

$$\Gamma = 3/32\ . \tag{2.45}$$

From (2.43) one recovers Moore's (1959) first order term

$$\varepsilon = -\frac{3}{32}W_a + O(W_a^2). \tag{2.46}$$

The surface of the bubble (2.30) becomes

$$r = r_1 = 1 - (0.09375W_a + 0.01180W_a^2 + 0.00211W_a^3)P_2$$
$$+ (0.00653W_a^2 + 0.00097W_a^3)P_4$$
$$- 0.00042W_a^3 P_6 + O(W_a^4). \tag{2.47}$$

Axis-ratio x

This is the ratio of the transverse and longitudinal axes of the bubble so that from Figure 2.2 one gets

$$x = \frac{c}{b} = \frac{[r_1]_{\theta=\pi/2}}{[r_1]_{\theta=0}} \; . \tag{2.48}$$

Upon substituting from (2.47) for $r_1$ one gets

$$x = 1 + \frac{3}{2}(\Gamma W_a) + \frac{61}{20}(\Gamma W_a)^2 + \frac{45108121}{5821200}(\Gamma W_a)^3 + O(W_a^4) \tag{2.49}$$

The volume of the bubble in dimensionless form is found to be

$$V = \frac{4\pi}{3}(1 + \frac{3}{5}\varepsilon^2 + \frac{2}{35}\varepsilon^3) + O(\varepsilon^4). \tag{2.50}$$

$$\therefore \qquad \bar{r}_e = r_e/a = 1 + \frac{1}{5}\varepsilon^2 + \frac{2}{105}\varepsilon^3 + O(\varepsilon^4), \tag{2.51}$$

or in terms of $W_a$

$$\bar{r}_e = 1 + \frac{1}{5}(\Gamma W_a)^2 + \frac{272}{525}(\Gamma W_a)^3 + O(W_a^4). \tag{2.52}$$

Now since

$$W_a/W = 1/\bar{r}_e, \tag{2.53}$$

$\therefore$

$$W_a = W - \frac{9}{5120}W^3 + O(W^4). \tag{2.54}$$

Hence in terms of W, which is based on $r_e$, the above equations become

$$\varepsilon = - 0.09375W + 0.01180W^2 + 0.00194W^3 + 0(W^4), \tag{2.55}$$

$$\begin{aligned} r = r_1 = 1 &- (0.09375W + 0.01180W^2 + 0.00194W^3)P_2 \\ &+ (0.00653W^2 + 0.00097W^3)P_4 \\ &- 0.00042W^3P_6 + 0(W^4) \end{aligned} \tag{2.56}$$

and

$$x = 1 + 0.14062W + 0.0261W^2 + 0.0061W^3 + 0(W^4). \tag{2.57}$$

Similarly the stream function coefficients (2.37) expressed to the third order in W are

$$\left.\begin{aligned} B_0 &= - 0.02813W - 0.00814W^2 - 0.00196W^3 \\ B_1 &= 0.02813W + 0.00357W^2 + 0.00093W^3 \\ B_2 &= - 0.00335W^2 - 0.00056W^3 \\ B_3 &= 0.00051W^3. \end{aligned}\right) \tag{2.58}$$

The function x(W) given by equation (2.57) is now plotted in Figure 2.3 for the different order perturbations in W. On the same figure the curve W(x) for the "Two-point Theory" is also plotted. Comparison of the two theories shows that the perturbation solution converges towards that of the "Two-point Theory". However, detailed examination shows that the third order theory departure from the "Two-point Theory" is 4.1% at $x = 1.4$, 7.1% at $x = 1.6$, and 11.2 % at $x = 1.7$. Moore (1965) has shown that the maximum deviation of his theory from the exact one should not exceed 10% at $x = 2$. It is thus clear that although the perturbation theory is exact for small Weber numbers, its convergence is slow. One can try the methods of accelerating convergence described in Van Dyke (1964), p.202. Among these is Shank's method for improving slowly converging series, or even divergent. Applying this method to the series (2.57) for the expansion of (x - 1), the corresponding expression is found to be

$$x - 1 = \frac{367W}{2610 - 610W} \tag{2.59}$$

Again we plot this curve, Figure 2.4, in comparison with that of the "Two-Point Theory". One finds that they differ by 6.8% at $x = 2$ which is well within the estimated range for the exact theory. Thus it seems likely that this result is fairly close to the exact theory up to $x = 2$.

7. <u>The drag on the bubble</u>

As discussed in the introduction, at large Reynolds numbers viscosity does not affect the shape of the bubble. Moreover, as Levich (1962) has shown, the drag force D on the bubble can to leading order be calculated from the dissipation in the potential flow, and from the expression given by Lamb (1959), p.581, for the dissipation in a potential flow

$$DU = -\mu_o \int \hat{\underline{n}}.\nabla(\underline{q}^2)dS; \tag{2.60}$$

the integral being taken over the body surface, and $\underline{n}$ is normal into the fluid. dS is element of surface area and $\mu_o$ is the viscosity. In dealing with axisymmetric flows it is convenient to express (2.60) in terms of the spherical coordinates $r$ and $\mu$ and the stream function $\psi$.

Now from Figure 2.1 one gets

$$\underline{\hat{n}} = \sin\beta\ \underline{\hat{r}} - \cos\beta\ \underline{\hat{\theta}}\ , \qquad (2.61)$$

and

$$\nabla = (\underline{\hat{r}}\frac{\partial}{\partial r},\ \hat{\theta}\frac{1}{r}\frac{\partial}{\partial\theta}). \qquad (2.62)$$

dS is given by

$$dS = -2\pi r^2 d\mu \qquad (2.63)$$

and

$$q^2 = q_r^2 + q_\theta^2 = [(\frac{1}{r^2}\frac{\partial\psi}{\partial\mu})^2 + \frac{1}{\alpha}(\frac{1}{r}\frac{\partial\psi}{\partial r})^2]. \qquad (2.64)$$

Upon substituting for these expressions in (2.60) one gets, after some manipulations,

$$\begin{aligned}\overline{D} = 4\pi \int_{\mu=-1}^{1} & [\frac{1}{\sqrt{r^2 + \alpha\dot{r}^2}} \{\frac{1}{\alpha}(1 + \frac{\mu\dot{r}}{r})(\frac{\partial\psi}{\partial r})^2 \\ & + \frac{1}{r}(\dot{r}\frac{\partial\psi}{\partial r} - \frac{\partial\psi}{\partial\mu}).\ \frac{\partial^2\psi}{\partial r\partial\mu} + \frac{2}{r^2}(\frac{\partial\psi}{\partial\mu})^2 \\ & - \frac{r}{\alpha}\frac{\partial\psi}{\partial r}\frac{\partial^2\psi}{\partial r^2} + \frac{\alpha\dot{r}}{r^3}\frac{\partial\psi}{\partial\mu}\frac{\partial^2\psi}{\partial\mu^2}\}]_{r=r_1} d\mu,\end{aligned} \qquad (2.65)$$

where

$$\overline{D} = \frac{D}{Ua\mu_o} \qquad (2.66)$$

is the dimensionless drag.

The actual drag D is given by

$$D = \frac{1}{2}\rho U^2 \pi r_e^2\ C_D, \qquad (2.67)$$

where $C_D$ is the drag coefficient. Combining equations (2.51), (2.65) - (2.67) and making use of the expression

$$R = \frac{2r_e \rho U}{\mu_o} \tag{2.68}$$

for the Reynolds number, one gets

$$C_D = \frac{16}{R\bar{r}_e} \int_{\mu=-1}^{1} [\frac{1}{\sqrt{r^2 + \alpha \dot{r}^2}} \{\frac{1}{\alpha}(1 + \frac{\mu \dot{r}}{r})(\frac{\partial \psi}{\partial r})^2$$

$$+ \frac{1}{r}(\dot{r}\frac{\partial \psi}{\partial r} - \frac{\partial \psi}{\partial \mu})\frac{\partial^2 \psi}{\partial r \partial \mu} + \frac{2}{r^2}(\frac{\partial \psi}{\partial \mu})^2$$

$$- \frac{r}{\alpha}\frac{\partial \psi}{\partial r}\frac{\partial^2 \psi}{\partial r^2} + \frac{\alpha \dot{r}}{r^3}\frac{\partial \psi}{\partial \mu}\frac{\partial^2 \psi}{\partial \mu^2}\}]_{r=r_1} d\mu. \tag{2.69}$$

This integral is evaluated after tedious but straightforward calculations, using the expressions for the B's in equation (2.58). The final result is

$$C_D = \frac{48}{R}[1 + 0.1875W + 0.02959W^2 + 0.00476W^3 + O(W^4)]. \tag{2.70}$$

It must be emphasized that this formula is correct only to $O(R^{-1})$. The calculation of the term of $O(R^{-3/2})$ requires the boundary-layer structure to be determined and this has not been attempted.

Moore (1965) pursuing his analysis for an ellipsoidal bubble, obtained an expression for the drag coefficient in terms of the axis-ratio. Invoking the details of the potential flow about an oblate ellipsoid of revolution, he calculated the dissipation in the flow. He then found the expression for $C_D$ corresponding to an ellipsoid, whose axis-ratio is x, in the form

$$C_D = \frac{48}{R}\,\frac{x^{4/3}(x^2-1)^{3/2}[(x^2-1)^{1/2}-(2-x^2)\sec^{-1}x]}{3[x^2\sec^{-1}x-(x^2-1)^{1/2}]^2} + O(R^{-3/2}). \tag{2.71}$$

In order to compare the results (2.70) and (2.71), it is convenient to adopt Moore's notation

$$C_D = \frac{48}{R}G(x) + O(R^{-3/2}), \tag{2.72}$$

so that the quantity in square brackets in equation (2.70) is also referred to as G.

Now expanding the function G(x), obtained from (2.71) and (2.72), to O(x - 1) (i.e. to $O(e^2)$, where e is the eccentricity of an ellipse in the meridian plane) and using the relation

$$W = \frac{64}{9}(x-1), \qquad \text{as } x \to 1, \tag{2.73}$$

(which may be obtained from either (2.49) or (2.57) since to this order $W_a = W$), one finds that it is identical with the linear term in equation (2.70). For further comparison, the graph of the functions G(x) derived from equations (2.70) and (2.71) are shown in Figure 2.5. Both curves demonstrate an increase in the drag with increasing oblateness. However, the present theory, which is not likely to be reliable beyond x = 1.4, seems to over-estimate the value of G(x).

# CHAPTER III

# THE VIRIAL METHOD AND ITS APPLICATION TO THE MOTION OF GAS BUBBLES

## 1. Introduction

The virial equations of the various orders are the moments of the relevant hydrodynamical equations. These moment equations are exact integral relations that must be satisfied by the solution of equation of motion and the boundary conditions. The moments themselves have simple physical interpretations.

Although the tensor virial equation has been known since Lord Rayleigh (1900), its usefulness in hydrodynamic problems has only recently been exploited. It has been revived by Chandrasekhar (1961, 1965, 1969) and Lebovitz (1961) in problems of astrophysical interest. More recently Rosenkilde (1969) extended the method to investigate the equilibrium and stability of an incompressible dielectric fluid drop situated in a uniform electric field. A general survey of the virial method and its recent applications are given in Chandrasekhar's book (1969).

It is the purpose of this chapter to find an appropriate extension to the tensor virial equation, for the study of the equilibrium of a gas bubble moving uniformly in an inviscid incompressible fluid which extends to infinity. Difficulties arise because the flow region is unbounded and a careful treatment of the integrals is needed.

## 2. The appropriate form of the tensor virial theorem

Consider the uniform translational motion of a bubble with velocity U, through an incompressible inviscid fluid under the action of surface tension forces. As shown in Figure 3.1, $\hat{\underline{n}}$ and $\hat{\underline{N}}$ are unit vectors normal to the surface elements $\delta S$ and $\delta\Sigma$ and are both drawn in the outward directions relative to the closed surfaces S and $\Sigma$. Here, S is the surface of the bubble and $\Sigma$ denotes the surface of a fixed sphere with a centre C and large radius R. The region enclosed between S and $\Sigma$ is of volume V and is wholly occupied by a fluid of uniform density $\rho$. $P_g$ is the gas pressure inside the bubble and is an unknown constant.

In the present problem it is convenient to employ a system of rectangular cartesian coordinates which is moving with the bubble. Its origin* O coincides with the centre of the bubble and has velocity $U_i$. Also, as illustrated in Figure 3.1, the axis $Ox_3$ is taken parallel to the velocity of the bubble so that

$$U_1 = U_2 = 0, \quad U_3 = U. \tag{3.1}$$

Let $u_i(x_1, x_2, x_3, t)$ be the fluid velocity relative to $\Sigma$. The combination of a moving frame $Ox_1x_2x_3$ and a velocity field $u_i(x_1, x_2, x_3, t)$ relative to a fixed frame is slightly unusual, but has advantage for the present problem. One remarks that since $\Sigma$ is at large distance and since $u_i$ falls off rapidly with distance from the bubble, $u_i$ does not depend on t - it would, of course, if $\Sigma$ were

---

* at time t = 0, O and C are taken coincident.

at a finite distance. Thus we can drop the time dependence of $u_i$ and obtain the momentum equation in the form

$$\rho u_k \frac{\partial u_i}{\partial x_k} - \rho U_k \frac{\partial u_i}{\partial x_k} = - \frac{\partial P}{\partial x_i} . \tag{3.2}$$

The advantage of this formulation is that certain integrals over $\Sigma$ will vanish on account of the smallness of $u_i$. The equation of continuity is

$$\frac{\partial u_i}{\partial x_i} = 0. \tag{3.3}$$

Unless otherwise stated, the summation convention applies to repeated indices in the above equations only.

Now to obtain the second-order virial equation, we have simply to multiply equation (3.2) by $x_j$ and integrate over the entire volume V occupied by the fluid. Thus the first moment of the equation of motion is

$$\int_V \rho x_j u_k \frac{\partial u_i}{\partial x_k} dV - \int_V \rho x_j U_k \frac{\partial u_i}{\partial x_k} dV = - \int_V x_j \frac{\partial P}{\partial x_i} dV, \tag{3.4}$$

where

$$dV = dx_1\, dx_2\, dx_3 \tag{3.5}$$

is the volume element. Applying the divergence theorem to the right-hand side of (3.4) gives

$$- \int_V x_j \frac{\partial P}{\partial x_i} dV = \int_S x_j P dS_i - \int_\Sigma x_j P d\Sigma_i + \delta_{ij} \int_V P dV, \tag{3.6}$$

where $\delta_{ij}$ is the Kronecker delta and

$$dS_i = n_i\, dS; \quad d\Sigma_i = N_i d\Sigma. \tag{3.7}$$

Here $n_i$ and $N_i$ denote the components of $\hat{\underline{n}}$ and $\hat{\underline{N}}$ respectively.

At this stage one defines the tensor

$$R_{ij} = -\frac{1}{2} \int_\Sigma x_i\, P\, d\Sigma_i, \tag{3.8}$$

and the quantity

$$\Pi = \int_V P dV. \tag{3.9}$$

The tensor $R_{ij}$ represents the effect of the disturbance on the pressure at the surface $\Sigma$. In general this tensor is non-zero, even when $\Sigma$ recedes to infinity. The scalar quantity $\Pi$ accounts for the microscopic motion of the fluid particles.

Now the external pressure on S, adjacent to S, is given by Laplace's formula

$$P - P_g = -\sigma \operatorname{div} \hat{\underline{n}}, \tag{3.10}$$

where the constant $\sigma$ denotes the surface tension. (The divergence of the unit outward normal to a point on S is equal to the first curvature at that point, see appendix (2A)).

By use of the boundary condition (3.10), the first integral on the right-hand side of (3.6) may be rewritten in the form

$$\int_S x_j\, PdS_i = -\sigma \int_S x_j \operatorname{div} \underline{n}\, dS_i + P_g \int_S x_j\, dS_i$$

or

$$\int_S x_j\, PdS_i = -2C_{ij} + K_{ij} \tag{3.11}$$

where

$$C_{ij} = \frac{1}{2}\sigma \int_S x_j \operatorname{div} \underline{\hat{n}}\, dS_i \tag{3.12}$$

is the Surface-Energy Tensor. This terminology has been adopted by Rosenkilde (1967a) where he modified Chandrasekhar's version for $C_{ij}$. To justify this, he proved that the trace of $C_{ij}$ is

$$C = \sigma \int_S dS = \sigma A, \tag{3.13}$$

A being the total surface area of the surface S, and thus agreeing with the usual thermodynamic definition of the surface energy. The tensor $K_{ij}$ in (3.11) is given by

$$K_{ij} = P_g \int_S x_j \, dS_i, \tag{3.14}$$

and will be identified as "the gas tensor".

Now combining equations (3.6)-(3.14) one gets

$$-\int_V x_j \frac{\partial P}{\partial x_i} dV = -2C_{ij} + 2R_{ij} + K_{ij} + \Pi\delta_{ij}. \tag{3.15}$$

The next task is to transform the left-hand side of equation (3.4) into simpler integrals.

Consider first the relation

$$\begin{aligned}\frac{\partial}{\partial x_k}(u_i u_k x_j) &= u_i u_k \delta_{kj} + u_k x_j \frac{\partial u_i}{\partial x_k} + x_j u_i \frac{\partial u_k}{\partial x_k} \\ &= u_i u_j + x_j u_k \frac{\partial u_i}{\partial x_k} + x_j u_i \frac{\partial u_k}{\partial x_k}.\end{aligned} \tag{3.16}$$

The last term on the right-hand side of this equation vanishes on applying equation (3.3). Thus (3.16) becomes

$$x_j u_k \frac{\partial u_i}{\partial x_k} = \frac{\partial}{\partial x_k}(u_i u_k x_j) - u_i u_j. \tag{3.17}$$

Multiplying this equation by $\rho$ and integrating over the volume V one gets, after an application of the divergence theorem,

$$\int_V \rho x_j u_k \frac{\partial u_i}{\partial x_k} dV = - \int_S \rho u_i u_k x_j dS_k +$$

$$\int_\Sigma \rho u_i u_k x_j d\Sigma_k - \int_V \rho u_i u_j dV. \tag{3.18}$$

We can perform some further useful transformations once we have introduced the assumption of irrotational flow. Then

$$u_i = \frac{\partial \Phi}{\partial x_i}, \tag{3.19}$$

where $\Phi$ is the velocity potential. On substituting for $u_i$ from (3.19) one gets

$$- \int_V \rho u_i u_j dV = -\rho \int_V u_j \frac{\partial \Phi}{\partial x_i} dV. \tag{3.20}$$

Now on using the relation

$$u_j \frac{\partial \Phi}{\partial x_i} = \frac{\partial}{\partial x_i} (\Phi u_i) - \Phi \frac{\partial u_j}{\partial x_i} \tag{3.21}$$

and applying the divergence theorem, equation (3.20) becomes

$$- \int_V \rho u_i u_j dV = \int_S \rho \Phi u_j dS_i - \int_\Sigma \rho \Phi \, u_j \, d\Sigma_i$$

$$+ \int_V \rho \Phi \frac{\partial u_j}{\partial x_i} dV. \tag{3.22}$$

Now we write

$$L_{ij} = - \frac{1}{2} \int_S \rho x_j u_i u_k dS_k \tag{3.23}$$

$$L'_{ij} = \frac{1}{2} \int_\Sigma \rho x_j u_i u_k d\Sigma_k \tag{3.24}$$

$$N_{ij} = -\frac{1}{2} \int_V \rho \Phi \frac{\partial u_j}{\partial x_i} dV \tag{3.25}$$

$$T_{ij} = -\frac{1}{2}\int_S \rho\Phi u_j dS_i \tag{3.26}$$

and

$$T'_{ij} = \frac{1}{2}\int_\Sigma \rho\Phi u_j d\Sigma_i, \tag{3.27}$$

where $T_{ij}$ is the kinetic-energy tensor. The contraction of $T_{ij}$ gives

$$T = -\frac{1}{2}\int_S \rho\Phi \underline{u}.\hat{\underline{n}} dS = -\frac{1}{2}\int_S \rho\Phi\frac{\partial\Phi}{\partial n}\, dS, \tag{3.28}$$

which is the kinetic energy associated with the macroscopic motion of the liquid. The set of equations (3.18)-(3.28) now gives

$$\int_V \rho x_j u_k \frac{\partial u_i}{\partial x_k}\, dV = 2L_{ij} + 2L'_{ij} - 2T_{ij} - 2T'_{ij} - 2N_{ij}. \tag{3.29}$$

Consider next the second integral on the left-hand side of equation (3.4). As $U_k$ is a constant, it is possible to write

$$\begin{aligned} -\int_V \cdot\, x_j U_k \frac{\partial u_i}{\partial x_k}\, dV &= -U_k \int_V \rho x_j \frac{\partial u_i}{\partial x_k}\, dV \\ &= -U_k \int_V \frac{\partial}{\partial x_k}(u_i x_j) dV + \rho U_k \int_V u_i \delta_{ij} dV \\ &= \int_S \rho u_i x_j U_k dS_k - \int_\Sigma \rho u_i x_j U_k d\Sigma_k + \rho U_j \int_V u_i dV, \end{aligned} \tag{3.30}$$

after an application of the divergence theorem. In a similar manner one gets

$$\begin{aligned} \rho U_j \int_V u_i dV &= \rho U_j \int_V \frac{\partial\Phi}{\partial x_i}\, dV \\ &= -\rho U_j \int_S \Phi\, dS_i + \rho U_j \int_\Sigma \Phi\, d\Sigma_i. \end{aligned} \tag{3.31}$$

To make further simplifications it is useful to define the tensors

$$M_{ij} = -\frac{1}{2} \int_S \rho u_i x_j U_k dS_k \tag{3.32}$$

$$M'_{ij} = \frac{1}{2} \int_\Sigma \rho u_i x_j U_k d\Sigma_k \tag{3.33}$$

$$Q_{ij} = \frac{1}{2} \int_S \rho \Phi U_j dS_i \tag{3.34}$$

$$Q'_{ij} = -\frac{1}{2} \int_\Sigma \rho \Phi U_j d\Sigma_i, \tag{3.35}$$

so that combining equations (3.30)-(3.35) gives

$$-\int_V \rho x_j U_k \frac{\partial u_i}{\partial x_k} dV = -2M_{ij} - 2M'_{ij} - 2Q_{ij} - 2Q'_{ij}. \tag{3.36}$$

Finally, on substituting from equations (3.15), (3.29) and (3.36) into (3.4) one gets

$$\begin{aligned} 2L_{ij} + 2L'_{ij} = {} & 2T_{ij} + 2T'_{ij} + 2N_{ij} + 2R_{ij} \\ & + 2M_{ij} + 2M'_{ij} + 2Q_{ij} + 2Q'_{ij} \\ & - 2C_{ij} + K_{ij} + \Pi\delta_{ij}, \end{aligned} \tag{3.37}$$

which is the tensor virial equation of the second order. It provides a set of nine moment equations since

$$i,j = 1,2,3. \tag{3.38}$$

3. Method of Solution

The application of the virial method requires the selection of a trial shape. This will be taken to be

$$\frac{x_1^2}{a_1^2} + \frac{x_2^2}{a_2^2} + \frac{x_3^2}{a_3^2} = 1, \tag{3.39}$$

with

$$a_1 = a_2, \tag{3.40}$$

so that it is an ellipsoid of revolution whose axis of symmetry $Ox_3$ is parallel to the velocity of the bubble. Moreover, we will assume that $a_1 > a_3$, so that the ellipsoid is oblate. This trial shape has the advantage that relatively simple expressions for the velocity field are available e.g. in Lamb (1959).

In order to evaluate the various tensorial quantities appearing in the virial equation, one requires two other coordinate systems. The system of oblate spheroidal coordinates and a related system, adopted by Rosenkilde (1967b) in order to suppress some of the manipulations.

Consider first the system of coordinates employed in connection with oblate spheroids of revolution. This is related to rectangular cartesian coordinates by the equations

$$x_1 = \bar{\omega} \cos \gamma; \quad x_2 = \bar{\omega} \sin \gamma; \quad x_3 = k\alpha\beta, \tag{3.41}$$

where

$$\bar{\omega} = k[(1 + \alpha^2)(1 - \beta^2)]^{1/2}. \tag{3.42}$$

The domain of the variables $\alpha$, $\beta$, $\gamma$ is given by:

$$0 < \alpha < \infty; \; -1 \leq \beta \leq 1; \; 0 \leq \gamma \leq 2\pi. \tag{3.43}$$

As shown in Figure 3.2, which is copied from Happel and Brenner (1965) with slight modifications, the surfaces $\alpha = \alpha_o$ (const.) are oblate spheroids of revolution about the z-axis and are given by

$$\frac{\bar{\omega}^2}{k^2(1 + \alpha_o^2)} + \frac{z^2}{k^2\alpha_o^2} = 1. \tag{3.44}$$

Comparing this with equations (3.39) and (3.40) we see that

$$a_1 = a_2 = k(1 + \alpha_o^2)^{1/2}; \quad a_3 = k\alpha_o. \tag{3.45}$$

On denoting the eccentricity of the meridian section by e one gets

$$e^2 = 1 - (a_3/a_1)^2 = 1 - x^{-2} = (1 + \alpha_o^2)^{-1}, \tag{3.46}$$

where x is the axis-ratio. The line elements $h_\alpha$, $h_\beta$ and $h_\gamma$ defined by

$$dS^2 = h_\alpha^2\, d\alpha^2 + h_\beta^2\, d\beta^2 + h_\gamma^2\, d\gamma^2$$

are

$$h_\alpha = k(D/L)^{1/2}, \; h_\beta = k(D/E)^{1/2}, \; h_\gamma = k(LE)^{1/2}, \tag{3.47}$$

where

$$\left.\begin{aligned} &D = \alpha^2 + \beta^2, \quad D_o = \alpha_o^2 + \beta^2 \\ &L = 1 + \alpha^2, \; L_o = 1 + \alpha_o^2 \\ &E = 1 - \beta^2. \end{aligned}\right\} \tag{3.48}$$

The motion due to an oblate ellipsoid ($\alpha = \alpha_o$) relative to a fixed frame moving with velocity U parallel to its axis of revolution in an infinite mass of liquid, as given in Lamb (1959) p.144, is

$$\Phi = c_o\beta(\alpha \cot^{-1}\alpha - 1), \tag{3.49}$$

where

$$c_o = -kU/\left(\frac{\alpha_o}{L_o} - \cot^{-1}\alpha_o\right) = -Ua_1/[(1 - e^2)^{1/2} - \frac{1}{e}\sin^{-1}e]. \tag{3.50}$$

It is now a straightforward matter to obtain the velocity components along the cartesian axes in the form

$$\left.\begin{aligned} &u_1 = \frac{c_o\beta x_1}{k^2 LD}, \quad u_2 = \frac{c_o\beta x_2}{k^2 LD}, \\ &u_3 = c_o[D\cot^{-1}\alpha - \alpha]/kD. \end{aligned}\right\} \tag{3.51}$$

Also their derivatives are found to be

$$\left.\begin{aligned}
\frac{\partial u_1}{\partial x_1} &= \frac{c_o\beta}{k^2LD} - \frac{c_o\beta E}{k^2LD^3}\,(5\alpha^4 + 3\alpha^2 + \alpha^2\beta^2 - \beta^2)\cos^2\gamma \\
\frac{\partial u_2}{\partial x_2} &= \frac{c_o\beta}{k^2LD} - \frac{c_o\beta E}{k^2LD^3}\,(5\alpha^4 + 3\alpha^2 + \alpha^2\beta^2 - \beta^2)\sin^2\gamma \\
\frac{\partial u_3}{\partial x_3} &= \frac{c_o\beta}{k^2D^3}\,(3\alpha^2 - \beta^2 - 5\alpha^2\beta^2 - \beta^4).
\end{aligned}\right\} \tag{3.52}$$

We now proceed to evaluate the tensor $N_{ij}$ in (3.25). This is clearly a symmetric tensor since

$$N_{ij} = -\frac{1}{2}\int \rho\,\Phi\,\frac{\partial^2\Phi}{\partial x_i\,\partial x_j}\,dV. \tag{3.53}$$

Furthermore the trace of $N_{ij}$ vanishes by applying the equation of continuity. Now on substituting from equations (3.49) and (3.52) into (3.25) one gets

$$\left.\begin{aligned}
N_{33} = \frac{2\pi c_o^2 k\rho}{3}\int_{\alpha=\alpha_o}^{\infty} &[-4 - 15\alpha^2 + 13\alpha\cot^{-1}\alpha + \\
&30\alpha^3\cot^{-1}\alpha - 3(3\alpha^2 + 5\alpha^4)(\cot^{-1}\alpha)^2]\,d\alpha.
\end{aligned}\right\} \tag{3.54}$$

Evaluation of this integral gives

$$\left.\begin{aligned}
N_{33} = \frac{\Gamma}{3e^2(eH - S)^2}&[(6 + e^2)He^2 - (12 - 11e^2)eS \\
&+ 6(1 - e^2)\,HS^2],
\end{aligned}\right\} \tag{3.55}$$

Similarly one finds

$$\left.\begin{aligned}
N_{11} = N_{22} = \frac{\Gamma}{6e^2(eH-S)^2}&[(12 - 11e^2)eS - (6 + e^2)He^2 \\
&- 6(1 - e^2)HS^2],
\end{aligned}\right\} \tag{3.56}$$

where

$$\Gamma = \pi\rho U^2 a_1^3; \quad H = \sqrt{1 - e^2}; \quad S = \sin^{-1} e. \tag{3.57}$$

Consider next the tensors represented by integrals over the surface $\Sigma$. These tensors are evaluated by integrating over the surface $\Sigma$ as its radius $R \to \infty$. The appropriate system of coordinates is that of spherical polars $(R,\theta,\gamma)$, where $\theta$ is the angle between $Ox_3$ and the radius vector $\underline{R}$.

For large values of $\alpha$, the above potential takes the form

$$\left.\begin{aligned} \bar{\Phi} &\sim - c_o\beta[1 - \alpha(\frac{1}{\alpha} - \frac{1}{3\alpha^3} + \ldots)], \\ &\sim - \frac{c_o\beta}{3\alpha^2} = - \frac{c_o x_3}{3k\alpha^3} \quad \text{as} \quad \alpha \to \infty. \end{aligned}\right\} \tag{3.58}$$

Now

$$\left.\begin{aligned} R^2 &= x_1^2 + x_2^2 + x_3^2 = k^2\alpha^2[1 + \frac{1 - \beta^2}{\alpha^2}] \\ R &\sim k\alpha \qquad \text{as } \alpha \to \infty \end{aligned}\right\} \tag{3.59}$$

Hence

$$\bar{\Phi} \sim - \frac{c_o k^2 x_3}{3R^3} \quad \text{as } R \to \infty. \tag{3.60}$$

It follows that at large distances from the ellipsoidal bubble, the velocity potential assumes the same form as that of a double source whose axis coincides with the axis of translation $(Ox_3)$, so that the expression for $\bar{\Phi}$ is

$$\left.\begin{aligned} \bar{\bar{\Phi}} &= -\frac{Ua_1^3 e^3 H x_3}{3R^3(S - eH)} = -\frac{\bar{U}x_3}{R^3}, \text{ say,} \\ \text{where} & \\ \bar{U} &= \frac{Ua_1^3 e^3 H}{3(S - eH)} . \end{aligned}\right\} \tag{3.61}$$

From the definition of oblate spheroidal coordinates (3.41), it is a simple matter to show that

$$\beta \sim \cos\theta \qquad \text{as } R \to \infty. \tag{3.62}$$

Consequently, on the surface $\Sigma$ the coordinates of a point, the components of the unit outward normal $\hat{\underline{N}}$, and the element of surface area $d\Sigma$ are,

$$\left.\begin{aligned} & x_1 = R\sin\theta\cos\gamma,\ x_2 = R\sin\theta\sin\gamma,\ x_3 = R\cos\theta \\ & N_1 = \sin\theta\cos\gamma,\ N_2 = \sin\theta\sin\gamma,\ N_3 = \cos\theta \\ & \qquad d\Sigma = R^2 \sin\theta\, d\theta d\gamma, \\ & \qquad \text{as } R \to \infty. \end{aligned}\right\} \tag{3.63}$$

The resultant velocity q and its radial and transverse components are given by

$$\left.\begin{aligned} & q^2 = q_R^2 + q_\theta^2, \\ & q_R = \frac{\partial\Phi}{\partial R} \quad , \quad q_\theta = \frac{1}{R}\frac{\partial\Phi}{\partial\theta} \end{aligned}\right\} \tag{3.64}$$

Now from (3.61) and (3.64) one gets

$$q^2 = \frac{\bar{U}^2}{R^6}(1 + 3\cos^2\theta), \tag{3.65}$$

so that

$$(\text{Velocity}) \sim \frac{1}{R^3} \text{ as } R \to \infty. \tag{3.66}$$

An immediate result of this is that the tensors in (3.24) and (3.27)

$$L'_{ij} = T'_{ij} = 0 \text{ for all } i,j; \tag{3.67}$$

bearing in mind that

$$\bar{\Phi} \sim \frac{1}{R^2}, \text{ as } R \to \infty. \tag{3.68}$$

On evaluating the tensors $M'_{ij}$ in (3.33) and $Q'_{ij}$ in (3.35) one gets

$$\left.\begin{aligned} M'_{11} &= M'_{22} = \frac{2\Gamma e^3}{15(S - eH)}, \\ M'_{33} &= \frac{8\Gamma e^3}{45(S - eH)}, \\ M'_{ij} &= 0, \; i \neq j; \end{aligned}\right) \tag{3.69}$$

and

$$\left.\begin{aligned} Q'_{11} &= Q'_{22} = 0, \\ Q'_{33} &= \frac{2\Gamma e^3}{9(S - eH)}, \\ Q'_{ij} &= 0, \; i \neq j. \end{aligned}\right) \tag{3.70}$$

Consider next the evaluation of the tensor $R_{ij}$ in (3.8). Because the body is moving and $\Sigma$ is fixed the motion near $\Sigma$ is not strictly steady and we must use the unsteady form of Bernoulli's equation

$$\frac{\partial \bar{\Phi}}{\partial t} + \frac{1}{2} q^2 + \frac{P}{\rho} = 0. \tag{3.71}$$

Now as $R \to \infty$, $\bar{\Phi} \to \bar{\bar{\Phi}}$ and the $q^2$ term in (3.71) will not contribute to the integral in (3.8), so that we may take (3.71) to be

$$P = - \rho \frac{\partial \bar{\bar{\Phi}}}{\partial t}. \tag{3.72}$$

The evaluation of $\frac{\partial\overline{\overline{\Phi}}}{\partial t}$ offers no special difficulties. It only requires a simple geometrical consideration. We realize that the origin O is in motion along the axis of the bubble, so that only the $x_3$ coordinate of a point P (fixed in space) will be time dependent. This leads to the relations

$$\left.\begin{aligned} R \sin\theta &= \text{const.} \\ R\cos\theta &= -Ut + \text{const.} \end{aligned}\right) \qquad (3.73)$$

Using the expression

$$\frac{\partial\overline{\overline{\Phi}}}{\partial t} = \frac{\partial\overline{\overline{\Phi}}}{\partial R}\frac{\partial R}{\partial t} + \frac{\partial\overline{\overline{\Phi}}}{\partial \theta}\frac{\partial \theta}{\partial t},$$

one finally gets

$$\frac{\partial\overline{\overline{\Phi}}}{\partial t} = \frac{U\overline{U}}{R^3}(1 - 3\cos^2\theta), \qquad (3.74)$$

and from (3.72)

$$P = \frac{\rho U\overline{U}}{R^3}(3\cos^2\theta - 1). \qquad (3.75)$$

On substituting from (3.75) and (3.61) into (3.8), the components of the tensor $R_{ij}$ are found to be

$$\left.\begin{aligned} R_{11} &= R_{22} = -\frac{4\Gamma e^3}{45(eH-S)} \\ R_{33} &= \frac{8\Gamma e^3}{45(eH-S)} \\ R_{ij} &= 0 \qquad i \neq j, \end{aligned}\right) \qquad (3.76)$$

so that $R_{ij}$ is also a symmetric tensor.

The remaining tensors in equation (3.37) are all integrals which are to be evaluated on the surface S of the spheroid. However the tensor $K_{ij}$ in (3.14) may easily be evaluated with the help of the divergence theorem, in the following manner

$$K_{ij} = P_g \int_S x_j \, dS_i$$

$$= P_g \int_V \frac{\partial}{\partial x_i} (x_j) \, dV$$

$$= P_g V_b \delta_{ij} \tag{3.77}$$

where

$$V_b = \frac{4}{3}\pi a_3 a_1^2 \tag{3.78}$$

is the volume of the bubble.

By using the method developed by Rosenkilde (1967,b) we can evaluate the tensors $C_{ij}$, $T_{ij}$ and $Q_{ij}$ in (3.12), (3.26) and (3.34) respectively. Some length algebra, (see appendix (3A)), leads to

$$\left.\begin{aligned} C_{11} &= C_{22} = \frac{\pi\sigma a_1^2}{2e^3} [e(1 + e^2) - H^4 \tanh^{-1} e ], \\ C_{33} &= \frac{\pi\sigma a_1^2 H^2}{e^3} [(1 + e^2) \tanh^{-1} e - e ], \\ C_{ij} &= 0, \ i \neq j; \end{aligned}\right) \tag{3.79}$$

$$\left.\begin{aligned} T_{11} &= T_{22} = \frac{\Gamma(e - HS)[(3e - e^3)H - 3H^2S]}{3e^2(eH - S)^2}, \\ T_{33} &= \frac{2\Gamma(e - HS)[3eH - (3 - 2e^2)S]}{3e^2(eH - S)^2} \\ T_{ij} &= 0 \quad i \neq j; \end{aligned}\right) \tag{3.80}$$

and

$$\left.\begin{aligned} Q_{11} &= Q_{22} = 0, \\ Q_{33} &= -\frac{2\Gamma(e - SH)}{3(S - eH)}, \\ Q_{ij} &= 0, \ i \neq j. \end{aligned}\right) \tag{3.81}$$

Now using the summation over repeated indices, the tensor $L_{ij}$ in (3.23) may be written in the form

$$L_{ij} = -\frac{1}{2}\int_S \rho x_j u_i \underline{u}.\underline{\hat{n}}\, dS. \tag{3.82}$$

Similarly the tensor $M_{ij}$ in (3.32) becomes

$$M_{ij} = -\frac{1}{2}\int_S \rho x_j u_i \underline{U}.\underline{\hat{n}}\, dS. \tag{3.83}$$

But

$$\underline{u}.\underline{\hat{n}} = \underline{U}.\underline{\hat{n}} \text{ on } \alpha = \alpha_o; \tag{3.84}$$

it follows that

$$L_{ij} = M_{ij}. \tag{3.85}$$

It is therefore not necessary to evaluate these tensors since they cancel each other in the tensor virial equation (3.37). This completes the evaluation of the tensor quantities appearing in this equation. In particular since it has been found that all the tensors are diagonal , and $L'_{ij}$, $T'_{ij}$ are identically zero, equation (3.37) reduces to

$$\begin{aligned} 0 &= 2T_{ii} + 2N_{ii} + 2R_{ii} + 2M'_{ii} + 2Q_{ii} \\ &\quad + 2Q'_{ii} - 2C_{ii} + (P_g V_b + \Pi)\cancel{\delta_{ij}}, \end{aligned} \tag{3.86}$$

where use has been made of equations (3.77) and (3.85). Equation (3.86) provides a set of three equations (i = 1,2,3). Writing these explicitly one gets

$$\begin{aligned} 0 &= 2T_{11} + 2N_{11} + 2R_{11} + 2M'_{11} + 2Q_{11} \\ &\quad + 2Q'_{11} - 2C_{11} + (P_g V_b + \Pi), \end{aligned} \tag{3.87}$$

$$0 = 2T_{33} + 2N_{33} + 2R_{33} + 2M'_{33} + 2Q_{33}$$

$$+ 2Q'_{33} - 2C_{33} + (P_g V_b + \Pi), \tag{3.88}$$

where the equation for i = 2 has been eliminated since it is identical with the first one. Now eliminating the unknown constant $(P_g V_b + \Pi)$ from (3.87) and (3.88) and substituting for each element its corresponding value from the above equations, one gets

$$W = \frac{2H^{1/3}(S-eH)^2[(3e-e^3) - (1-e^2)(3+e^2)\tanh^{-1}e\,]}{e^4(3S - 2Se^2 - 3He)} \tag{3.89}$$

or in terms of the axis-ratio x,

$$W = \frac{2x^{-7/3}(hx^2-g)^2[gx(3x^2-g^2) - (3x^2+g^2)\tanh^{-1}(g/x)\;]}{g^4(3hx^2 - 2hg^2 - 3g)} \tag{3.90}$$

where

$$g = \sqrt{x^2 - 1}\;; \quad h = \sec^{-1}x, \tag{3.91}$$

and

$$W = \frac{2r_e \rho U^2}{\sigma} \tag{3.92}$$

is the Weber number based on $r_e$, the equivalent spherical radius for the bubble.

The above expression for W in terms of the axis-ratio constitutes the main result of this chapter. Another useful result is the expression for the gas pressure $P_g$, which may be obtained from the contracted form of the virial equation (3.86). The trace of this equation is

$$0 = 2(T + N + R + M' + Q + Q' - C) + 3(P_g V_b + \Pi) \tag{3.93}$$

Considering the value of each quantity, from the preceding results, one finds

$$N = R = 0, \tag{3.94}$$

and,

$$M' + Q + Q' = \tfrac{1}{2}\rho V_b U^2. \tag{3.95}$$

Therefore equation (3.93) reduces to

$$0 = T + \tfrac{1}{2}\rho V_b U^2 - C + \tfrac{3}{2}(P_g V_b + \Pi). \tag{3.96}$$

This represents the scalar form of the virial theorem appropriate for a gaseous bubble rising in an infinite liquid. Here, we recall that T is the kinetic energy of the liquid, $\Pi$ is the microscopic energy of the liquid particles, C is the surface energy and $V_b$ is the volume of the bubble. The expressions for T, C, and $V_b$ are found from equations (3.80), (3.79) and (3.78), respectively. The integral (3.9) for $\Pi$ is evaluated in appendix (3B). Substituting for these quantities in equation (3.96) one obtains the expression

$$P_g = \frac{2[gx + \tanh^{-1}(g/x)]}{gWx^{1/3}} + \frac{[3hx^3 + 2g^3(1 - x) - 3gx^3]}{6(hx^3 - gx)} \tag{3.97}$$

for the dimensionless gas pressure, $P_g$, in terms of the axis-ratio x and the Weber number W, and where g and h are given by equation (3.91).

## 4. Conclusions

On expanding the expression (3.90) as $x \to 1$ (i.e. neglecting $W^2$), one finds

$$x = 1 + \frac{9}{64} W, \tag{3.98}$$

which agrees with the analytic theory. Thus the exact solution is an oblate ellipsoid if $W^2$ is neglected.

The series solution, using the method of accelerating convergence, is compared with the virial theory in Figure 3.3. The maximum difference between the two curves is only 5% up to axis-ratio 3. This is very gratifying in view of the fact that the method of accelerating convergence is known to bring about a considerable improvement in the accuracy.

Let us now compare the virial theory with the "Two-point Theory". It has already been shown that the leading terms in both theories are identical and the exact solution is an oblate ellipsoid if $W^2$ is neglected. Consider now Figure 3.4 in which the theory of accelerating convergence, the virial theory, and the "Two-point Theory" are represented. One finds that for $x = 2$ the difference in the latter two theories is 1.4%, for $x = 3$, 6.2%, and for $x = 4$, 11.6%. One may be tempted to assume that the difference between them is an indication of the error involved in the spheroidal approximation. This may not be the case in view of the simplifying assumptions made in both theories. However, Moore (1965) has shown that his "Two-point Theory" is reliable up to $x = 2$. This at least ensures that either of these theories is not far from the exact one, up to $x = 2$.

One fact that emerges from Figure 3.4 is that, up to $x = 2.5$, the theory of accelerating convergence is closer to the virial than the "Two-point Theory". It seems therefore that, up to $x = 2.5$, the virial theory is closer to the exact one than the "Two-point Theory" is. This is likely to be the case since the theory of accelerating convergence may be expected to be more accurate than the other theories up to this value of x.

Further examination of Figure 3.3 shows that there is a maximum Weber number of 3.271 at $x = 3.72$ in the virial theory, as compared to 3.745 at $x = 6.0$ in the "Two-point Theory". Although the latter result is well outside the range of validity of the "Two-point Theory" approximation, it is striking that the virial theory exhibits the same sort of behaviour, though at a smaller axis-ratio of 3.72. This seems to support Moore's conjecture that "there is a maximum Weber number of ... above which the symmetric shape is impossible".

Finally we use the method of direct assessment adopted by Moore (1965). Basically, one has to find an expression for the error arising from the fact that the boundary condition, that the sum of the dynamic pressure and the surface tension pressure is constant on the bubble surface, cannot be satisfied exactly, at every point, on the surface of the bubble. A convenient measure of this error is the fractional change in the first curvature necessary to make the above condition satisfied at every point on the surface. Moore gave an estimate of the maximum percentage error   for the "Two-point Theory".

In Figure 3.5 these calculations are extended by giving the percentage error for different axis-ratios and at different points on the surface of the bubble. In Figure 3.6 the curves corresponding to the virial theory, using the same technique as before , are traced. This set of curves indicates that the virial theory is more accurate than the "Two-point Theory", whose corresponding curves are traced in Figure 3.5. It also shows that in the virial method, the boundary condition is, in essence, satisfied on a mean surface, thus using an averaging process.

The virial theory being so good, suggests that a perturbation to the shape, using the results offered by the virial theory, might give a very accurate solution.

# CHAPTER IV

## SLIGHTLY DISTORTED ELLIPSOIDAL BUBBLES

### 1. Introduction

It has been seen that for small values of the Weber number ($W < \frac{1}{10}$) the bubble will deform into an oblate spheroid. This suggests that when we examine larger distortions we should take as our starting point the oblate spheroid. Even for Weber numbers of $O(1)$ the bubble might be expected not to be too different in shape from an oblate spheroid of the same axis-ratio.

The system of coordinates suitable for the present formulation is that of oblate spheroidal coordinates $(\alpha,\beta,\gamma)$ which has been discussed in the preceding chapter.

Unfortunately it is not possible to adopt the method of Chapter II in this section. The difficulty arises from the fact that the perturbed first curvature for an ellipsoidal surface is an irrational function of $\beta$. This means that Legendre polynomials of all orders enter at the first stage of the iteration.

Precisely as in Chapter II, it is assumed that a bubble having a prescribed volume $V$ is placed in a uniform stream $U$. The bubble is surrounded by an infinite incompressible fluid which is moving irrotationally. Further assumptions regarding viscosity $\mu_o$, the gas pressure $P_g$, and motion of the gas, also carry throughout. The notation of Chapter III, unless otherwise stated is applicable here. Also the expressions representing the physical parameters e.g. $W$, $R$,...etc., remain unaltered.

The first part of this chapter explains, briefly, the reason for the divergence of the perturbation method of Chapter II. Failure of the theory is predicted at an axis-ratio $x = \sqrt{2}$, due to an improper representation of the velocity field at this value. There is a remarkable analogy between this problem and that of a two-dimensional motion of an ellipse. This is because in the latter problem, the velocity field diverges at precisely the same axis-ratio, $x = \sqrt{2}$.

The main part of this chapter deals with two problems having a common principle underlying their methods of approach. This is basically the selection of an ellipsoid $\alpha = \alpha_o$ which is closest to the true shape of the bubble.

In the first problem, an approximate method based on the hypothesis that the true shape of the bubble will differ little from an ellipsoid $\alpha_o$ having the same value, is devised. In view of this assumption, it is plausible to use the flow field about $\alpha_o$ in order to determine the dynamic pressure on the surface of the true shape. Two cases are considered:

(a) in which the Weber number, and consequently $\alpha_o$, are given by the "Two-point Theory".

(b) W and $\alpha_o$ are given by the virial theory.

The second problem examines the effect of gravity, as well as surface tension, on the shape of the bubble. The formulation of the problem resembles the case of surface tension alone. The shape of the bubble is obtained by perturbing an ellipsoid $\alpha_o$ assuming that the flow field about the true shape is the same as that about $\alpha_o$. This leads to a differential equation in terms of the Froude number, which is unknown. This difficulty is resolved by expressing the Froude number in terms of the drag on the ellipsoid $\alpha_o$, and this is a known quantity. The numerical solution of the differential equation is then accomplished using a similar procedure to that of the "symmetric case", of surface tension. The problem is solved for different values of the M number. The shapes of bubbles for both the "symmetric case" and the case of gravity are traced in comparison with the ellipsoids $\alpha_o$. Theoretical curves for the drag coefficient are plotted. Also comparisons are given with some experimental results.

Before considering these problems in detail, let us first introduce the velocity field in oblate spheroidal coordinates and compare it with its counterpart in spherical polar coordinates.

2. The velocity field

In oblate spheroidal coordinates Laplace's equation

$$\nabla^2 \Phi = 0, \tag{4.1}$$

where $\Phi$ is the velocity potential, takes the form

$$\frac{\partial}{\partial\alpha}(L \frac{\partial\Phi}{\partial\alpha}) + \frac{\partial}{\partial\beta}(E \frac{\partial\Phi}{\partial\beta}) + (\frac{1}{E} - \frac{1}{L})\frac{\partial^2\Phi}{\partial\gamma^2} = 0, \tag{4.2}$$

where L and E are as defined in Chapter III. Using the method of separation of variables, a fundamental solution of (4.2) which is symmetrical about the axis of revolution and is appropriate to the region outside a spheroid of the family $\alpha = \alpha_o$ (const.) is given by

$$\Phi = \sum_{n=o}^{\infty} b_n P_n(\beta) q_n(i\alpha). \tag{4.3}$$

Here $b_n$ are complex constants, $P_n(\beta)$ are Legendre functions of the first kind while $q_n(i\alpha)$ are those of the second kind. For the properties of these functions see appendix (4A).

The expressions for the normal and tangential components of the velocity are

$$u_n = \frac{1}{h_\alpha}\frac{\partial\Phi}{\partial\alpha}; \qquad u_t = \frac{1}{h_\beta}\frac{\partial\bar{\Phi}}{\partial\beta}, \tag{4.4}$$

respectively.

For an ellipsoid $\alpha_o$ in a uniform stream U, parallel to its axis of revolution, the expression for the slip velocity $u_\beta^{(o)}$ is readily calculated in the form

$$u_\beta^{(o)} = \frac{Uc_o E^{1/2}}{L_o D^{1/2}}, \tag{4.5}$$

where

$$c_o = 1/(\cot^{-1}\alpha_o - \frac{\alpha_o}{L_o}). \tag{4.6}$$

We now hope to throw some light on the cause of divergence in the systematic perturbation method of Chapter II. To proceed, we assume that $\alpha_o$ is large and consider the expansion of $u_\beta^{(o)}$ in powers of $\alpha_o^{-1}$. There is no difficulty in obtaining the formal expansion, however, it is only valid for $\alpha_o > 1$. At $\alpha_o = 1$, the main source of trouble is going to be the series expansion for $\cot^{-1}\alpha_o$ which occurs in (4.6). This is best illustrated by the following quotation from Van Dyke (1964) p.202 "... the numerical series

$$\pi = 4(1 - \frac{1}{3} + \frac{1}{5} - \frac{1}{7} + \ldots)$$

which converges, but with painful slowness..., and 400,000 terms would be required for six-figure accuracy." It is rather dismaying to find from the relation

$$x = \sqrt{(1 + \alpha_o^2)} / \alpha_o, \tag{4.7}$$

that at this value of $\alpha_o$ the corresponding axis-ratio is only $\sqrt{2}$. This explains why the series method, of Chapter II, breaks down at an early stage in the perturbation. The origin of the term $\cot^{-1}\alpha_o$ is the $q_n(i\alpha)$'s in the velocity potential (4.3), see appendix (4A). Thus the dependence of the velocity term on the expansion of $\cot^{-1}\alpha_o$ shows that the velocity field is improperly represented, due to the requirement of an infinitely large number of terms before one gets a reasonable degree of accuracy.

It is interesting to note that the same sort of behaviour occurs in the two-dimensional motion of an ellipse. This treatment is given in Van Dyke (1964) pp. 50-52. He shows that the formal expansion of the velocity is only justified for $x < \sqrt{2}$. This confirms the above result and makes evident the source of trouble in both the two and three-dimensional theories.

### 3. Mathematical formulation

A bubble of prescribed volume V is placed in a uniform stream U parallel to its axis of revolution, see Figure 4.1. The bubble is surrounded by an infinite incompressible fluid which is moving irrotationally. The motion of the gas, inside the bubble, whose constant pressure is $P_g$, is assumed to be negligible. The system of oblate spheroidal coordinates $(\alpha,\beta,\gamma)$ is used. The shape of the bubble is represented by the surface of revolution

$$G = \alpha - \alpha_o - g(\beta) = 0, \tag{4.8}$$

where $\alpha = \alpha_o$ is the ellipsoid which has the same volume as the exact shape and is closest to it in some sense. We will call this the "basic ellipsoid". In the subsequent approximate theory, $\alpha_o$ is given by either the "Two-point Theory" or the virial theory.

Thus we seek a gas pressure $P_g$, a constant $\alpha_o$ and a continuous function $g(\beta)$ such that

(a) $P_S - \frac{1}{2} u_t^2 + J\sigma = P_g$

(b) Volume of $G = V$,

where in (a), J is the first curvature in oblate spheroidal coordinates, for the surface (4.8), and $u_t$ is the slip velocity. The derivation of J proceeds on the same lines as the corresponding one in spherical polar coordinates, in Chapter II. Following the same steps in appendix (2A) one obtains

$$J = \frac{kH}{[D(L + E\dot{g}^2)]^{3/2}} \tag{4.9}$$

where

$$H = \{L(2L - E)\alpha + L(2L - 3E)\beta\,\dot{g}$$

$$- ELD\ddot{g} + (3L - 2E)\alpha E\dot{g}^2 + E(L - 2E)\beta\dot{g}^3\}. \tag{4.10}$$

The size of the bubble enters the above equations through k and it will be convenient to remove this dependence by introducing the equivalent spherical radius $r_e$. Since the basic ellipsoid is chosen to have the same volume as the true shape

$$r_e = k(\alpha_o L_o)^{1/3}. \tag{4.11}$$

Then if

$$W = 2r_e\rho U^2/\sigma\ , \tag{4.12}$$

the above boundary condition (a) can be written in the form

$$2\Delta P + \frac{4(\alpha_o L_o)^{1/3}}{W} J = u_t^2, \tag{4.13}$$

where

$$\Delta P = P_S - P_g. \tag{4.14}$$

The expression (4.9) for the first curvature is now

$$J = \frac{H}{[D(L + E\dot{g}^2)]^{3/2}}\ , \tag{4.15}$$

where H is given by (4.10).

Consider now the surface (4.8), for small g, such that

$$\alpha = \alpha_o + g(\beta) + O(g^2). \tag{4.16}$$

Substituting for this in (4.15) leads to

$$J = J_o + \bar{J} + O(g^2), \tag{4.17}$$

where

$$J_o = \frac{(2L_o - E)\alpha_o}{L_o^{1/2} D_o^{3/2}} \tag{4.18}$$

is the first curvature for the ellipsoid $\alpha_o$

and

$$\bar{J} = \frac{1}{L_o^{3/2} D_o^{5/2}} [L_o D_o (2L_o - 3E)\beta \dot{g} - L_o D_o^2 E \ddot{g}$$

$$+ (-2L_o^3 + 4L_o^2 - L_o^2 E - 2L_o E + E^2) g ] \quad + O(g^2). \tag{4.19}$$

Similarly the slip velocity $u_t$ corresponding to the surface (4.16) may be written in the form

$$u_t = u_\beta^{(o)} + u_\beta^{(1)} + \ldots \tag{4.20}$$

where $u_\beta^{(o)}$ is the slip velocity on the ellipsoidal surface $\alpha_o$ and is given by (4.5). The second term $u_\beta^{(1)}$ represents the velocity perturbation.

Upon substituting from (4.17) and (4.20) into the equilibrium condition (4.13) one finds

$$(\alpha_o L_o)^{1/3}(J_o + \bar{J}) - \frac{W}{4}(u_\beta^{(o)2} + \Lambda)$$

$$= - \frac{W\Delta P}{2} + O(g^2) \tag{4.21}$$

where

$$\Lambda = u_\beta^{(1)2} + 2u_\beta^{(o)} u_\beta^{(1)} + \dots , \tag{4.22}$$

is the velocity perturbation term. Now from Chapter II one recalls that the velocity corrections "lag" one step in the perturbation scheme behind the shape corrections. To apply this in the present case, one requires the condition that

$$\Lambda W \sim O(g^2) \tag{4.23}$$

If this is satisfied, then equation (4.21) reduces to

$$(\alpha_o L_o)^{1/3}(J_o + \bar{J}) - \frac{W}{4} u_\beta^{(0)2} = - \frac{W\Delta P}{2} + O(g^2). \tag{4.24}$$

This is the basis of the approximate method which we shall introduce in the next section.

## 4. Linearized Two-point Theory

We now realize that even if it were practical to obtain all the terms in a perturbation scheme based on $\alpha_o^{-1}$, this would necessarily fail at $\alpha_o = 1$, $(x = \sqrt{2})$. To avoid this difficulty, we have devised an approximate method based on the hypothesis that the true shape of the bubble will differ little from the "basic ellipsoid". If this is so, we can use the flow field about this ellipsoid to determine the dynamic pressure on the surface of the true shape. Then the equilibrium condition (4.24) becomes a differential equation for g which is solved numerically.

Upon substituting from (4.19) into (4.24) one gets

$$A(\beta,x)\ddot{g} + B(\beta,x)\dot{g} + C(\beta,x)g \;=\; F(\beta,x)$$

$$+ a(x) + O(g^2), \tag{4.25}$$

which is a linear second-order non-homogeneous differential equation in g. The function $F(\beta,x)$ is given by

$$F(\beta,x) = \frac{W}{4}\, u_\beta^{(0)2} - (\alpha_o L_o)^{1/3}\, J_o(\beta) - \frac{W}{2}\Delta P, \tag{4.26}$$

stressing the dependence of $J_o$ on $\beta$.

The "Two-point Theory" described above is equivalent to choosing W so that

$$F(0,x_o) \;=\; F(1,x_o) = 0. \tag{4.27}$$

Thus if we pick our closest ellipsoidal approximation in this way, equation (4.26) can be rewritten in the form

$$F(\beta,x) = \frac{W}{4}\, u_\beta^{(0)2} + [J_o(1) - J_o(\beta)]\; (\alpha_o L_o)^{1/3} \tag{4.28}$$

The constant a(x) in equation (4.25) is a correction term for $\Delta P$ in (4.26), due to the surface perturbation, and it varies with the axis-ratio x. The coefficients A, B and C in (4.40) are given by

$$\left.\begin{aligned}
A(\beta,x) &= -\frac{E(\alpha_o L_o)^{1/3}}{(D_o L_o)^{1/2}}\,, \\
B(\beta,x) &= \frac{\beta(2L_o - 3E)(\alpha_o L_o)^{1/3}}{D_o^{\;3/2} L_o^{\;1/2}} \\
C(\beta,x) &= \frac{1}{D_o^{5/2}\; L_o^{3/2}}(-2L_o^3 + 4L_o^2 - L_o^2 E - 2L_o E + E^2)(\alpha_o L_o)^{1/3}
\end{aligned}\right\} \tag{4.29}$$

In particular,

$$A(\pm 1,x) \;=\; B(o,x) = 0. \tag{4.30}$$

Thus for any given value $x = x_o$, the functions A,B,C and F in equation (4.25) are all known, where the corresponding value for W in (4.28) is obtained on substituting for $x_o$ into (1.9). However, the unknown constant a(x) has still to be determined. It is also clear from (4.30) that equation (4.25) has a regular singularity at $\beta = \pm 1$.

It is evident now that equation (4.25) requires three conditions to determine the general solution. To accomplish this, let us utilize the assumption that the bubble has fore and aft symmetry. This implies that the coordinate axes in a meridian section of the bubble Figure 4.1, are normals to the trace of the bubble. In other words,

$$\left.\frac{d\bar{\omega}}{dz}\right|_{\beta=o} = 0 \tag{4.31}$$

and

$$\left.\frac{dz}{d\bar{\omega}}\right|_{\beta=1} = 0, \tag{4.32}$$

where

$$\left.\begin{aligned} \bar{\omega} &= k[(1+\alpha^2)(1-\beta^2)]^{1/2}, \\ z &= k\alpha\beta, \\ \alpha &= \alpha_o + g(\beta). \end{aligned}\right) \tag{4.33}$$

Performing the differentiation in (4.31), with the understanding that $\alpha > 0$, for all $\beta$, the condition is found to be equivalent to

$$\dot{g}(\beta) = 0 \quad \text{at} \quad \beta = 0. \tag{4.34}$$

The latter condition (4.32), for the slope to be zero at the pole, is satisfied by any regular solution of the differential equation (4.25). Therefore we shall impose regularity of the solution at the pole. This leads to, from (4.25) and (4.27),

$$B(1,x)\dot{g}(1) + C(1,x)g(1) = a(x). \tag{4.35}$$

A third condition is necessary in order to determine the unknown constant $a(x)$ in (4.25). Now as the volume of the bubble is to be prescribed, we normalize its value to that of the ellipsoid $\alpha_o$. This is equivalent to the relation

$$\int_0^1 g(\beta)D_o d\beta = 0,$$

The conditions on (4.25) can now be summarized as follows:

$$\left.\begin{array}{lll} (1a) & \dot{g}(\beta) = 0, & \text{at } \beta = 0, \\ (2a) & B(1,x)g(1) + C(1,x)g(1) = a(x), & \\ (3a) & \int_0^1 g(\beta)D_o d\beta = 0. & \end{array}\right) \tag{4.36}$$

Let us now embark on solving the problem numerically. This is accomplished here by using the method described by Fox (1957), Chapter 8. The basic process is to solve the boundary-value problem using an initial-value technique. One starts by solving the problem with some arbitrary initial conditions, combining the solutions to satisfy all the given boundary conditions.

Consider now the non-homogeneous equation (4.25) together with the corresponding homogeneous equation

$$A(\beta,x)\ddot{g} + B(\beta,x)\dot{g} + C(\beta,x)g = 0. \tag{4.37}$$

Denote these equations by I and II respectively Equation I can now be integrated completely with the two point boundary conditions (1a) and (2a). The numerical procedure is as follows:

(1) Guess a value for $a(x)$.

(2) Define $g_I(\beta)$ to satisfy I and such that at $\beta = 1$,

$$\left.\begin{aligned} B(1,x)\dot{g}_I(1) + C(1,x)g_I(1) &= a(x), \\ g_I(1) &= 1. \end{aligned}\right\} \tag{4.38}$$

(3) Define $g_{II}(\beta)$ to satisfy II and such that at $\beta = 1$,

$$\left.\begin{aligned} B(1,x)\dot{g}_{II}(1) + C(1,x)g_{II}(1) &= 0, \\ g_{II}(1) &= 1. \end{aligned}\right\} \tag{4.39}$$

Clearly

$$g(\beta) = g_I(\beta) + tg_{II}(\beta), \tag{4.40}$$

satisfies I and boundary condition (2a). Now choose t such that $g(\beta)$ satisfies boundary condition (1a). This yields

$$t = -\dot{g}_I(o)/\dot{g}_{II}(o). \tag{4.41}$$

(4) Choose a(x) such that (3a) is satisfied. This can be achieved using the following iterative procedure. The integral in (3a) is denoted by y, where y is now a function of a, and so one has to find a value for a such that y vanishes. Suppose that $(a + \delta a)$ is the exact value for which y is zero. Then we have

$$y(a + \delta a) = 0.$$

Expanding this by Taylor's theorem one gets

$$y(a + \delta a) = y(a) + \delta a \frac{dy}{da} + \ldots = 0.$$

$$\therefore \quad \delta a = - y(a)/(\tfrac{dy}{da}). \tag{4.42}$$

Now to calculate dy/da let the initial $\delta a$ be $\delta a_o$. Then

$$\frac{dy}{da} = \frac{y(a + \delta a_o) - y(a)}{\delta a_o}$$

Hence by (4.42) one finds

$$\delta a_1 = - \frac{y(a)}{\dfrac{y(a + \delta a_o) - y(a)}{\delta a_o}},$$

where $\delta a_1$ is the new value for $\delta a$. Thus the general equation used to correct a is

$$\delta a_{n+1} = - y(a_n) \frac{y(a_n + \delta a_n) - y(a_n)}{\delta a_n}, \tag{4.43}$$

where

$$a_{n+1} = a_n + \delta a_n, \tag{4.44}$$

and $a_n$ is the nth approximation to a.

The numerical integration of equation I is carried out using the fourth-order Runge-Kutta method with step width

$$\delta\beta = 0.002. \tag{4.45}$$

Upon reducing $\delta\beta$ to 0.0002, no significant change has been detected in the results. It seems therefore there is no appreciable build up of error resulting from reducing the step width to this value.

The solution is started with a prescribed value of $x = x_o$, say. This fixes the values of $\alpha_o$ and W. Also the coefficients A, B and C together with $J_o$ and $u_\beta^{(o)}$ are computed at the specified number of points on the surface of the bubble, using the value of $x_o$.

In order to start the integration of I, the value of a(x) is required. However, this is not known a priori, in consequence it has to be determined by a trial-and-error solution. A value is guessed for it and the integration is then started from the pole and towards the equator (i.e. along the direction of the flow). In order to force the regularity of the solution at $\beta = 1$, the integration is started a few steps away from $\beta = 1$, precisely at $\beta = 0.996$. This is accomplished by finding the series solution of I in the neighbourhood of $\beta = 1$ and selecting a few terms of the power series of the regular solution. This, however, has been found to have no merits, in this problem, over the case when the integration is started exactly at $\beta = 1$. Both results are found to be identical, to the required degree of accuracy. This result is, otherwise, expected from the fact that the singularity, in equation I, is regular at $\beta = 1$.

An iteration program, using a digital computer, is then started. In each case for a given value of the axis-ratio, $x_o$, the constant $a(x)$ is incremented successively and at each stage the program iterated until convergence has been obtained for the number of decimal places retained for a.

In the iteration process it has been found that to avoid running into a loop of oscillating convergence, it is necessary to add a fraction of $\delta a_n$ at a time instead of the whole increment as in (4.44). The relation that has been employed instead is

$$a_{n+1} = a_n + \frac{2}{5}\,\delta a_n \tag{4.46}$$

This has given rise to an average of about ten iterations necessary to obtain an accuracy of $a(x)$ to three decimal places.

The program required about ten minutes of computer time. It should be noted here that the iterative procedure was set to stabilize three decimal places. By reducing the tolerances in the iteration process and reducing $\delta\beta$, greater accuracy could have been obtained but of course more machine time would have been involved.

The results are tabulated below, Table (1). The shapes of the bubbles are traced in "continuous" line, while those of the corresponding ellipsoids, $\alpha_o$, are in "broken" lines, Figures 4.2-4.3. The curve of W against the corrected axis-ratio, $x_c$, is plotted in Figure 4.6 together with that of the "Two-point Theory".

5. Linearized Virial Theory

We have seen that the virial theory is less in error than the "Two-point Theory", and this suggests we use it as the basis of our approximation.

Now replacing the expression for the Weber number (1.9) by that obtained from the Virial Theory, (3.90), the problem is solved again. The $\Delta P$ in equation (4.25) is absorbed into a(x) so that equation (4.28) is dropped. There are no other modifications required in the numerical scheme.

The results obtained are tabulated below, Table (2). The bubble shapes are traced in Figures 4.4-4.5, in similar manner to that of the previous case. Figure 4.6 gives a comparison between the "Two-point Theory", the virial theory and their linearized versions.

Having studied six different methods for obtaining a relation between the Weber number and the axis-ratio, let us compare these results at some specified axis-ratio. This comparison is shown in Table (3) for x = 1.1. The comparison is restricted to three decimal places since the linearized theories are accurate to this order. It is apparent that the Weber numbers for the linearized theories are closer to that of the "accelerated convergence" method, than their initial values are. This tendency is in agreement with the view that the "accelerated convergence" result is supposed to be closer to the exact theory for this range of W, and thus justifying this sort of behaviour. Also the series solution indicates its tendency to diverge even at such a relatively small value of W, bearing in mind that terms of $O(W^4)$ are neglected.

## 6. The effect of gravity

Hitherto, our investigations were confined to motions which take no account of gravity effect. This section is devoted to examining the effect of gravitational forces, in the presence of surface tension, on a rising bubble.

Gravity forces become significant when the hydrostatic pressure is comparable with the hydrodynamic pressure, i.e.

$$\rho g^* r_e \sim \rho U^2$$

where $g^*$ is the acceleration due to gravity. Now in steady state the drag force = buoyancy force, i.e.

$$\frac{1}{2}\rho U^2 \pi r_e C_D = \frac{4}{3}\pi r_e{}^3 \rho g^*$$

or

$$C_D = \frac{8g^* r_e}{3U^2}, \tag{4.47}$$

where $C_D$ is the drag coefficient. It is now apparent that gravity becomes important when $C_D$ is of $O(1)$.

We now proceed to extend the above numerical method by introducing gravity as well as retaining the surface tension forces. Apart from minor modifications, the method is practically the same as that for surface tension alone. In the present case Bernoulli's equation is

$$P + \frac{1}{2}\rho(u_\alpha^2 + u_\beta^{(o)2}) + \rho g^* h = \text{const.}, \tag{4.48}$$

where h is the length indicated in Figure 4.7. Substituting for h from the figure and absorbing the constant L in the right-hand side, (4.48) becomes, on the surface of the bubble,

$$P + \frac{1}{2}\rho u_\beta^{(o)2} - \rho g^* z = \text{const.} \tag{4.49}$$

Now taking the surface of the bubble as in (4.16) and assuming that it has the same velocity field as that of the unperturbed ellipsoid $\alpha_o$, one gets in the dimensionless form, the equation

$$\left.\begin{aligned} &A(\beta,x)\ddot{g} + B(\beta,x)\dot{g} + C(\beta,x)g = \\ &F(\beta,x) - \frac{WZ}{r_e F_r} + \text{const.}, \end{aligned}\right\} \tag{4.50}$$

where the Froude number $F_r$ is defined by

$$F_r = \frac{U^2}{2r_e g^*} \tag{4.51}$$

Equation (4.50) is similar to (4.25), with the terms having the same meaning. Now for a point on the surface of the bubble

$$z = \alpha\beta = \alpha_o\beta + \beta g(\beta) + O(g^2), \tag{4.52}$$

in dimensionless form. Combining equations (4.50) and (4.52) one gets on the surface of the bubble

$$A(\beta,x)\ddot{g} + B(\beta,x)\dot{g} + C(\beta,x)g = \overline{F}(\beta,x) + \overline{a}(x), \tag{4.53}$$

where

$$\bar{C} = C(\beta,x) + \frac{\beta W}{F_r r_e}, \qquad \text{and} \qquad \bar{F}(\beta,x) = F(\beta,x) - \frac{\alpha_o \beta W}{F_r r_e}, \tag{4.54}$$

with $\bar{a}(x)$ playing the same role as $a(x)$ in equation (4.25).

The Froude number, which appears in equation (4.50), remains to be determined. This is obtained from the unperturbed theory. From equations (4.47) and (4.51) one obtains the relation

$$F_r = \frac{4}{3C_D}, \tag{4.55}$$

so that we may also assert that for $F_r$ of $O(1)$, gravity forces come into play.

Consider now the physical parameters

$$M = \frac{g^* \mu_o^4}{\rho\sigma^3}, \quad R = \frac{2r_e \rho U}{\mu_o} \quad \text{and} \quad W = \frac{2r_e \rho U^2}{\sigma} \tag{4.56}$$

where M is the M-number, responsible for the physical properties of the fluid. From equations (4.47) and (4.56) one finds the relation

$$C_D = \frac{4}{3} M R^4 W^{-3}. \tag{4.57}$$

Now availing ourselves with the expression (2.71), for $C_D$, obtained by Moore (1965), it will be possible to find $F_r$ and R for any ellipsoid whose axis-ratio is known. This is accomplished by prescribing values for M and x. Then W may be found from (1.9), or (3.90), in case of the virial theory. The corresponding value for G(x) in (2.72) is also determined. Combining equations (2.72) and (4.57) one finds

$$R = \left(\frac{36W^3G(x)}{M}\right)^{1/5} , \qquad (4.58)$$

which determines the value of the Reynolds number. It is then a simple matter to determine $C_D$ and $F_r$.

Having found the necessary parameters, we now proceed to the numerical solution of equation (4.53). This resembles that of equation (4.25). One starts by a given ellipsoid $\alpha_o$ whose axis-ratio is $x_o$. The M-number is selected to run through the values $10^{-10}$, $10^{-11}, \ldots, 10^{-16}$, the problem being solved for each of these numbers. Knowing $x_o$ and M, one determines $r_e$, W,G(x), R,$C_D$,$F_r$ and U, where the expression used for W may be obtained from either the "Two-point Theory" (1.9) or the virial theory (3.90). It is important to notice that in our procedure the Weber number is the key parameter and once it is specified, the rest of the parameters including the shape of the bubble are determined. However, as we have seen that the virial theory is less in error than the "Two-point Theory", we shall only trace the shapes arising from the virial theory.

Apart from the fact that the numerical integration now runs from the forward stagnation point to the rear stagnation point, the other steps and assumptions are all applied as in the symmetric case. The shapes of the bubbles are traced in "continuous" lines while those of the ellipsoids, $\alpha_o$, are in "broken" lines, Figures 4.8-4.14. The results are tabulated below, Table (4). In Figure 4.15 a family of curves are drawn, showing the variation of the Weber number with the axis-ratio, for different M-numbers. These are compared with the curve W(x) representing the virial theory (symmetric case). It is apparent that for bubbles having the same axis-ratio, the effect of gravity is less pronounced as the M-number decreases. In other words departures from symmetric shapes are smaller. It may be remarked that the corrected axis-ratio, $x_c$, for cases of large dents at the rear of the bubble is considerably exaggerated. It is only meaningful when the rear of the bubble is nearly flat.

It is a simple matter to calculate the values of R, $C_D$ or $F_r$, corresponding to $x_o$ in Table (3), using their relevant expressions. The variation of $C_D$ with R, for different M-numbers, is shown in Figure 4.16. The results indicate a minimum of $C_D$ at W $\doteq$ 1.91, corresponding to $x_o$ = 1.44. Similar computations using the "Two-point Theory", gave a minimum value of $C_D$ at the same value for $x_o$ but at a Weber number of 1.92. Moore (1965) included the effect of boundary-layer in computing $C_D$, and R and obtained a result similar to ~~while using~~ an empirical result of Peebles and Garber (1953), ~~to calculate R~~. He found that the minimum of $C_D$ occurs at $W \doteq 1.8$. Other features predicted by his theory are also observed in the present one. It seems to support his speculations that "... the drag coefficient is not very sensitive to the shape of the bubble once the axis-ratio is fixed,...". Again the theory predicts the rise of $C_D$, with R, after reaching its minimum value but not so sharply pronounced as in Moore's theory. This is probably because boundary-layer effects have not been included in the present work.

## 7. Comparison with experiment

The most extensive experimental results with which we can compare the theoretical predictions are those of Haberman and Morton (1953). Comparisons are also made with recent experimental results of Jones (1965) and Schwerdtfeger (1968). The theory is tested by comparing its predictions of the velocity of rise as a function of $r_e$. An attempt is also made to compare the shapes of bubbles. The results are tabulated below, Tables (5) - (8). The shapes of bubbles are also traced, in the previous manner, in Figures 4.20-4.22. Plots of U as a function of $r_e$ for air bubbles in methyl alcohol and in water, and for argon bubbles in mercury are shown in Figures 4.17-4.19. Reasonable agreement is found between theory and experiment. Comparison of the theory for water shows a slightly higher value for U than the corresponding experimental values of Haberman and Morton (1953). Also the maximum value of U occurs at a larger $r_e$ than that given by experiment. Moore (1965) noticed such discrepancy in comparing his theory for methyl alcohol with Haberman and Morton's experimental curve. The present theory for methyl alcohol reveals similar features. In particular it is also observed that for $x > 2$ reasonable agreement between theory and experiment still exists. It is interesting to note that the virial theory gives, for all three liquids, a maximum value of U at an axis-ratio $x_o = 1.9$ with a corresponding value of $W \doteqdot 2.70$. Similar calculations using the "Two-point Theory" give $x_o = 1.9$ and $W \doteqdot 2.73$, correspondingly. It seems therefore that, for low M liquids, the axis-ratio x is a crucial parameter in the sense that, once it is fixed, it is possible to determine the drag coefficient and the velocity of rise irrespective of the bubble shape. It is necessary to make further investigations on this point, in view of the fact that the present theory does not account for the presence of boundary-layer on the bubble.

Comparison of the theory with the experimental results of Schwerdtfeger (1968) for the rise of argon bubbles in mercury, shows fair agreement. It seems that consistent experimental investigations are necessary in the region where U is increasing to its maximum value, as $r_e$ increases. This is a regime dominated by laminar flow and information about it is of considerable value for comparison with experimental and theoretical results.

The size of bubbles dealt with in this work are of the order of a few millimetres. It is therefore not surprising that experimenters find it rather difficult to obtain clear photographs of such bubbles. Haberman and Morton (1953) give photographs of air bubbles in water and in methyl alcohol. Also Jones (1965) gives a photograph of air bubbles in water. The present theoretical shapes, Figures 4.20 - 4.21 are several hundreds times larger than the experimental shapes, which do not exceed the size of a dot in some cases. It seems desirable, therefore, to do more experiments with a view to obtaining enlarged photographs. Figure 4.22 shows the shapes of argon bubbles in mercury. The problem of vision is another handicap facing the experimenter who wants to photograph three-dimensional bubbles in liquid metals. It is thereforenot easy to make comparison between theoretical and experimental shapes, in such cases.

The bubble shapes in Figures 4.20-4.22 are characterized by a dent at the rear stagnation point. The size of the dent increases with increase in the Weber number. This effect is noted to be more pronounced in water and methyl alcohol than in mercury. In other words, for high M liquids, the rate of dent growth, as the Weber number increases, is faster than in low M liquids. It is therefore likely that, in low M liquids, gravitational forces are more dominant than surface tension forces.

In view of the simplifying assumptions used, it is possible that the above shapes may not be correct beyond the stage when the rear of the bubble is flat. Walters and Davidson (1962,3) in their theoretical and experimental work on accelerating bubbles, under the action of gravitational forces alone, observed a tongue of liquid forming at the back of the bubble. The bubble distorts into the form of a mushroom and ultimately into an umbrella shape. Although a comparison of these shapes with those of the present theory may be irrelevant, it might well be the case that, the natural development of a bubble shape from spherical to spheroidal to a spherical cap, follows similar lines.

# R E F E R E N C E S

## REFERENCES

Batchelor, G.K. and Davies, R.M. (Editors). 1956. Surveys in Mechanics. Cambridge: University Press.

Batchelor, G.K. 1967. An introduction to fluid dynamics. Cambridge: University Press.

Chandrasekhar, S. 1961. Hydrodynamic and hydromagnetic stability. Oxford: University Press.

Chandrasekhar, S. 1965. The stability of a rotating liquid drop. Proc. Roy. Soc., Series A, Vol. 286, 1-26.

Chandrasekhar, S. 1969. Ellipsoidal figures of equilibrium. New Haven and London: Yale University Press.

Davies, R.M. and Taylor, G.I. 1950. The mechanics of large bubbles rising through extended liquids and through liquids in tubes. Proc. Roy. Soc., Series A. Vol. 200, 375-390.

Fox, L. 1957. Numerical solution of two-point boundary problems. Oxford: University Press.

Haberman, W.L. and Morton, R.K. 1953. An experimental investigation of the drag and shape of air bubbles rising in various liquids. David Taylor Model Basin, Rep. No. 802.

Happel, J. and Brenner, H. 1965. Low Reynolds number hydrodynamics. Prentice-Hall.

Harper, J.F., Moore, D.W., and Pearson J.R.A. 1967. The effect of the variation of surface tension with temperature on the motion of bubbles and drops. J. Fluid Mech. Vol. 27, 361-366.

Harper, J.F. 1970. Viscous drag in steady potential flow past a bubble. Chemi. Eng. Science. Vol. 25, 342-343.

Hartunian, R.A. and Sears, W.R. 1957. On the instability of small gas bubbles moving uniformly in various liquids. J. Fluid Mech. Vol. 3, 27-47.

Jones, D.R.M. 1965. Ph.D. dissertation. University of Cambridge.

Lamb, H. 1959. Hydrodynamics. Sixth edition. Cambridge: University Press.

Lebovitz, N.R. 1961. The virial tensor and its application to self gravitating fluids. Astrophys. J. Vol. 134, 500-536.

Levich, V. 1962. Physico-Chemical hydrodynamics. New York: Prentice Hall.

Macrobert, T.M. 1967. Spherical harmonics. Third edition. Pergamon Press.

Moore, D.W. 1959. The rise of a gas bubble in a viscous liquid. J. Fluid. Mech. Vol. 6, 113-130.

Moore, D.W. 1963. The boundary layer on a spherical gas bubble. J. Fluid. Mech. Vol. 16, 161-176.

Moore, D.W. 1965. The velocity of rise of distorted gas bubbles in a liquid of small viscosity. J. Fluid Mech. Vol. 23, 749-766.

Peebles, F.N. and Garber, H.J. 1953. Studies of the motion of gas bubbles in liquids. Chem. Eng. Prog. Vol. 49, 88-97.

Rayleigh, Lord. 1900. On a theorem analogous to the virial theorem. Scientific Papers, 1892-1901. Vol. 4, 491-493. Cambridge: University Press.

Rosenkilde, C.E. 1967a. Surface-Energy tensors. J. Math. Phys. Vol. 8, 84-88.

Rosenkilde, C.E. 1967b. Surface-Energy tensors for ellipsoids. J. Math. Phys. Vol. 8., 88-97.

Rosenkilde, C.E. 1969. A dielectric fluid drop in an electric field. Proc. Roy. Soc., Series A. Vol. 312, 473-494.

Saffman, P.G. 1956. On the rise of air bubbles in water. J. Fluid Mech. Vol. 1, 249-275.

Schwerdtfeger, K. 1968. Velocity of rise of argon bubbles in mercury. Chem. Eng. Science. Vol. 23, 937-938.

Siemes, W. 1954. Gasblasen in Flüsigkeiten. Chemie. Ing. Tech. Vol. 26, 614-630.

Taylor, G.I. 1964. Disintegration of water drops in an electric field. Proc. Roy. Soc. Vol. 280, 383-397.

Van Dyke, M. 1964. Perturbation methods in fluid mechanics. New York and London: Academic Press.

Walters, J.K. and Davidson, J.F. 1962. The initial motion of a gas bubble formed in an inviscid liquid. I. J. Fluid Mech. Vol. 12, 408-416.

Walters, J.K. and Davidson, J.F. 1963. The initial motion of a gas bubble formed in an inviscid liquid. II. J. Fluid Mech. Vol. 17, 321-340.

Weatherburn, C.E. 1930. Differential geometry of three dimensions. Vol. II. Cambridge: University Press.

Winnikow, S. and Chao, B.T. 1966. Droplet motion in purified systems. Phys. Fluids Vol. 9, 50-61.

# APPENDICES

## APPENDIX (2A)

### First curvature of a surface

In this appendix we give a summary of the method discussed by Weatherburn (1930) pp. 86-87, for the derivation of the first curvature of a surface. In order to avoid any ambiguities in the sign of the normal, we shall define $\hat{\underline{n}}$ to be the unit normal, to the surface, directed away from the centre of curvature. Thus for an ellipsoidal surface, $\hat{\underline{n}}$ denotes the unit outward normal. The first curvature, J, of a surface is then given by

$$J = \operatorname{div} \hat{\underline{n}}. \tag{1}$$

Consider now a family of surfaces

$$G(x,y,z) = \text{const.}, \tag{2}$$

where x,y,z are taken to be orthogonal curvilinear coordinates. This is a special case of the more general one, for oblique coordinates, treated by Weatherburn. The unit normal $\hat{\underline{n}}$ at any point on the surface G may then be expressed by

$$\hat{\underline{n}} = F\nabla G, \tag{3}$$

where

$$F = 1/|\nabla G|. \tag{4}$$

Substituting from (3) into (1), the expression for the first curvature of the surface (2) becomes

$$J = F\nabla^2 G + \nabla F . \nabla G, \tag{5}$$

or

$$J = F\nabla^2 G + \hat{\underline{n}} . \nabla \log G. \tag{6}$$

For our purpose, we shall take G to be a surface of revolution of the form

$$G = x - k - \ell g(y) = 0, \tag{7}$$

where k and $\ell$ are constants and g is a single-valued continuous function of y.

## APPENDIX (3A)

## EVALUATION OF SOME INTEGRALS

By definition

$$A_i = \int_0^\infty \frac{a_1 a_2 a_3 dt}{\Delta_1 (a_i^2 + t)}, \qquad (i = 1,2,3), \tag{1}$$

where

$$\Delta_1^2 = (a_1^2 + t)(a_2^2 + t)(a_3^2 + t). \tag{2}$$

These integrals can be expressed in terms of the incomplete elliptic integrals

$$E(\theta,\phi) = \int_0^\phi (1 - \sin^2\theta \sin^2 g)^{1/2}\, dg \tag{3}$$

and

$$F(\theta,\phi) = \int_0^\phi (1 - \sin^2\theta \sin^2 g)^{-1/2}\, dg \tag{4}$$

of the two kinds with the definitions

$$\sin\theta = \left(\frac{a_1^2 - a_2^2}{a_1^2 - a_3^2}\right)^{1/2} \text{ and } \cos\phi = \frac{a_3}{a_1} \tag{5}$$

when $a_1 = a_2 > a_3$ the integrals defining the $A_i$ give

$$\left.\begin{aligned} A_1 &= A_2 = \frac{H}{e^3}(S - eH), \\ A_3 &= \frac{2}{e^3}(e - HS), \end{aligned}\right) \tag{6}$$

where e, H and S are as defined in Chapter III. The $B_i$'s are defined by

$$B_i = \int_0^\infty \frac{dt}{\Delta_2 (a_i^2 + t^2)}, \tag{7}$$

where

$$\Delta_2^2 = (a_1^2 + t^2)(a_2^2 + t^2)(a_3^2 + t^2). \tag{8}$$

Again we use the incomplete elliptic integrals (3) and (4), where now

$$\sin\theta = \frac{a_1}{a_2}\left(\frac{a_2^2 - a_3^2}{a_1^2 - a_3^2}\right)^{1/2}, \cos\phi = \frac{a_3}{a_1} \tag{9}$$

and $$t = a_3(\sin^2\phi - \sin^2 g)^{-1/2} \sin g. \tag{10}$$

For the oblate spheroid ($a_1 = a_2 > a_3$), these integrals give

$$\left.\begin{aligned} B_1 = B_2 &= (2a_1^4 e^2)^{-1}[(1 + e^2)(\tanh^{-1} e)/e - 1], \\ B_3 &= (a_1^4 e^2)^{-1}[(1 - e^2)^{-1} - (\tanh^{-1} e)/e]. \end{aligned}\right\} \tag{11}$$

The integrals $I_i$ are defined by

$$I_1 = \int_{t=o}^{\infty} \frac{dt}{(a_1^2 + t^2)^{5/2}}, \tag{12}$$

$$I_2 = \int_{t=o}^{\infty} \frac{t^2 dt}{(a_1^2 + t^2)^{5/2}}, \tag{13}$$

and

$$I_3 = \int_{t=o}^{\infty} \frac{dt}{(a_1^2 + t^2)^{5/2}(a_3^2 + t^2)}. \tag{14}$$

These integrals may then be evaluated, using the substitution (10), so that one finally gets

$$\left.\begin{aligned} I_1 &= \frac{2}{3a_1^4}, \qquad I_2 = \frac{1}{3a_1^2}, \\ I_3 &= \frac{1}{3Ha_1^6 e^5}[3S - e(3 + 2e^2)H]. \end{aligned}\right\} \tag{15}$$

The evaluation of the tensors $C_{ij}$, $T_{ij}$ and $Q_{ij}$ given by equations (3.12), (3.26) and (3.34) respectively, is facilitated by using the transformation of coordinates given in Rosenkilde (1967, b) p.90. The case of revolutional symmetry, $a_1 = a_2$, will suffice for this work. Therefore after correcting a misprint in the expression for $x_3$ in the text and putting $a_1 = a_2$ one gets

$$\left.\begin{aligned} x_1 &= a_1^2 b_1^{-1/2} \cos\gamma \\ x_2 &= a_1^2 b_1^{-1/2} \sin\gamma \\ x_3 &= b_1^{-1/2} , \end{aligned}\right) \tag{16}$$

where

$$b_i = a_i^2 + t^2, \; i = 1,2,3. \tag{17}$$

The components of the unit outward normal $\hat{\underline{n}}$ are

$$\left.\begin{aligned} n_1 &= a_3 b_3^{-1/2} \cos\gamma \\ n_2 &= a_3 b_3^{-1/2} \sin\gamma \\ n_3 &= b_3^{-1/2}\, t. \end{aligned}\right) \tag{18}$$

The element of surface area is

$$dS = a_1^4 b_1^{-2} b_3^{1/2}\, dt\, d\gamma. \tag{19}$$

The variables t and $\gamma$ have the ranges $0 \leq t \leq \infty$ and $o \leq \gamma \leq 2\pi$. This transformation has the advantage that the above tensors may be expressed in terms of standard incomplete elliptic integrals given here.

The surface-energy tensor $C_{ij}$ defined by (3.12) is evaluated by

Rosenkilde (1967 b) for the ellipsoidal surface (3.39) in terms of the elliptic integrals $B_i$. The resulting expressions are

$$\left.\begin{aligned} C_{ij} &= 0 \quad (i \neq j) \\ C_{ii} &= (a_1 a_2 a_3)^2 \sigma (B_j + B_k) \quad (i \neq j \neq k). \end{aligned}\right\} \tag{20}$$

The case corresponding to an oblate spheroid ($a_1 = a_2$) is easily obtained on substituting for the $B_i$'s from equation (11).

The expressions for the velocity potential and the velocity components in equations (3.49) - (3.51) are now transformed in terms of the parameter t, using the relation

$$\beta = t\, b_1^{-1/2} \qquad (\text{on } \alpha = \alpha_o), \tag{21}$$

which is obtained from comparison of the above coordinate system with that of oblate spheroidal coordinates. The resulting expressions, on the surface $\alpha = \alpha_o$, are

$$\Phi = C_o t(\alpha_o \cot^{-1}\alpha_o - 1) b_1^{-1/2} \tag{22}$$

$$u_1 = \frac{C_o t}{L_o b_3} \cos\gamma, \tag{23}$$

$$u_2 = \frac{C_o t}{L_o b_3} \sin\gamma, \tag{24}$$

$$u_3 = \frac{Ut^2}{b_3} + \frac{C_o a_3}{b_3}(\alpha_o \cot^{-1}\alpha_o - 1), \tag{25}$$

$$u_{n_o} = \frac{Ut}{b_3^{1/2}}, \tag{26}$$

where $u_{n_o}$ is the velocity component normal to the surface $\alpha = \alpha_o$.

On substituting from equations (18), (19) (22) - (25) into (3.26), one can express the integrals in the form

$$
\left.\begin{aligned}
T_{11} &= T_{22} = \frac{\pi\rho c_o^2 a_1^4 a_3 \lambda}{L_o}(I_1 - a_3^2 I_3), \\
T_{33} &= 2\pi\rho c_o a_1^4 \lambda[-(c_o a_3 \lambda + U a_3^2) I_1 + U I_2 + (c_o a_3^2 \lambda + U a_3^4) I_3], \\
T_{ij} &= 0 \qquad\qquad i \neq j;
\end{aligned}\right\} \tag{27}
$$

where

$$
\lambda = 1 - \alpha_o \cot^{-1}\alpha_o \tag{28}
$$

and $I_1$, $I_2$, $I_3$ are given by equation (15).

In a similar manner, on substituting from equations (18), (19) and (22) into (3.34) the components of the tensor $Q_{ij}$ are found to be

$$
\left.\begin{aligned}
Q_{11} &= Q_{22} = 0, \\
Q_{33} &= -\frac{2\pi\rho U^2 a_1^3 (e - SH)}{3(S - eH)}, \\
Q_{ij} &= 0, \qquad i \neq j.
\end{aligned}\right\} \tag{29}
$$

## APPENDIX (3B)

## EVALUATION OF THE MICROSCOPIC ENERGY ($\Pi$)

To evaluate the integral (3.9) for $\Pi$, one requires the value of the pressure at a field point. This may be obtained from the convenient form of Bernoulli's equation,

$$\frac{P}{\rho} - \underline{U}.\ \mathrm{grad}\,\Phi + \frac{1}{2}(\mathrm{grad}\,\Phi)^2 = 0, \tag{1}$$

relative to the moving frame. Then substituting for P from this equation into (3.9), making use of the divergence theorem, Laplace's equation, and the equation of continuity, one finds

$$\Pi = -\frac{\rho}{2}\int_S \Phi\underline{U}.\underline{dS} + \rho\int_\Sigma \Phi\underline{U}.\underline{d\Sigma} \ . \tag{2}$$

Upon substituting for the expressions in this equation and performing the integrations one finally gets, on letting $R \to \infty$ on $\Sigma$,

$$\Pi = \frac{2\Gamma(3e - 3HS - 2e^3H)}{9(S - eH)} \tag{3}$$

## APPENDIX (4A)

### Legendre Functions.

The $P_n(\beta)$ in equation (4.3) satisfy Legendre's differential equation of integral order n,

$$\frac{d}{d\beta}\left[(1-\beta^2)\frac{dP_n}{d\beta}\right] + n(n+1)P_n = 0. \tag{1}$$

They are polynomials in $\beta$ and offer no difficulty. They satisfy the following recurrence relations, see MacRobert (1967) p.91,

$$(2n+1)P_n = \dot{P}_{n+1} - \dot{P}_{n-1}, \tag{2}$$

$$(1-\beta^2)\dot{P}_n = nP_{n-1} - n\beta P_n, \tag{3}$$

$$(n+1)P_{n+1} - (2n+1)\beta P_n + nP_{n-1} = 0, \tag{4}$$

$$nP_n = \beta\dot{P}_n - \dot{P}_{n-1}, \tag{5}$$

$$(1-\beta^2)\dot{P}_n = \frac{n(n+1)}{2n+1}(P_{n-1} - P_{n+1}). \tag{6}$$

The functions $q_n(i\alpha)$, however, have imaginary argument. They satisfy the same equation (1) with $\beta$ replaced by $(i\alpha)$, viz.

$$\frac{d}{d\alpha}\left[(1+\alpha^2)\frac{dq_n}{d\alpha}\right] - n(n+1)q_n = 0. \tag{7}$$

Their only singularities are at $\pm 1$ on the real $\alpha$ axis. Hence they always remain finite on the imaginary axis. In particular

$$q_n(i\infty) = 0. \tag{8}$$

They are alternately odd and even. Furthermore $q_n(i\alpha)$ is either real or purely imaginary, so that by a proper choice of the constants $b_n$ in equation (4.3), it is always possible to make $q_n(i\alpha)$ real. In fact $i^{n+1}q_n(i\alpha)$ is always real, see MacRoberts p.196. Therefore, retaining the same notation, one may write

$$q_n(i\alpha) = i^{-n-1}\, q_n(\alpha), \tag{9}$$

where $q_n$ are real and have real arguments. The $q_n(i\alpha)$ satisfy the same recurrence relations (2)-(6). On replacing $P_n(\beta)$ by $q_n(i\alpha)$ from equation (9) into equations (2)-(6) and replacing $\beta$ by $i\alpha$, one gets the following recurrence formulae for $q_n(\alpha)$.

$$(2n + 1)q_n = -\,(\dot{q}_{n+1} + \dot{q}_{n-1}), \tag{10}$$

$$(1 + \alpha^2)\dot{q}_n = n\alpha q_n - nq_{n-1}, \tag{11}$$

$$(n + 1)q_{n+1} + (2n + 1)\alpha q_n - nq_{n-1} = 0, \tag{12}$$

$$nq_n = \alpha\dot{q}_n - \dot{q}_{n-1}, \tag{13}$$

$$(1 + \alpha^2)\dot{q}_n = -\,\frac{n(n + 1)}{2n + 1}\,(q_{n+1} + q_{n-1}). \tag{14}$$

The expressions for $q_o$, $q_1$ and $q_2$ as given in Lamb (1959) p.143 are,

$$\left.\begin{aligned} q_o &= \cot^{-1}\alpha \\ q_1 &= 1 - \alpha\cot^{-1}\alpha \\ q_2 &= \tfrac{1}{2}(3\alpha^2 + 1)\cot^{-1}\alpha - \tfrac{3}{2}\alpha. \end{aligned}\right\} \tag{15}$$

# TABLES

T A B L E. (1).Two-point Theory (symmetric.)

| No. | $x_o$ | $x_c$ | W |
|---|---|---|---|
| (a) | 1.04 | 1.040 | 0.2695 |
| (b) | 1.10 | 1.100 | 0.6237 |
| (c) | 1.30 | 1.300 | 1.4919 |
| (d) | 1.50 | 1.504 | 2.0563 |
| (e) | 1.70 | 1.718 | 2.4455 |
| (f) | 1.90 | 1.949 | 2.7265 |
| (g) | 2.00 | 2.076 | 2.8388 |
| (h) | 2.20 | 2.376 | 3.0223 |
| (i) | 2.40 | 2.848 | 3.1648 |
| (j) | 2.50 | 3.338 | 3.2244 |
| (k) | 2.60 | 4.970 | 3.2775 |

T A B L E. (2). Virial theory (symmetric.)

| No. | $x_o$ | $x_c$ | W |
|---|---|---|---|
| (a) | 1.04 | 1.040 | 0.2698 |
| (b) | 1.10 | 1.100 | 0.6255 |
| (c) | 1.30 | 1.301 | 1.4989 |
| (d) | 1.50 | 1.507 | 2.0608 |
| (e) | 1.70 | 1.714 | 2.4376 |
| (f) | 1.90 | 1.929 | 2.6975 |
| (g) | 2.00 | 2.041 | 2.7965 |
| (h) | 2.20 | 2.276 | 2.9499 |
| (i) | 2.40 | 2.552 | 3.0587 |
| (j) | 2.50 | 2.739 | 3.1006 |
| (k) | 2.60 | 3.074 | 3.1357 |
| (l) | 2.64 | 3.396 | 3.1481 |
| (m) | 2.66 | 3.729 | 3.1540 |
| (n) | 2.69 | 5.446 | 3.1624 |

T A B L E. (3). Comparison of the different theories.

| T H E O R Y. | X | W |
|---|---|---|
| Analytical Perturbation | 1.1 | 0.627 |
| Virial | 1.1 | 0.626 |
| Two-point | 1.1 | 0.624 |
| Linearized virial | 1.1 | 0.616 |
| Linearized Two-point | 1.1 | 0.614 |
| Exact theory (convergence accelerated.) | 1.1 | 0.610 |

TABLE. (4). Virial (with gravity.)

| No. | $x_o$ | W |
|---|---|---|
| (a) | 1.02 | 0.1385 |
| (b) | 1.06 | 0.3945 |
| (c) | 1.10 | 0.6255 |
| (d) | 1.16 | 0.9317 |
| (e) | 1.20 | 1.1128 |
| (f) | 1.30 | 1.4989 |
| (g) | 1.40 | 1.8090 |
| (h) | 1.50 | 2.0608 |
| (i) | 1.60 | 2.2672 |
| (j) | 1.70 | 2.4376 |
| (k) | 1.90 | 2.6975 |
| (l) | 2.10 | 2.8798 |
| (m) | 2.20 | 2.9499 |

T A B L E. (5). Summary of liquid properties.

| Liquid | Temperature deg C | Viscosity $\mu_o$ poises | Density $\rho$ gms/cc | Surface tension $\sigma$ dynes/cm | M number |
|---|---|---|---|---|---|
| Methyl alcohol. | 30 | 0.0052 | 0.782 | 21.8 | $8.9\times10^{-11}$ |
| Distilled (or filtered) Water. | 21 | 0.0098 | 0.998 | 72.6 | $2.4\times10^{-11}$ |
| Mercury. | (room temp.) 20 (estimated.) | 0.0155 | 13.546 | 48~~8~~3.0 | $3.7\times10^{-14}$ |

T A B L E. (6). Air bubbles in methyl alcohol ($M=8.9\times10^{-11}$.)

| No. | $x_o$ | W | R | $C_D$ | $F_r$ | $r_e$ Cm. | U cm./sec. |
|---|---|---|---|---|---|---|---|
| (a) | 1.02 | .1385 | 64.34 | .766 | 1.741 | .024 | 9.022 |
| (b) | 1.06 | .3945 | 121.84 | .426 | 3.129 | .030 | 13.573 |
| (c) | 1.10 | .6255 | 162.29 | .336 | 3.963 | .033 | 16.157 |
| (d) | 1.16 | .9317 | 209.17 | .281 | 4.748 | .037 | 18.674 |
| (e) | 1.20 | 1.1128 | 234.90 | .262 | 5.085 | .039 | 19.860 |
| (f) | 1.30 | 1.4989 | 287.31 | .240 | 5.553 | .044 | 21.871 |
| | 1.40 | 1.8090 | 328.61 | .234 | 5.704 | .047 | 23.078 |
| | 1.44 | 1.9159 | 342.95 | .233 | 5.712 | .049 | 23.420 |
| | 1.50 | 2.0608 | 362.65 | .235 | 5.685 | .051 | 23.823 |
| | 1.60 | 2.2672 | 391.56 | .239 | 5.571 | .054 | 24.274 |
| | 1.70 | 2.4376 | 416.62 | .247 | 5.402 | .056 | 24.529 |
| | 1.90 | 2.6975 | 458.40 | .267 | 4.995 | .062 | 24.670 |
| | 2.00 | 2.7965 | 476.17 | .279 | 4.780 | .064 | 24.622 |
| | 2.20 | 2.9499 | 507.16 | .306 | 4.360 | .069 | 24.385 |
| | 2.50 | 3.1006 | 545.36 | .352 | 3.786 | .076 | 23.835 |
| | 2.70 | 3.1651 | 566.89 | .387 | 3.450 | .081 | 23.407 |
| | 3.00 | 3.2261 | 594.93 | .443 | 3.012 | .087 | 22.734 |
| | 3.50 | 3.2677 | 633.64 | .548 | 2.432 | .097 | 21.620 |
| | 4.00 | 3.2667 | 665.55 | .668 | 1.996 | .108 | 20.577 |
| | 4.50 | 3.2432 | 692.83 | .802 | 1.663 | .117 | 19.624 |
| | 5.00 | 3.2078 | 716.78 | .949 | 1.405 | .127 | 18.762 |
| | 5.50 | 3.1663 | 738.20 | 1.110 | 1.201 | .136 | 17.982 |
| | 6.00 | 3.1219 | 757.65 | 1.285 | 1.038 | .146 | 17.274 |
| | 6.50 | 3.0766 | 775.51 | 1.474 | .905 | .155 | 16.632 |
| | 7.00 | 3.0315 | 792.07 | 1.677 | .795 | .164 | 16.045 |
| | 7.50 | 2.9872 | 807.55 | 1.893 | .704 | .173 | 15.508 |
| | 8.00 | 2.9441 | 822.09 | 2.124 | .628 | .182 | 15.014 |

TABLE. (7). Air bubbles in distilled water ($M=2.4\times10^{-11}$.)

| No. | $x_o$ | W | R | $C_D$ | $F_r$ | $r_e$ cm. | U cm./sec. |
|---|---|---|---|---|---|---|---|
| (a) | 1.02 | .1385 | 83.63 | .589 | 2.262 | .033 | 12.267 |
| (b) | 1.06 | .3945 | 158.35 | .328 | 4.067 | .042 | 18.454 |
| (c) | 1.10 | .6255 | 210.92 | .259 | 5.151 | .047 | 21.968 |
| (d) | 1.16 | .9317 | 271.86 | .216 | 6.170 | .053 | 25.390 |
| (e) | 1.20 | 1.1128 | 305.29 | .202 | 6.609 | .056 | 27.002 |
| (f) | 1.30 | 1.4989 | 373.41 | .185 | 7.216 | .062 | 29.736 |
| (g) | 1.40 | 1.8090 | 427.08 | .180 | 7.414 | .067 | 31.378 |
| | 1.44 | 1.9159 | 445.73 | .180 | 7.424 | .069 | 31.843 |
| | 1.50 | 2.0608 | 471.33 | .180 | 7.389 | .071 | 32.391 |
| | 1.60 | 2.2672 | 508.90 | .184 | 7.240 | .076 | 33.004 |
| | 1.70 | 2.4376 | 541.47 | .190 | 7.021 | .080 | 33.351 |
| | 1.90 | 2.6975 | 595.77 | .205 | 6.492 | .087 | 33.542 |
| | 2.00 | 2.7965 | 618.86 | .215 | 6.213 | .091 | 33.476 |
| | 2.20 | 2.9499 | 659.14 | .235 | 5.666 | .098 | 33.155 |
| | 2.50 | 3.1006 | 708.80 | .271 | 4.921 | .107 | 32.407 |
| | 2.70 | 3.1651 | 736.77 | .297 | 4.483 | .114 | 31.825 |
| | 3.00 | 3.2261 | 773.21 | .341 | 3.914 | .123 | 30.909 |
| | 3.50 | 3.2677 | 823.53 | .422 | 3.161 | .138 | 29.395 |
| | 4.00 | 3.2667 | 865.00 | .514 | 2.594 | .152 | 27.977 |
| | 4.50 | 3.2432 | 900.46 | .617 | 2.162 | .166 | 26.682 |
| | 5.00 | 3.2078 | 931.58 | .730 | 1.826 | .179 | 25.509 |
| | 5.50 | 3.1663 | 959.42 | .854 | 1.561 | .193 | 24.448 |
| | 6.00 | 3.1219 | 984.70 | .989 | 1.348 | .206 | 23.487 |
| | 6.50 | 3.0766 | 1007.92 | 1.134 | 1.176 | .219 | 22.613 |
| | 7.00 | 3.0315 | 1029.44 | 1.290 | 1.034 | .232 | 21.815 |
| | 7.50 | 2.9872 | 1049.55 | 1.457 | .915 | .244 | 21.085 |
| | 8.00 | 2.9441 | 1068.45 | 1.634 | .816 | .257 | 20.413 |

T A B L E. (8). Argon bubbles in mercury ($M=3.7\times10^{-14}$.)

| No. | $x_o$ | W | R | $C_D$ | $F_r$ | $r_e$ cm. | U cm./sec. |
|---|---|---|---|---|---|---|---|
| (a) | 1.02 | .1385 | 305.31 | .161 | 8.259 | .012 | 14.368 |
| (b) | 1.06 | .3945 | 578.13 | .090 | 14.849 | .015 | 21.614 |
| (c) | 1.10 | .6255 | 770.06 | .071 | 18.806 | .017 | 25.729 |
| (d) | 1.16 | .9317 | 992.53 | .059 | 22.528 | .019 | 29.737 |
| (e) | 1.20 | 1.1128 | 1114.60 | .055 | 24.129 | .020 | 31.626 |
| (f) | 1.30 | 1.4989 | 1363.30 | .051 | 26.347 | .022 | 34.828 |
| (g) | 1.40 | 1.8090 | 1559.24 | .049 | 27.067 | .024 | 36.751 |
| | 1.44 | 1.9159 | 1627.31 | .049 | 27.103 | .025 | 37.295 |
| (h) | 1.50 | 2.0608 | 1720.79 | .049 | 26.977 | .026 | 37.936 |
| (i) | 1.60 | 2.2672 | 1857.94 | .050 | 26.433 | .027 | 38.655 |
| (j) | 1.70 | 2.4376 | 1976.84 | .052 | 25.634 | .029 | 39.061 |
| (k) | 1.90 | 2.6975 | 2175.10 | .056 | 23.700 | .032 | 39.285 |
| (l) | 2.00 | 2.7965 | 2259.41 | .059 | 22.682 | .033 | 39.208 |
| (m) | 2.20 | 2.9499 | 2406.46 | .064 | 20.688 | .035 | 38.831 |
| | 2.50 | 3.1006 | 2587.76 | .074 | 17.965 | .039 | 37.955 |
| | 2.70 | 3.1651 | 2689.90 | .081 | 16.369 | .041 | 37.274 |
| | 3.00 | 3.2261 | 2822.94 | .093 | 14.290 | .045 | 36.202 |
| | 3.50 | 3.2677 | 3006.62 | .116 | 11.540 | .050 | 34.428 |
| | 4.00 | 3.2667 | 3158.04 | .141 | 9.472 | .055 | 32.767 |
| | 4.50 | 3.2432 | 3287.50 | .169 | 7.893 | .060 | 31.250 |
| | 5.00 | 3.2078 | 3401.11 | .200 | 6.667 | .065 | 29.877 |
| | 5.50 | 3.1663 | 3502.75 | .234 | 5.699 | .070 | 28.634 |
| | 6.00 | 3.1219 | 3595.04 | .271 | 4.923 | .075 | 27.508 |
| | 6.50 | 3.0766 | 3679.82 | .311 | 4.292 | .079 | 26.484 |
| | 7.00 | 3.0315 | 3758.41 | .353 | 3.773 | .084 | 25.550 |
| | 7.50 | 2.9872 | 3831.82 | .399 | 3.342 | .089 | 24.695 |
| | 8.00 | 2.9441 | 3900.82 | .448 | 2.979 | .093 | 23.908 |
| | 9.00 | 2.8624 | 4027.90 | .554 | 2.408 | .102 | 22.512 |
| | 10.00 | 2.7869 | 4143.20 | .672 | 1.985 | .111 | 21.307 |
| | 11.00 | 2.7173 | 4249.13 | .802 | 1.663 | .120 | 20.257 |
| | 12.00 | 2.6532 | 4347.40 | .944 | 1.413 | .129 | 19.332 |
| | 13.00 | 2.5940 | 4439.25 | 1.098 | 1.215 | .137 | 18.510 |
| | 14.00 | 2.5393 | 4525.65 | 1.264 | 1.055 | .146 | 17.774 |
| | 15.00 | 2.4886 | 4607.35 | 1.442 | .924 | .154 | 17.110 |
| | 16.00 | 2.4414 | 4684.92 | 1.633 | .816 | .162 | 16.508 |
| | 17.00 | 2.3974 | 4758.85 | 1.836 | .726 | .171 | 15.958 |
| | 18.00 | 2.3562 | 4829.54 | 2.052 | .650 | .179 | 15.455 |

# F I G U R E S

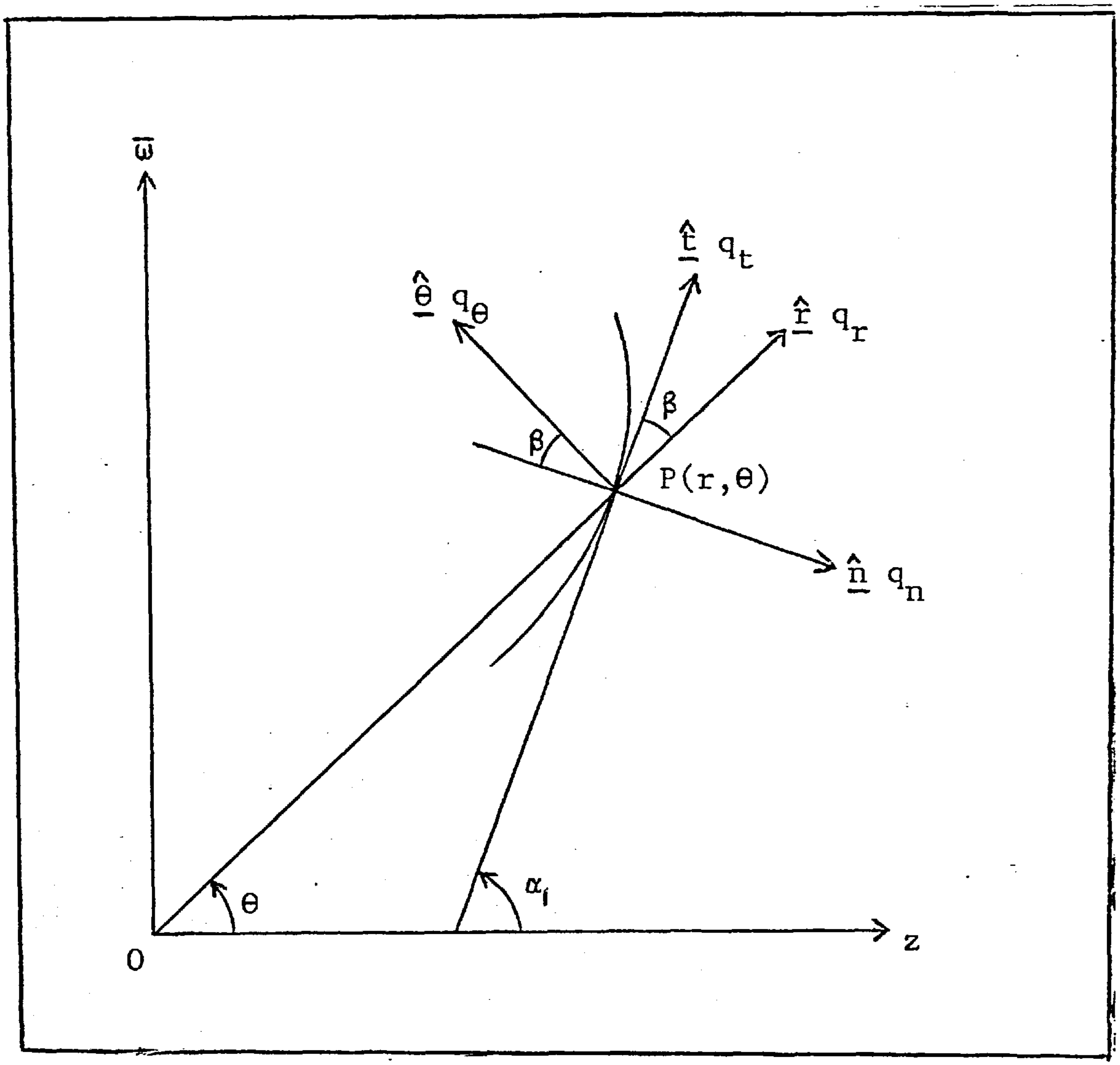


Fig. 2.1. A diagram representing the velocity components at a point P(r,θ) .Directions are specified by the unit vectors $\hat{\underline{r}}$,$\hat{\underline{\theta}}$,$\hat{\underline{t}}$ and $\hat{\underline{n}}$.

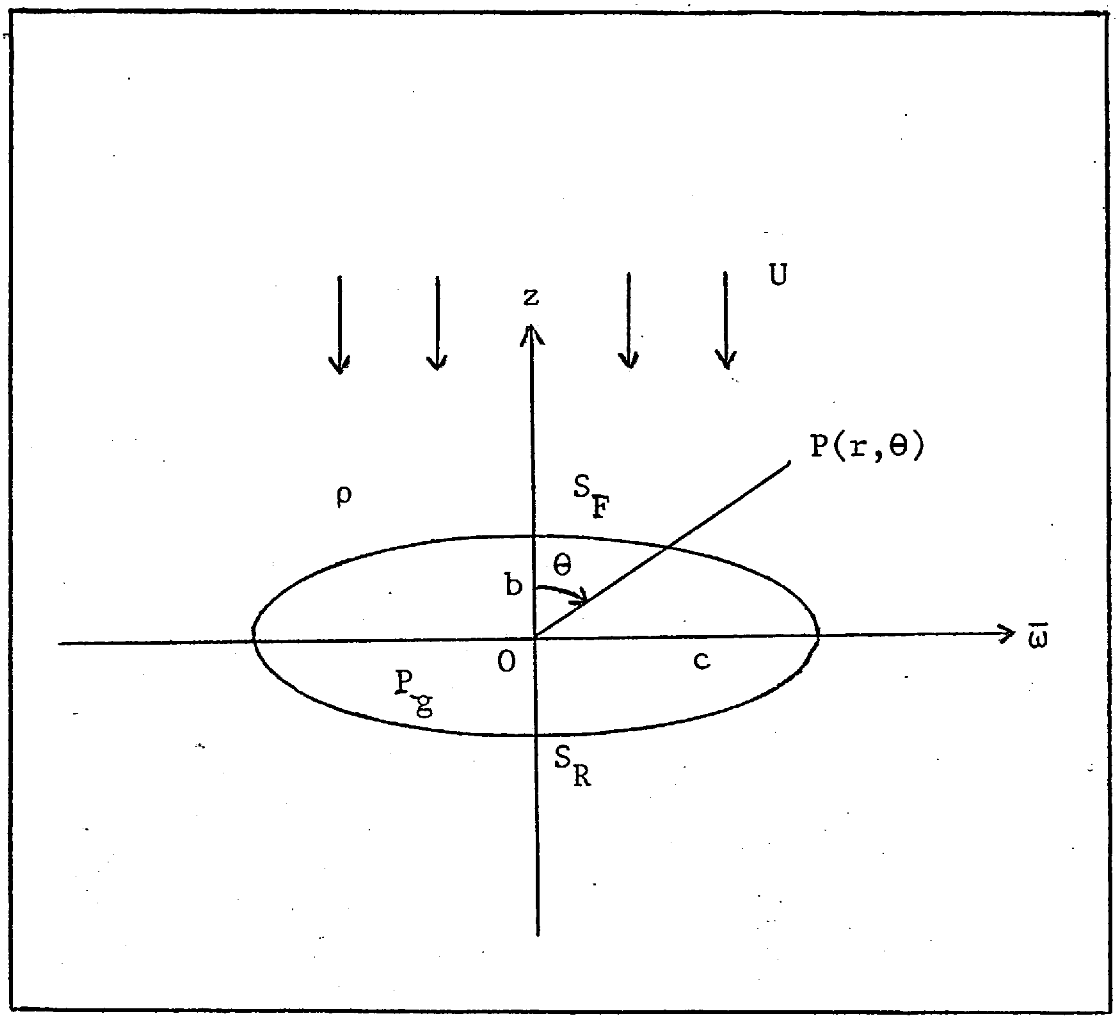


Fig. 2.2. A sketch in an axial plane of a stationary bubble in a stream with uniform velocity at infinity. $S_F$ , $S_R$ are the front and rear stagnation points respectively.

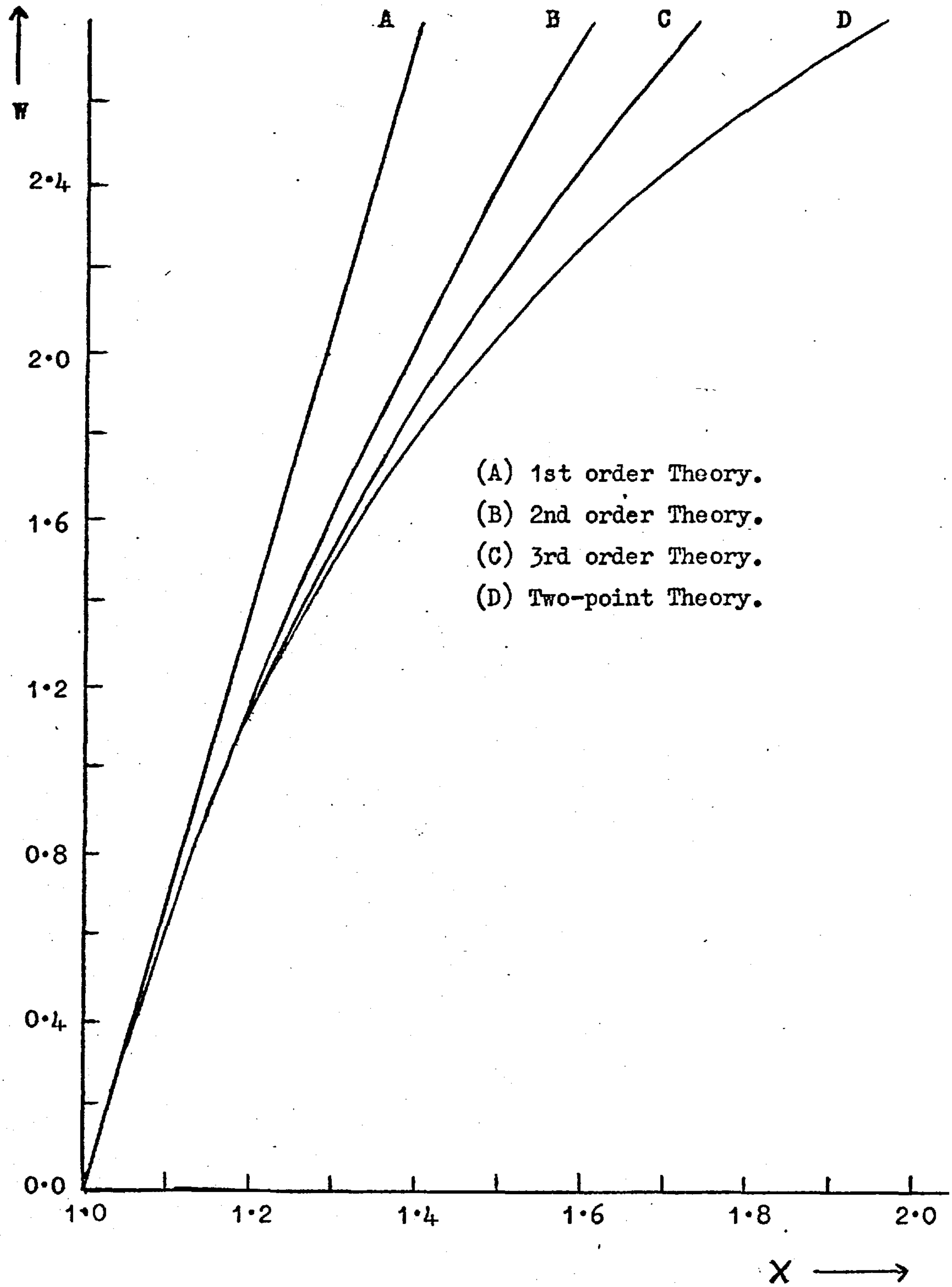


Fig. 2.3. The Weber number as a function of the axis-ratio.

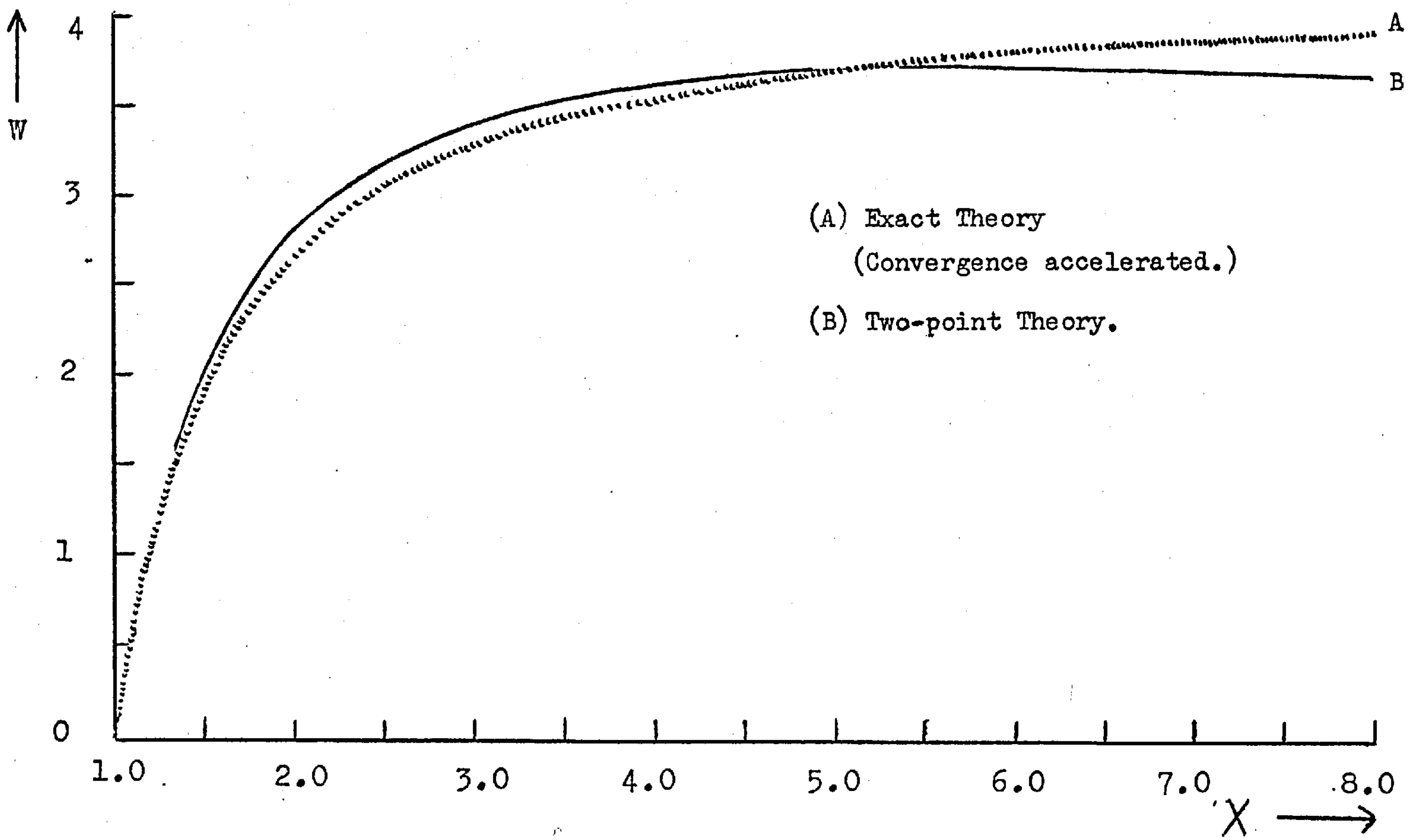


Fig. 2.4. Variation of the Weber number with the axis-ratio.

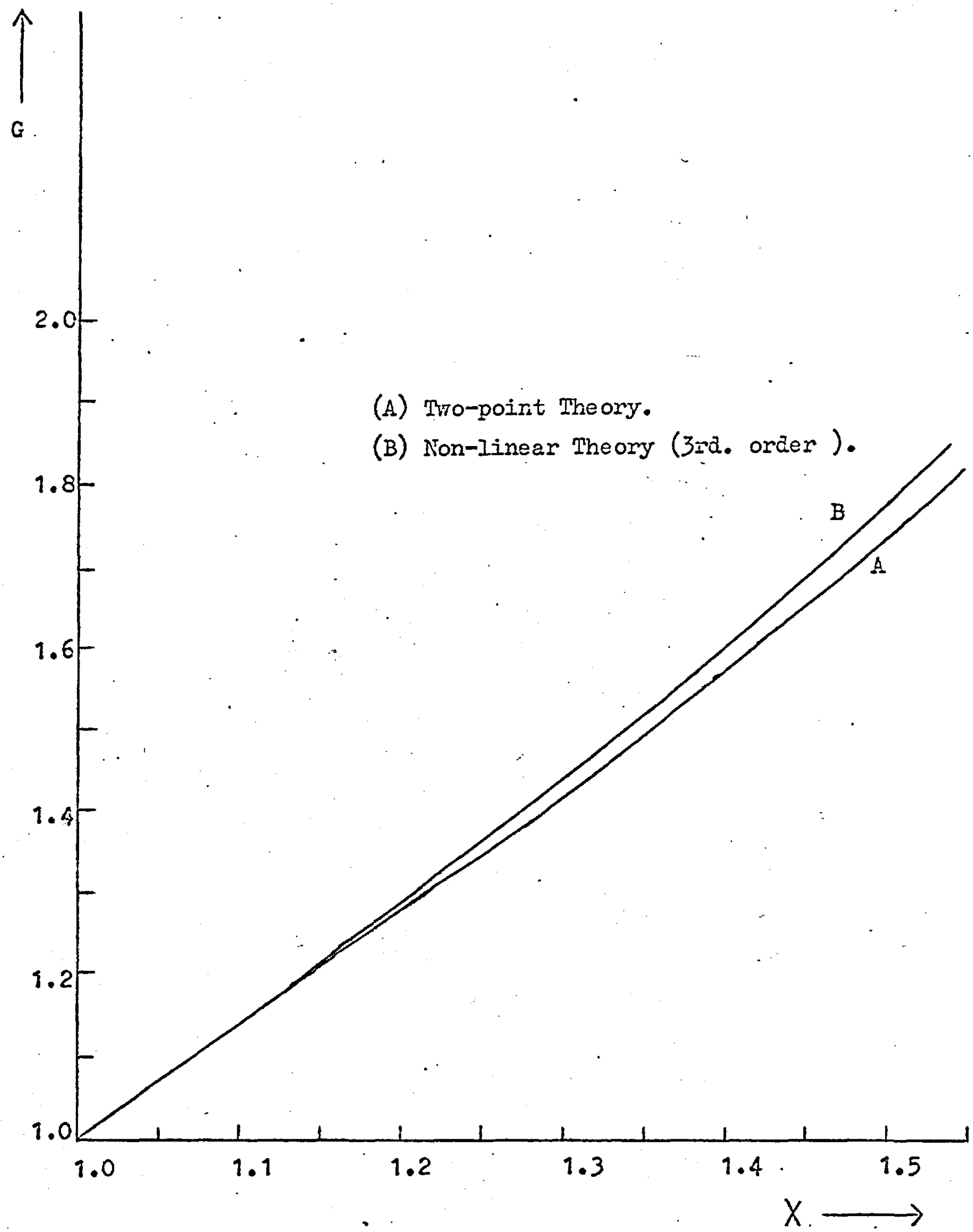


Fig. 2.5 The drag curves as a function of the axis-ratio.

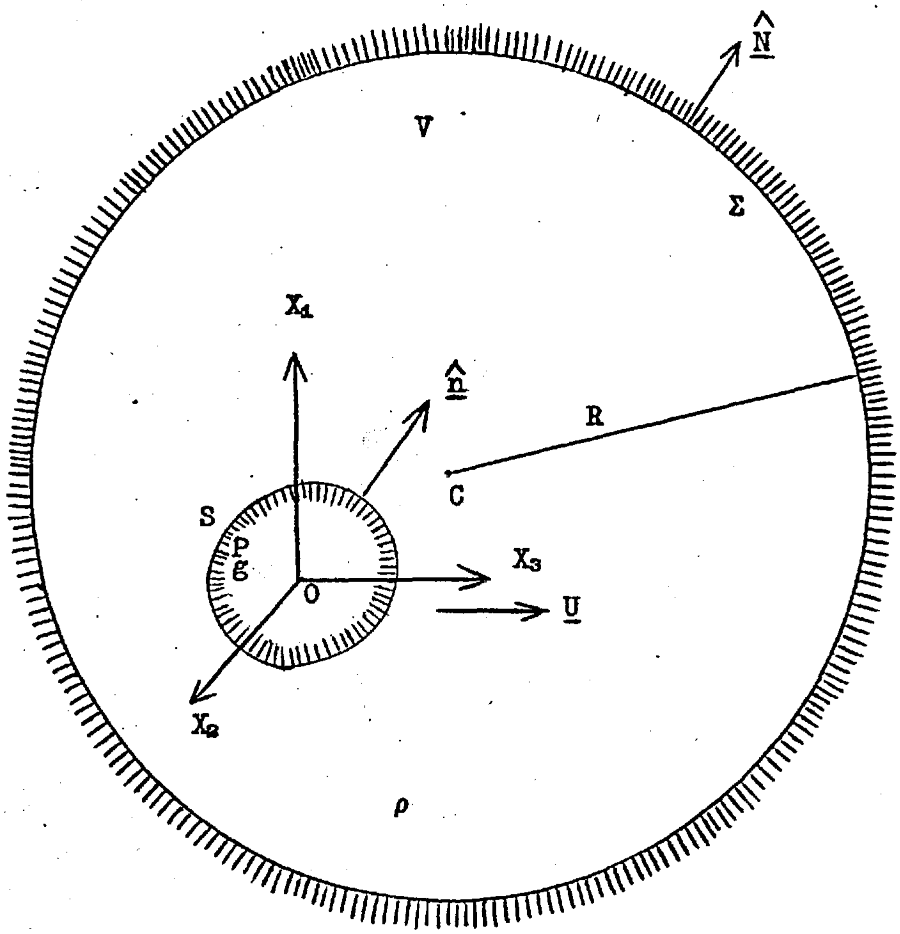


Fig. 3.1. Illustrating a body (S) translating uniformly through a fluid bounded externally by a large sphere (Σ).

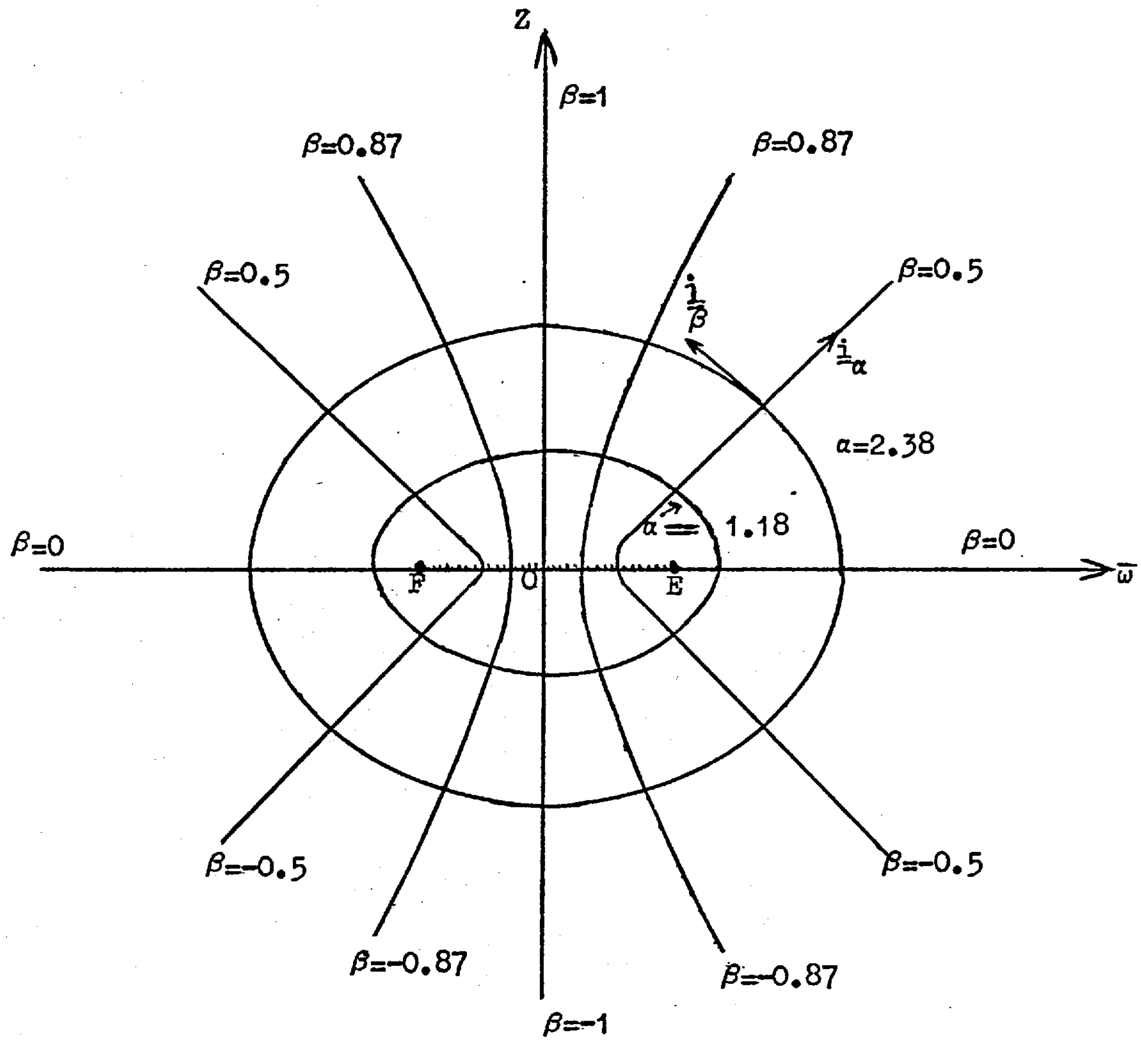


Fig. 3.2. Oblate spheroidal coordinates in a meridian plane. The two foci are E(k,0) and F(-k,0). The segment EF is represented by $\alpha=0$. The unit vectors $i_\alpha$ and $i_\beta$ represent the directions of increasing $\alpha$ and $\beta$ respectively.

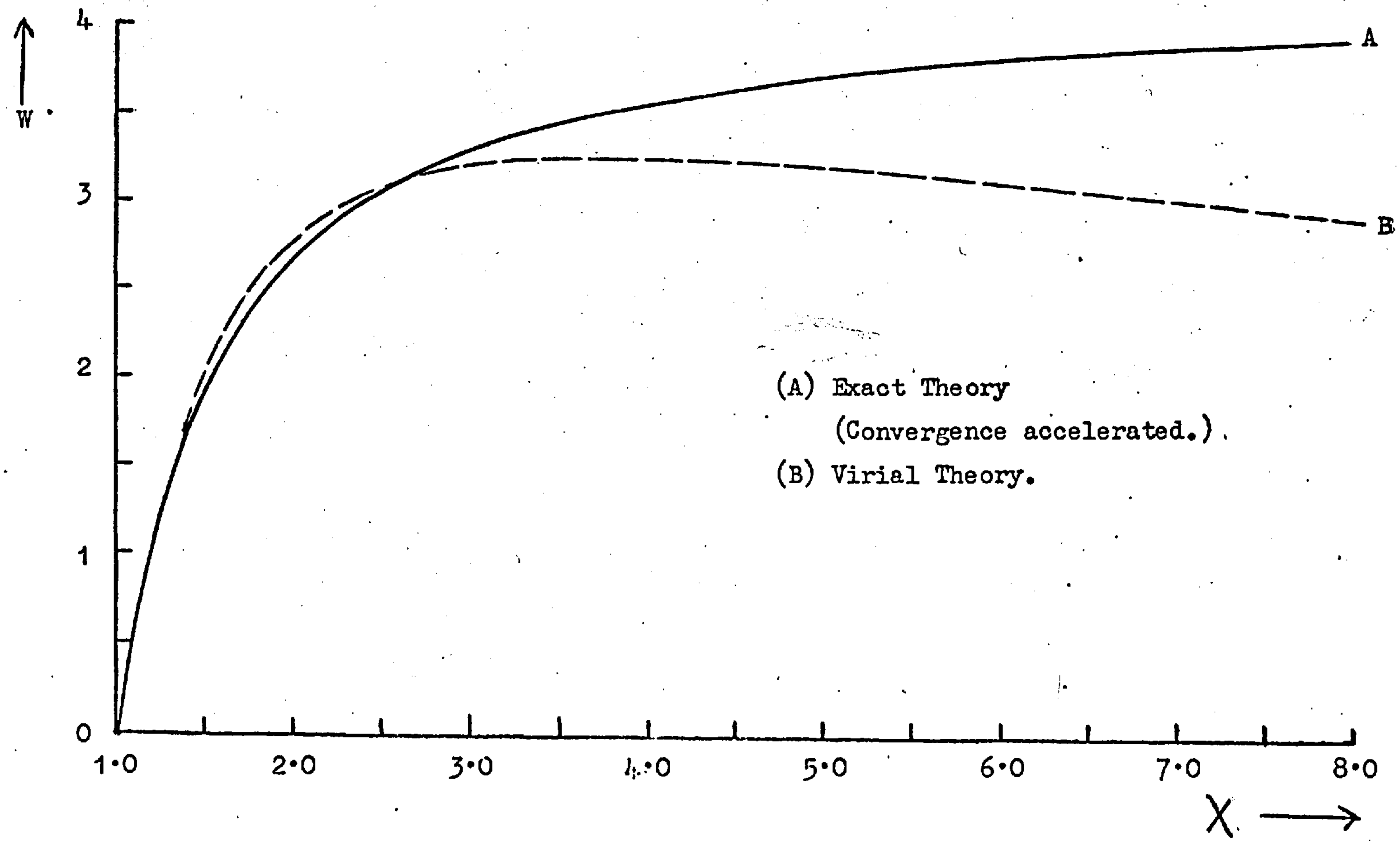


Fig. 3.3 Variation of the Weber number with the axis-ratio.

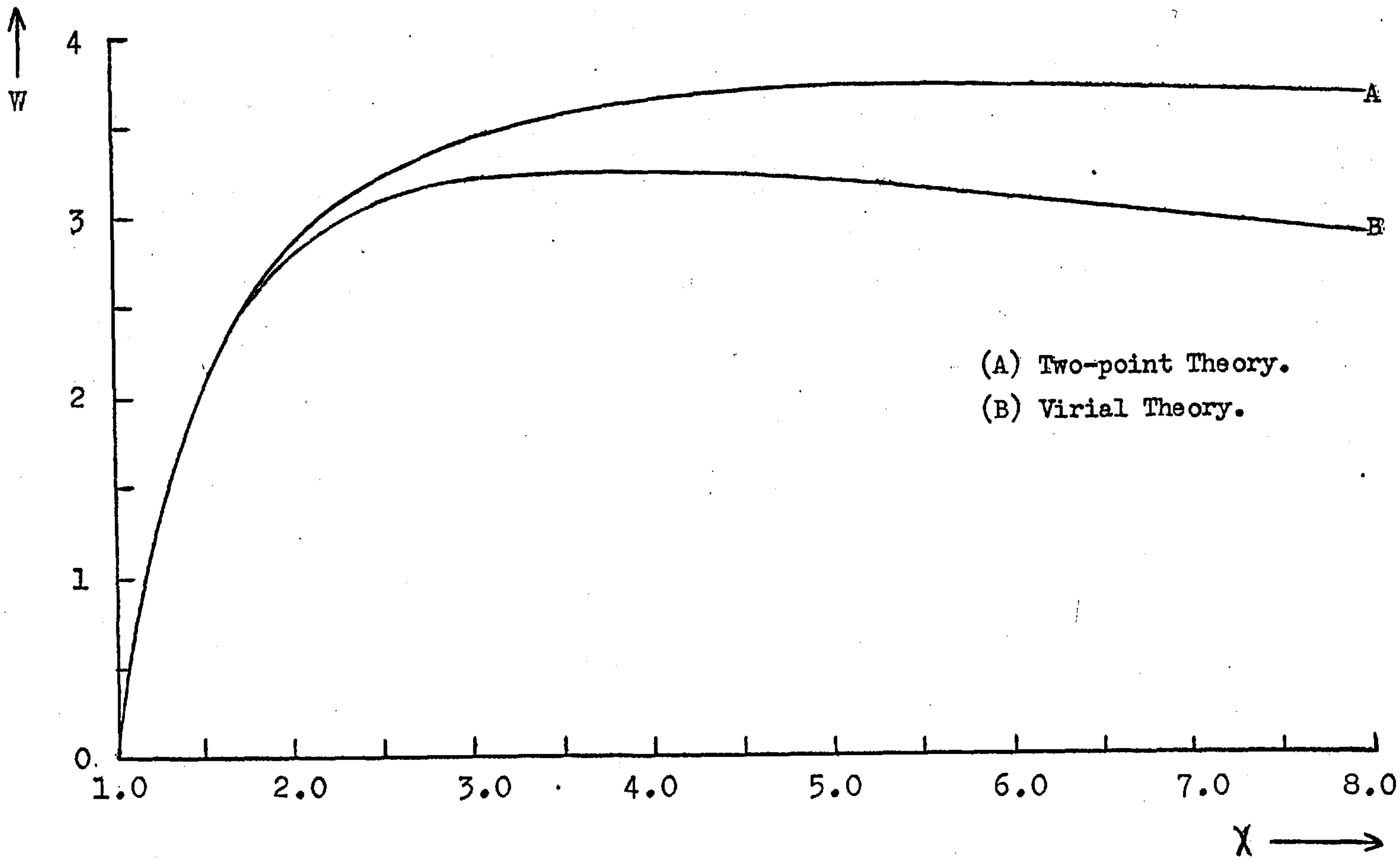


Fig. 3.4. Variation of the Weber number with the axis-ratio.

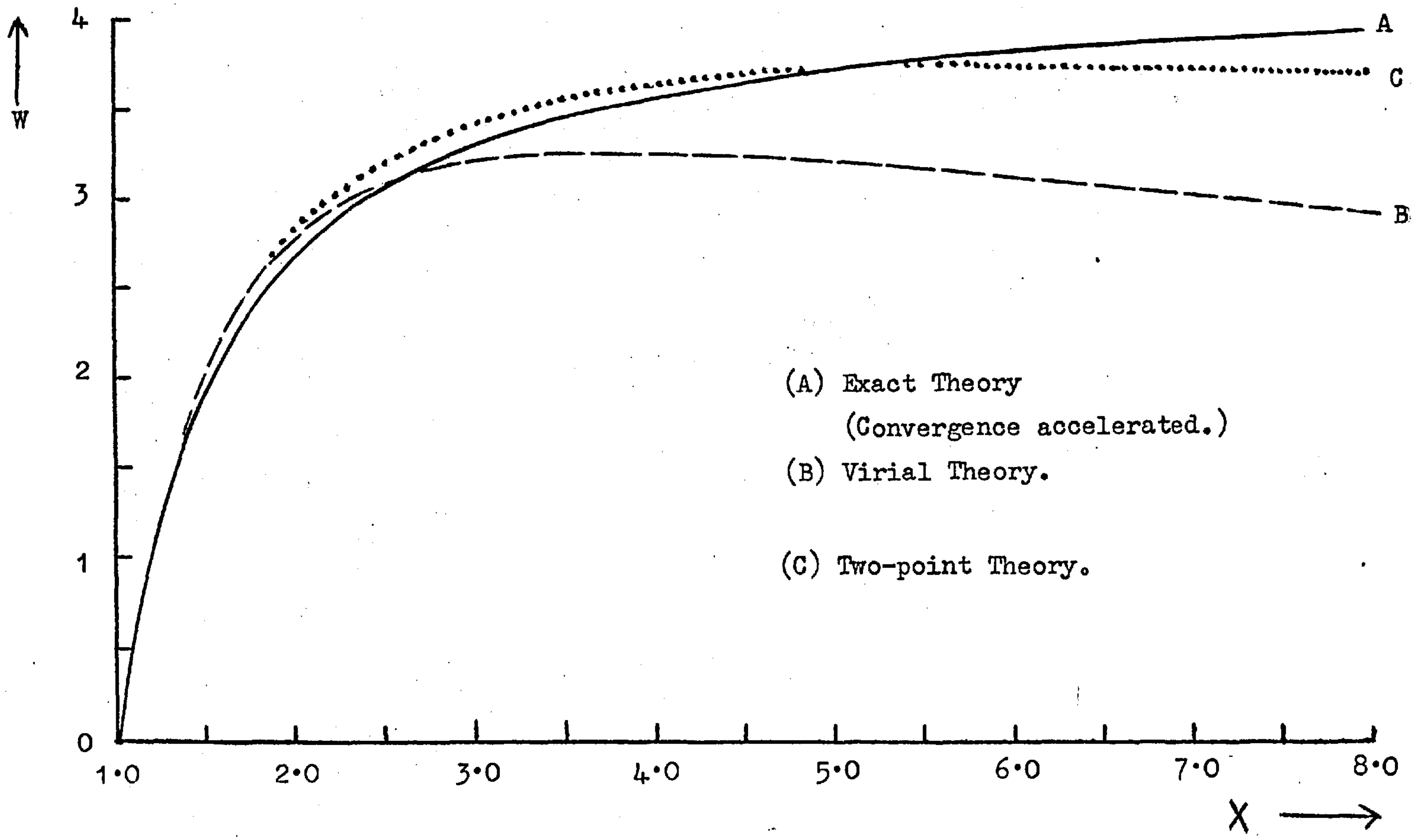


Fig.3.5. Variation of the Weber number with the axis-ratio.

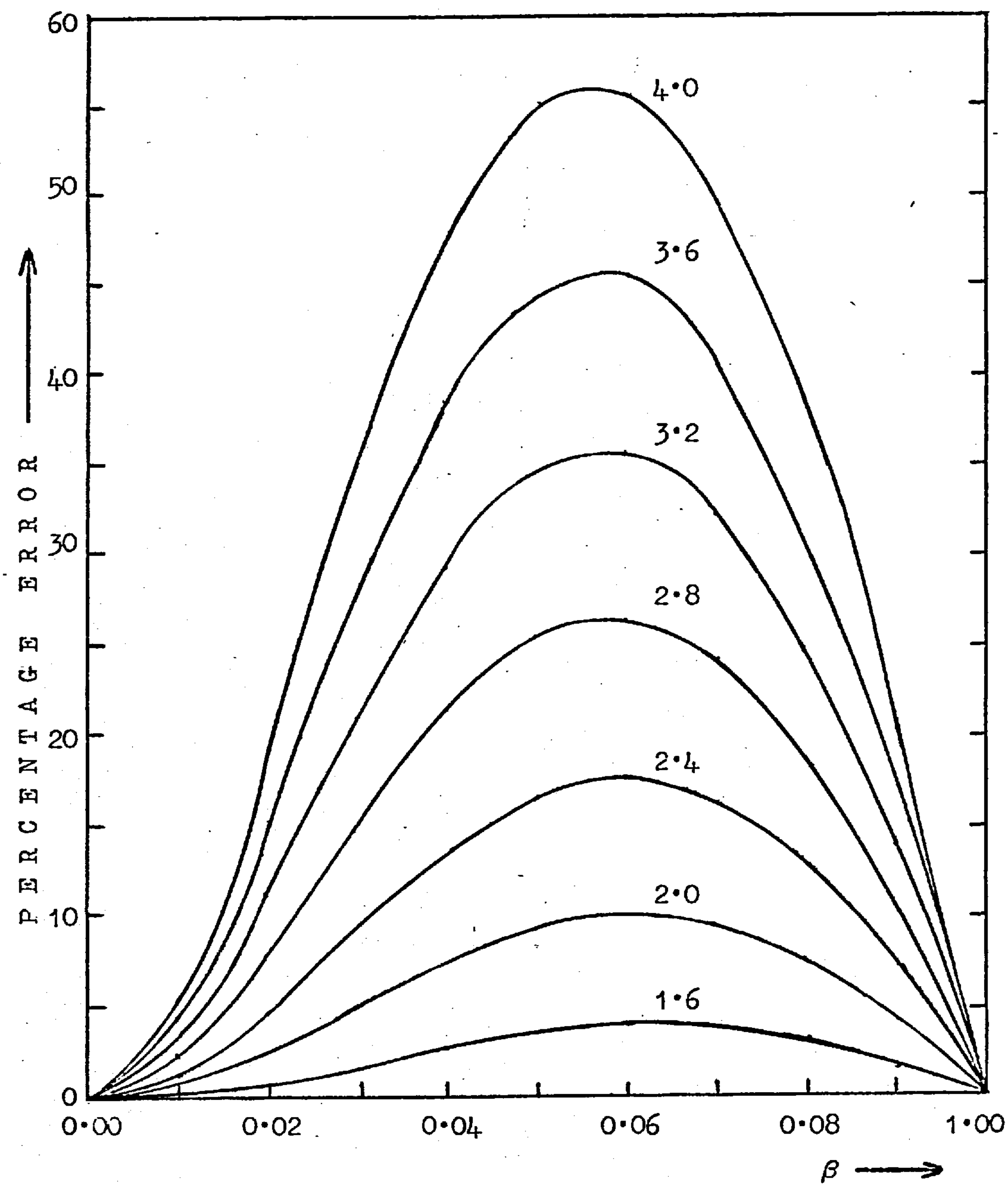


Fig. 3.6. Percentage error in the first curvature, for the Two-point Theory, at various points ($\beta$) on the bubble's surface. The figures on the curves indicate the axis-ratio.

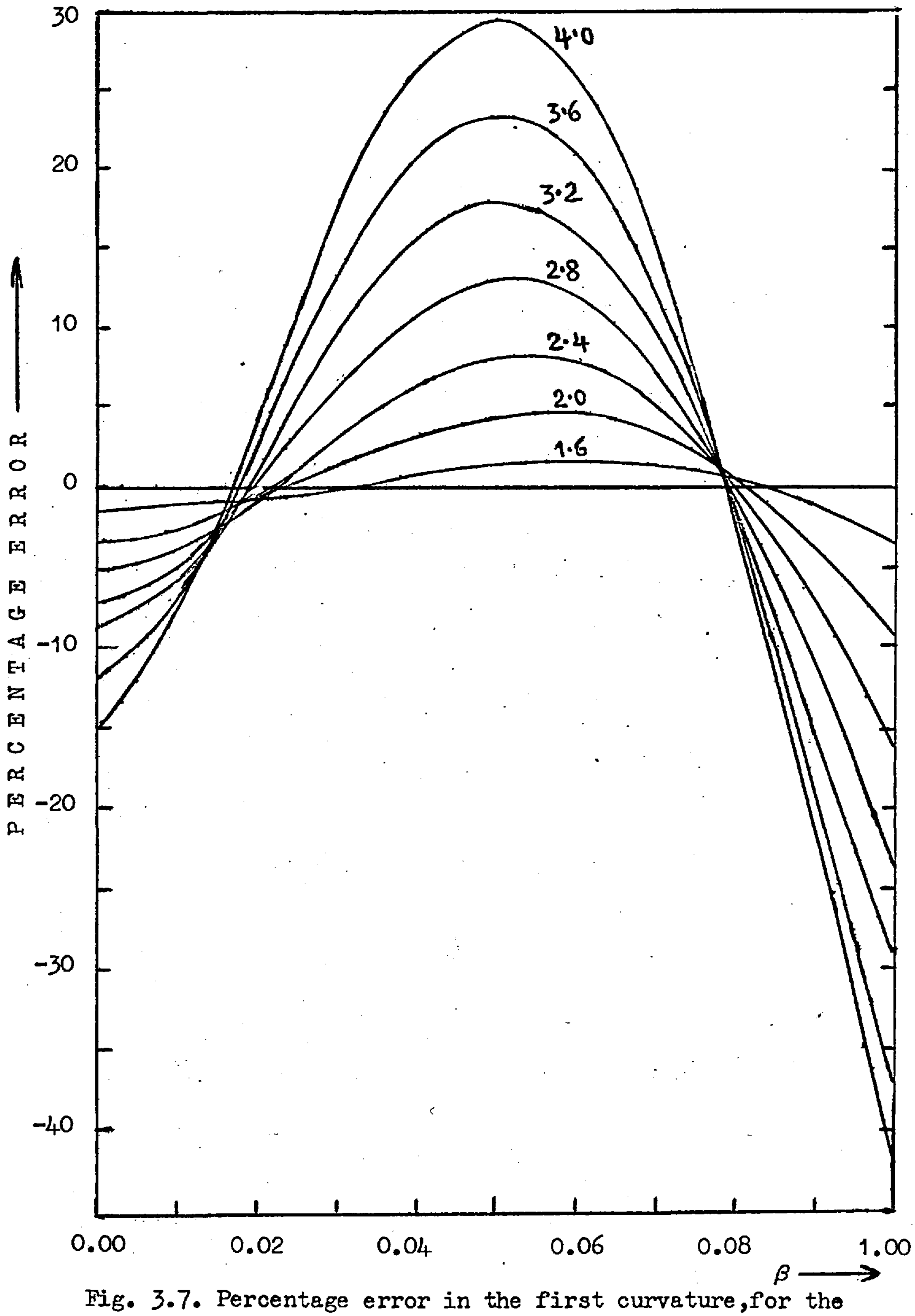


Fig. 3.7. Percentage error in the first curvature, for the virial theory, at various points ($\beta$) on the bubble surface. The figures on the curves indicate the axis-ratio.

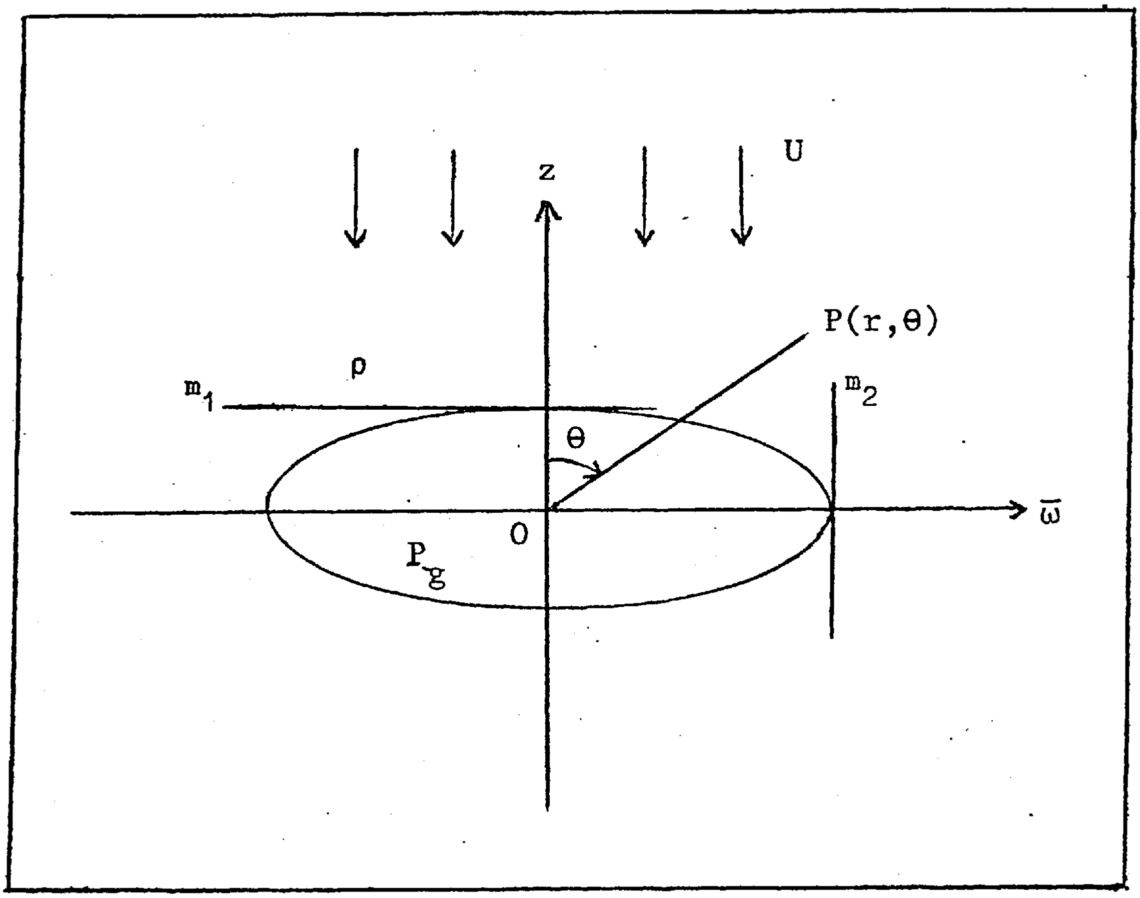


Fig. 4.1. A sketch of a bubble trace in an axial plane. $m_1$ and $m_2$ are the slopes at the pole and the equator. $\mu = \cos\theta$ and $\beta^2 = \mu^2(1+\alpha^2)/(\alpha^2+\mu^2)$.

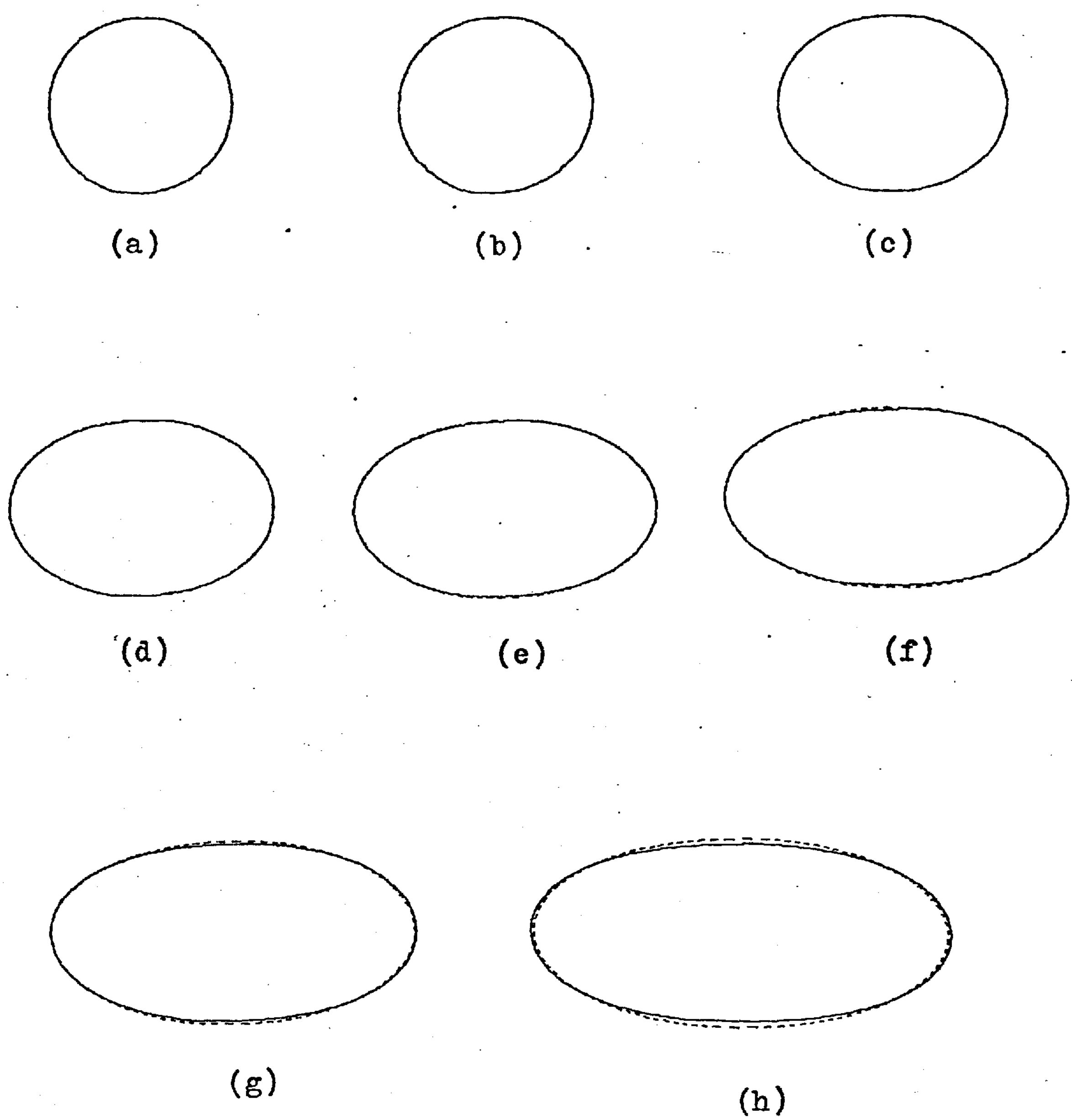


Fig. 4.2. symmetric case.

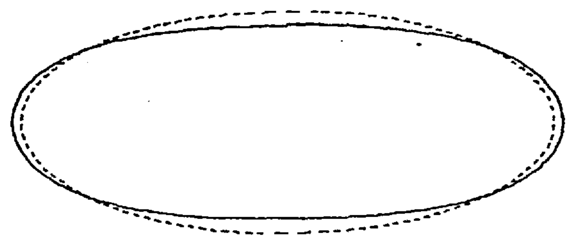

(i)

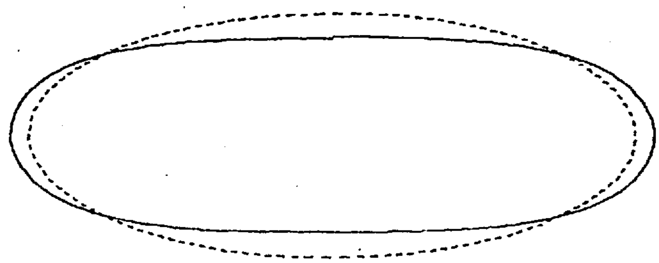

(j)

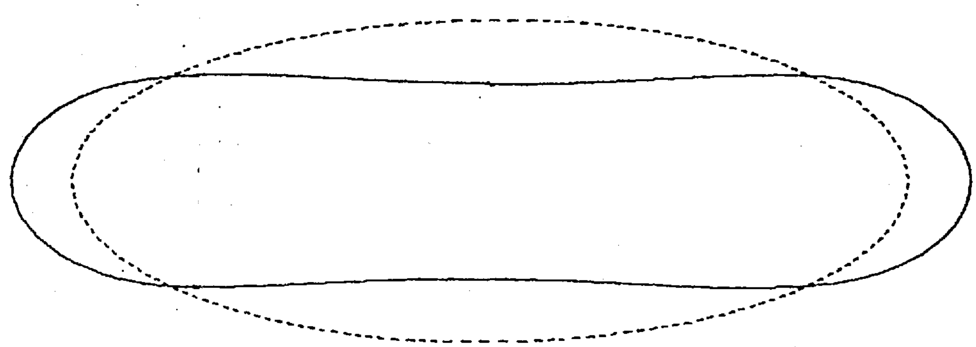

(k)

4.2. contd.

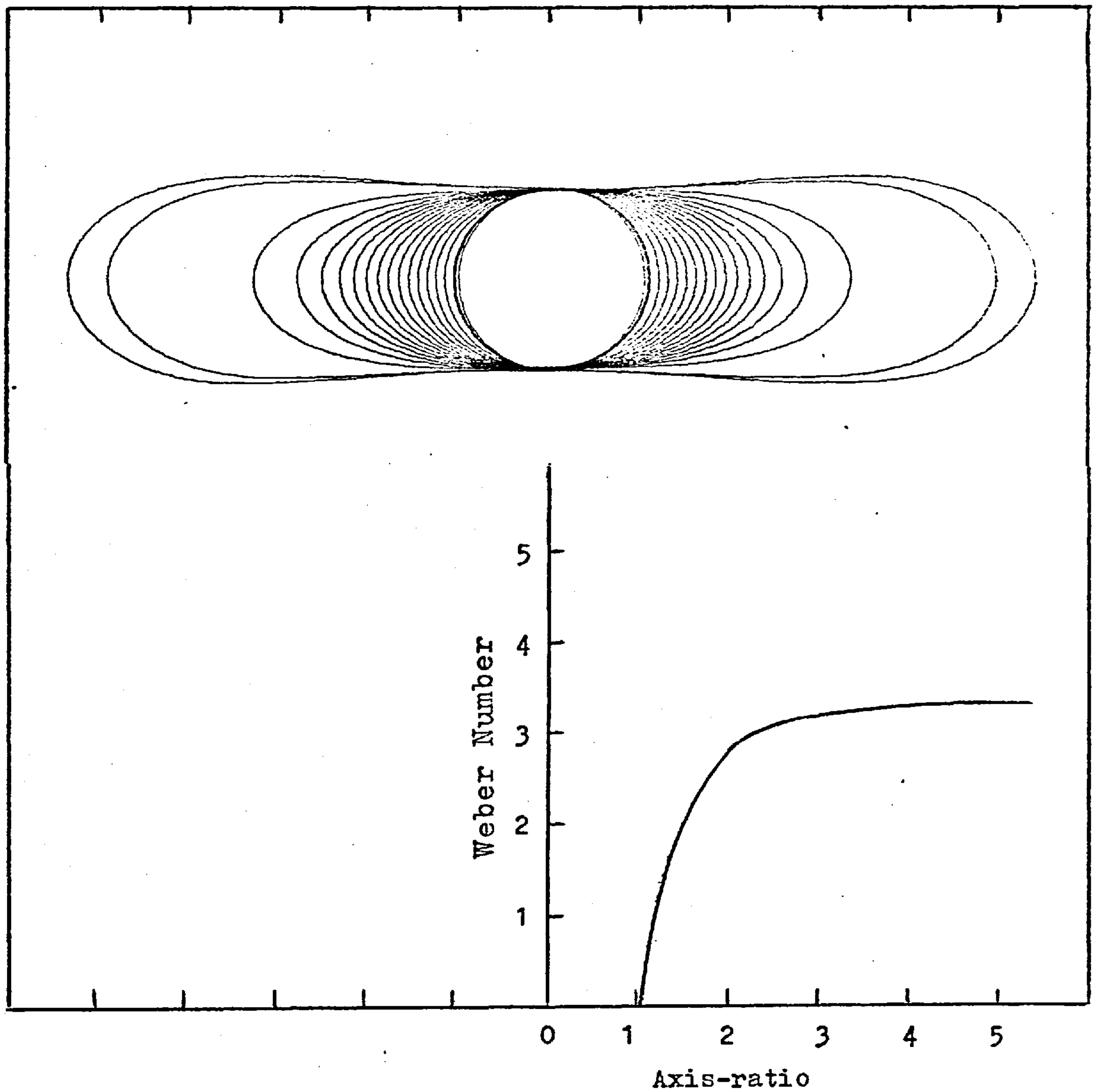


Fig.4.3. Variation of the Weber number with the axis-ratio for a family of symmetric bubbles obtained by linear perturbation of an oblate spheroid. The horizontal scale represents the same axis-ratio for both diagrams.
The relation between the Weber number and the axis-ratio is that given by the "Linearized Two-point Theory."

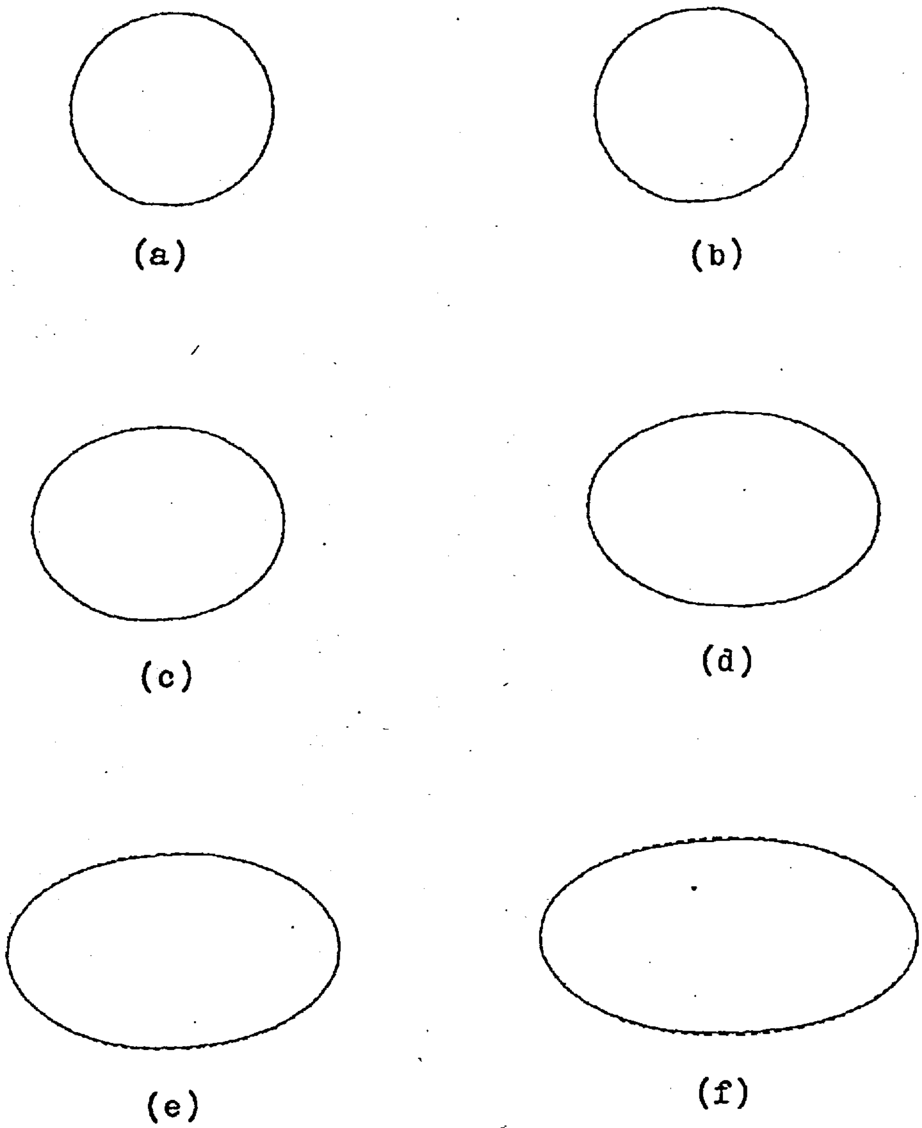


Fig. 4.4. symmetric Virial case.

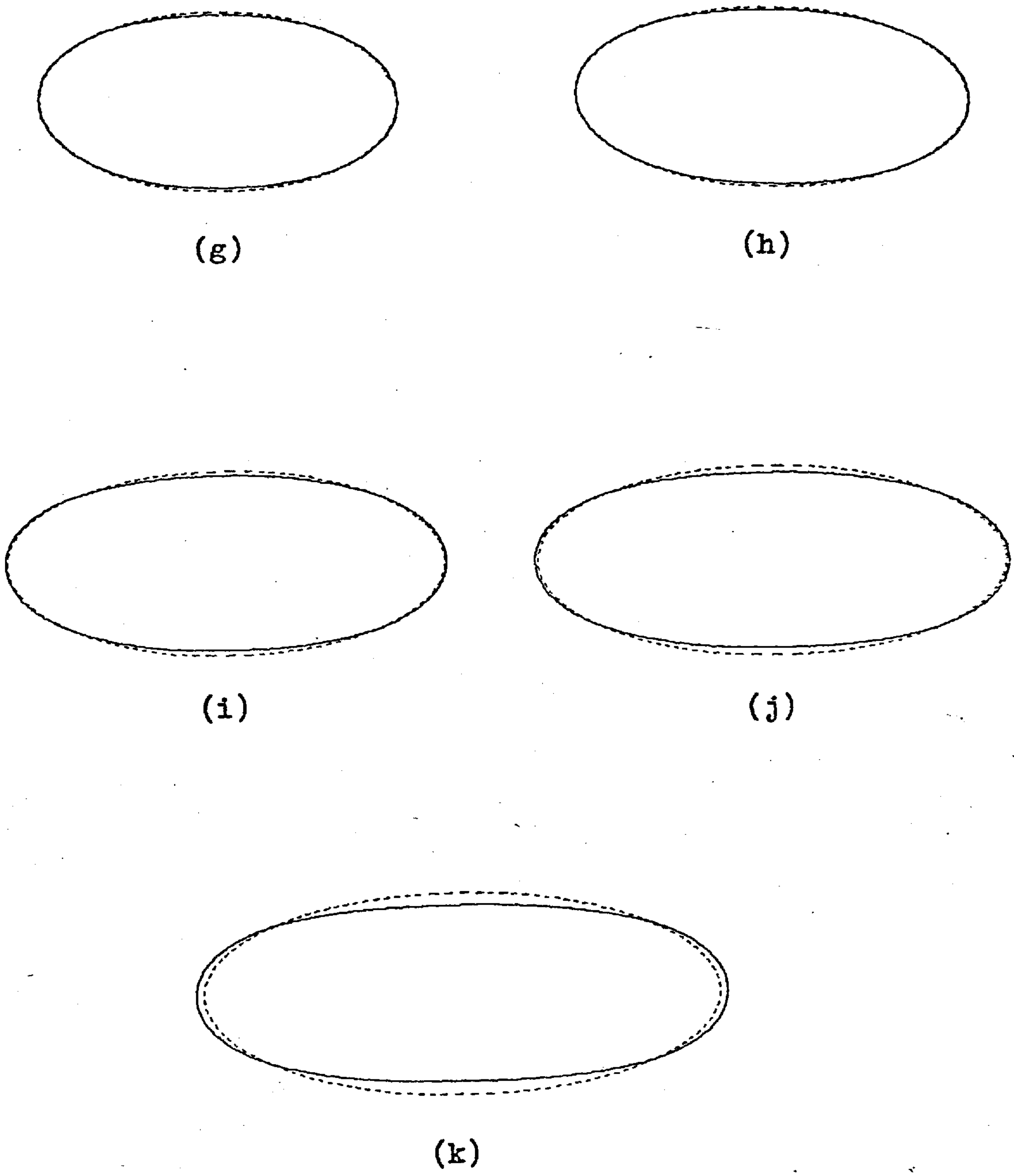


4.4. contd.

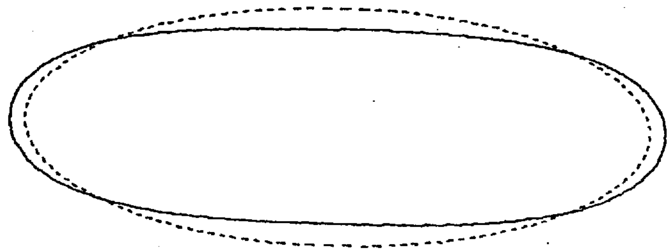

(l)

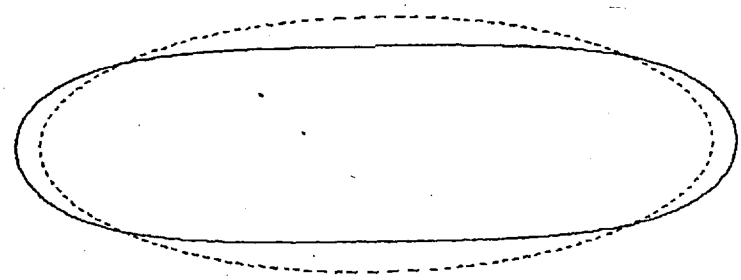

(m)

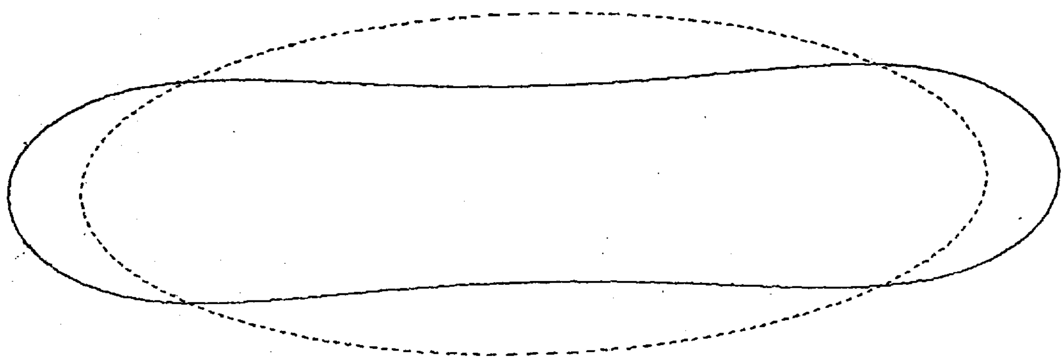

(n)

4.4. contd.

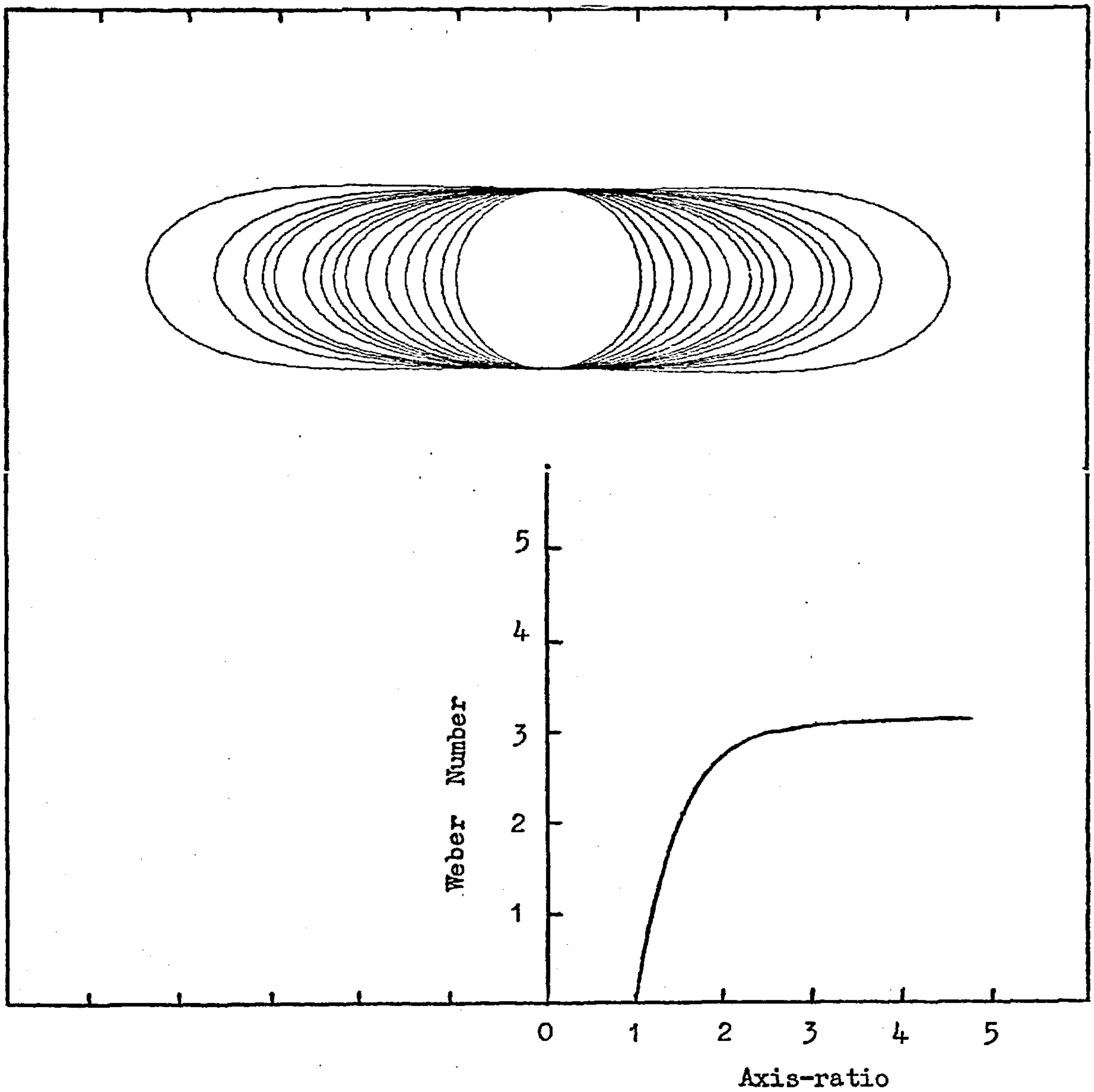


Fig. 4.5. Variation of the Weber number with the axis-ratio for for a family of symmetric bubbles obtained by linear perturbation of an oblate spheroid. The horizontal scale represents the same axis-ratio for both diagrams. The relation between the Weber number and the axis-ratio is that given by the "Linearized Virial Theory".

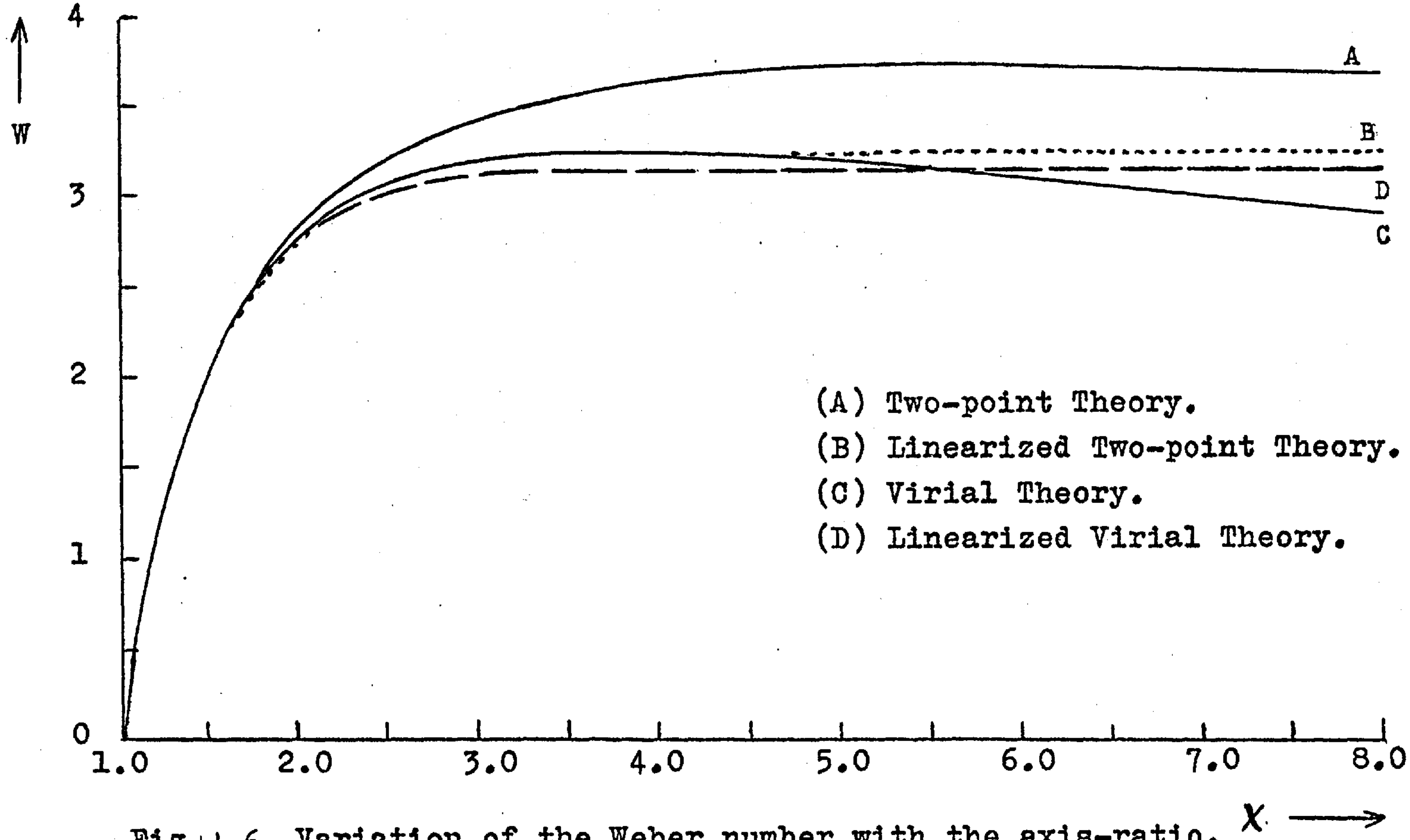


Fig. 4.6. Variation of the Weber number with the axis-ratio.

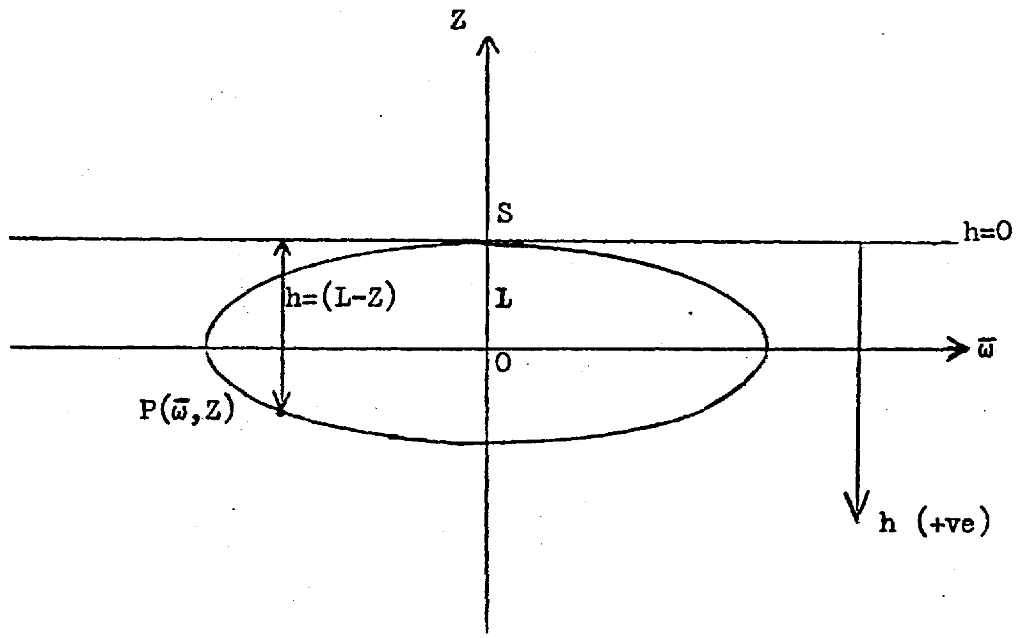


Fig.4.7. A sketch to determine the elevation for the hydrostatic pressure.

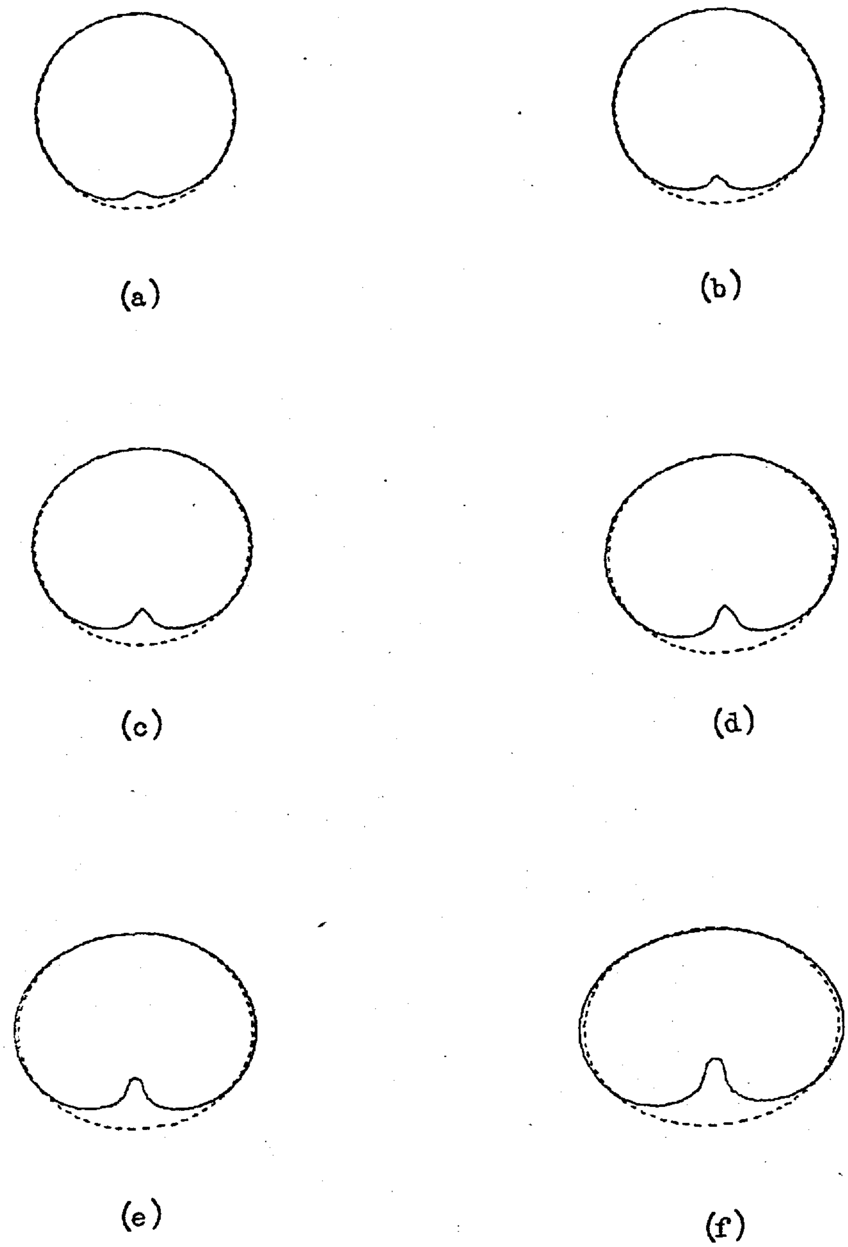


Fig. 4.8. Virial case $M=10^{-10}$.

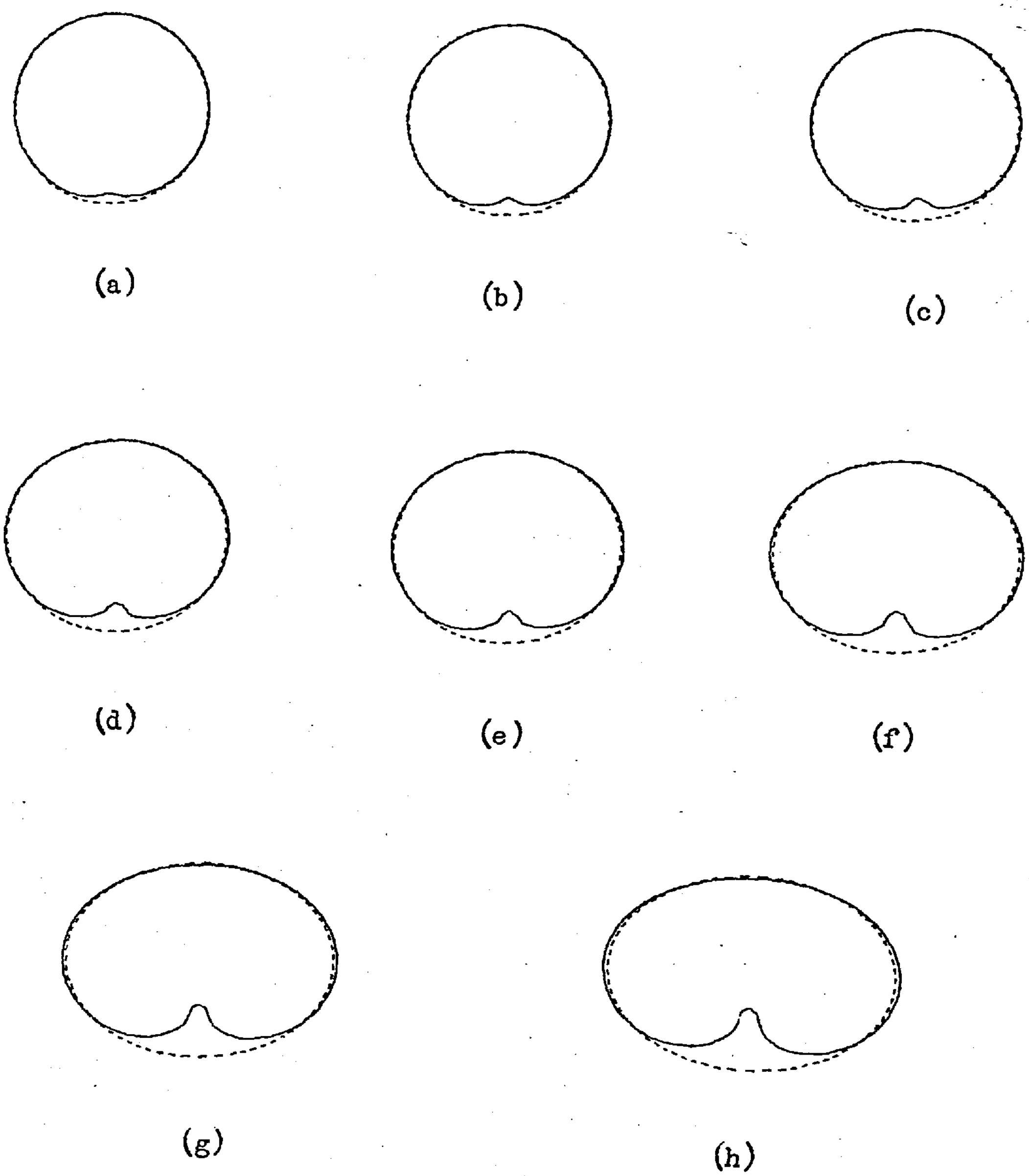


Fig. 4.9. Virial case $M=10^{-11}$.

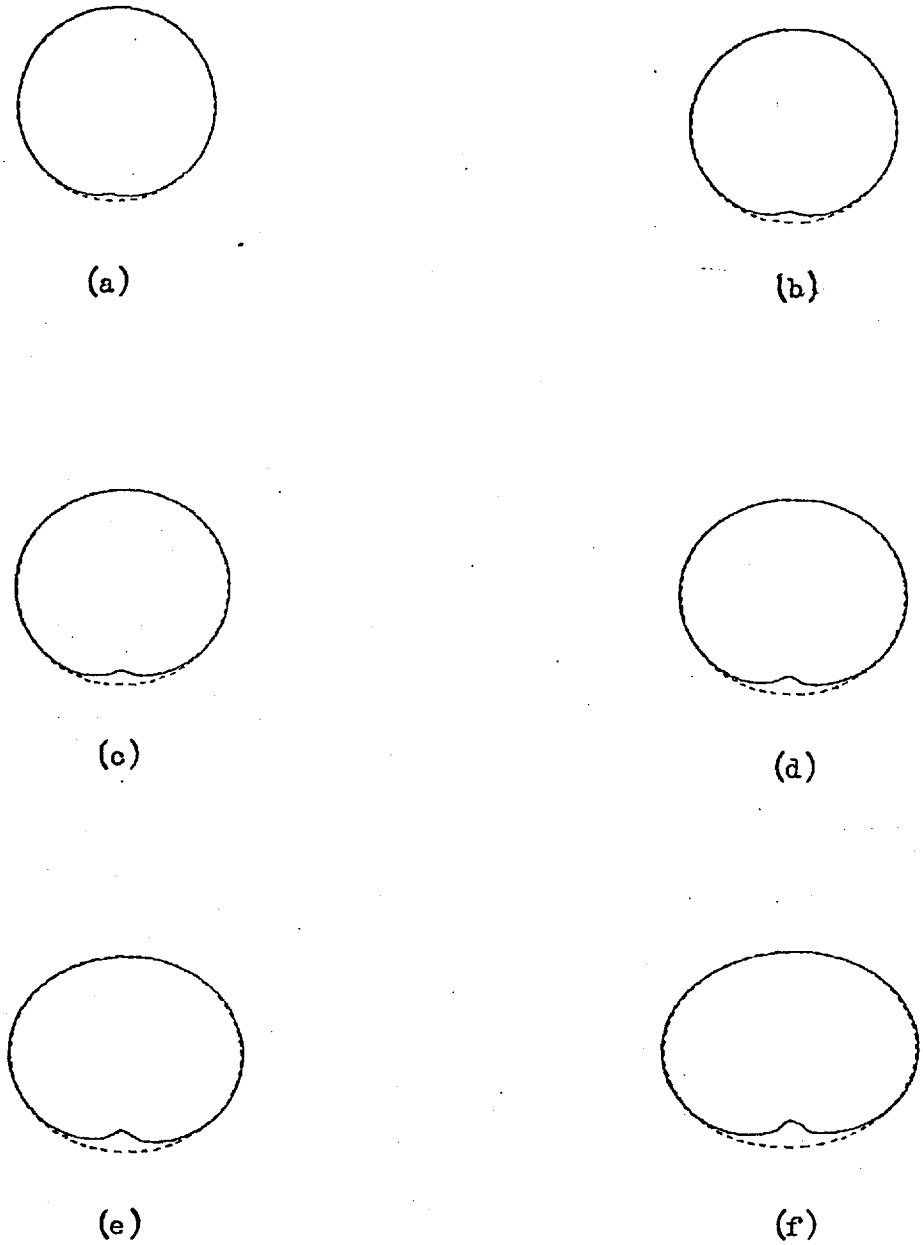


Fig. 4.10. Virial case $M=10^{-12}$.

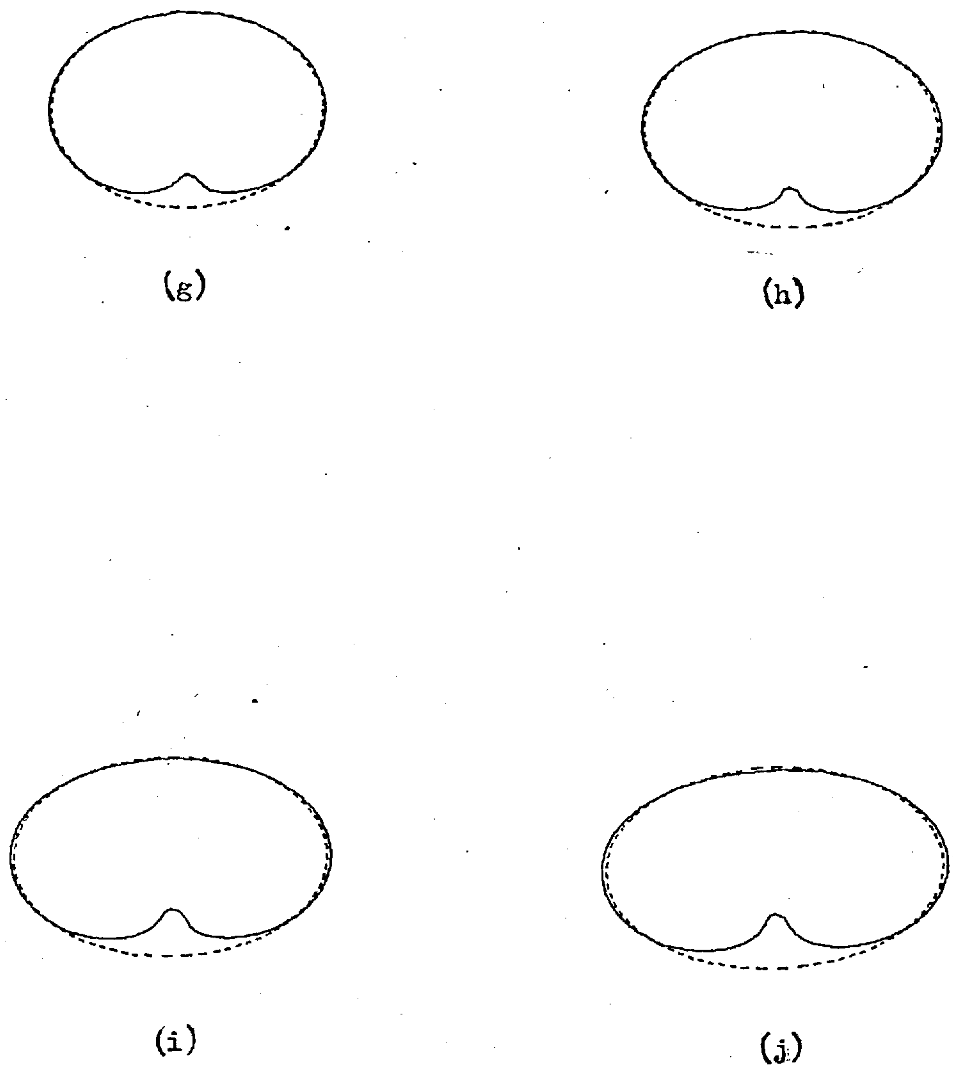


4.10. contd.

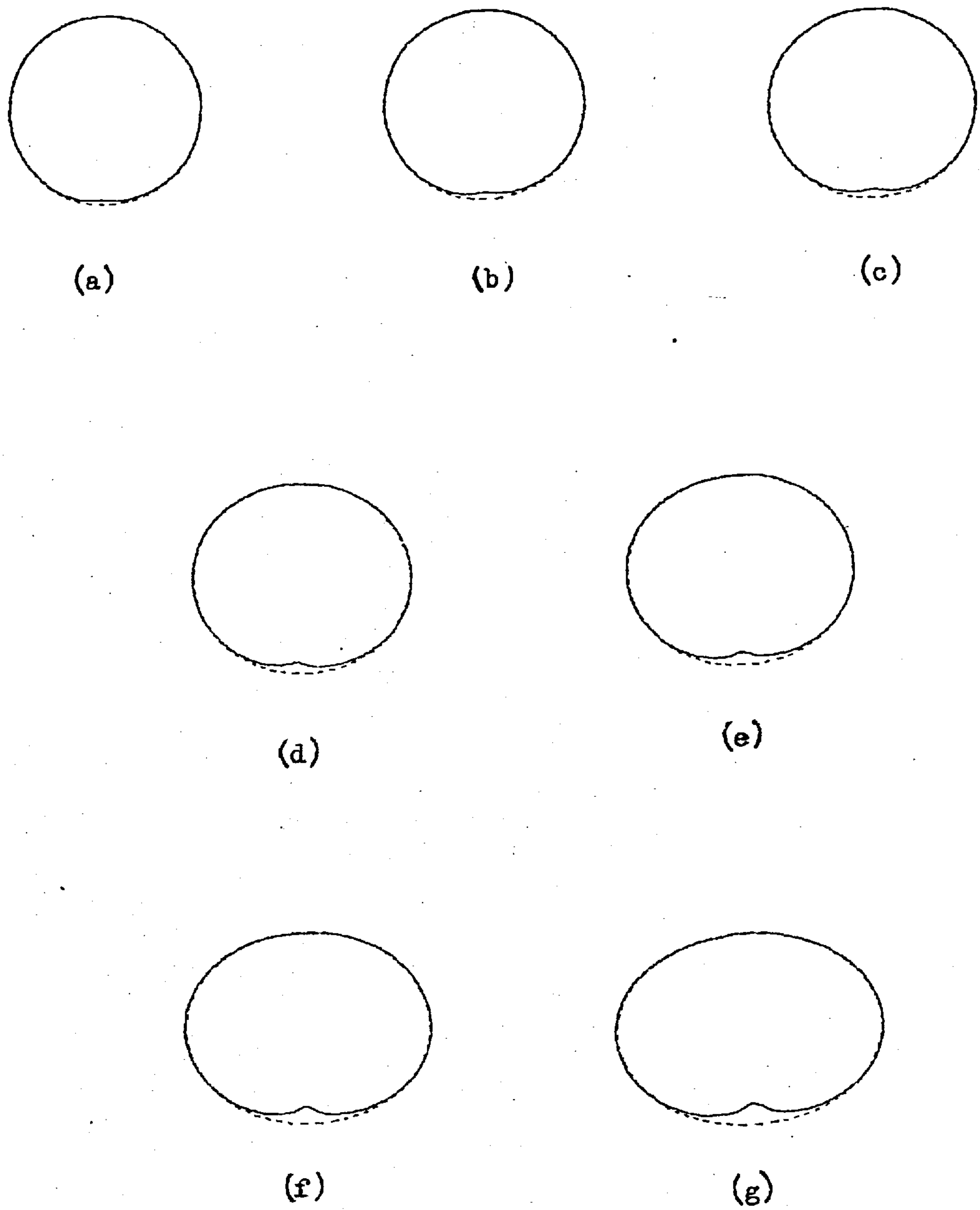


Fig. 4.11. Virial case $M=10^{-13}$.

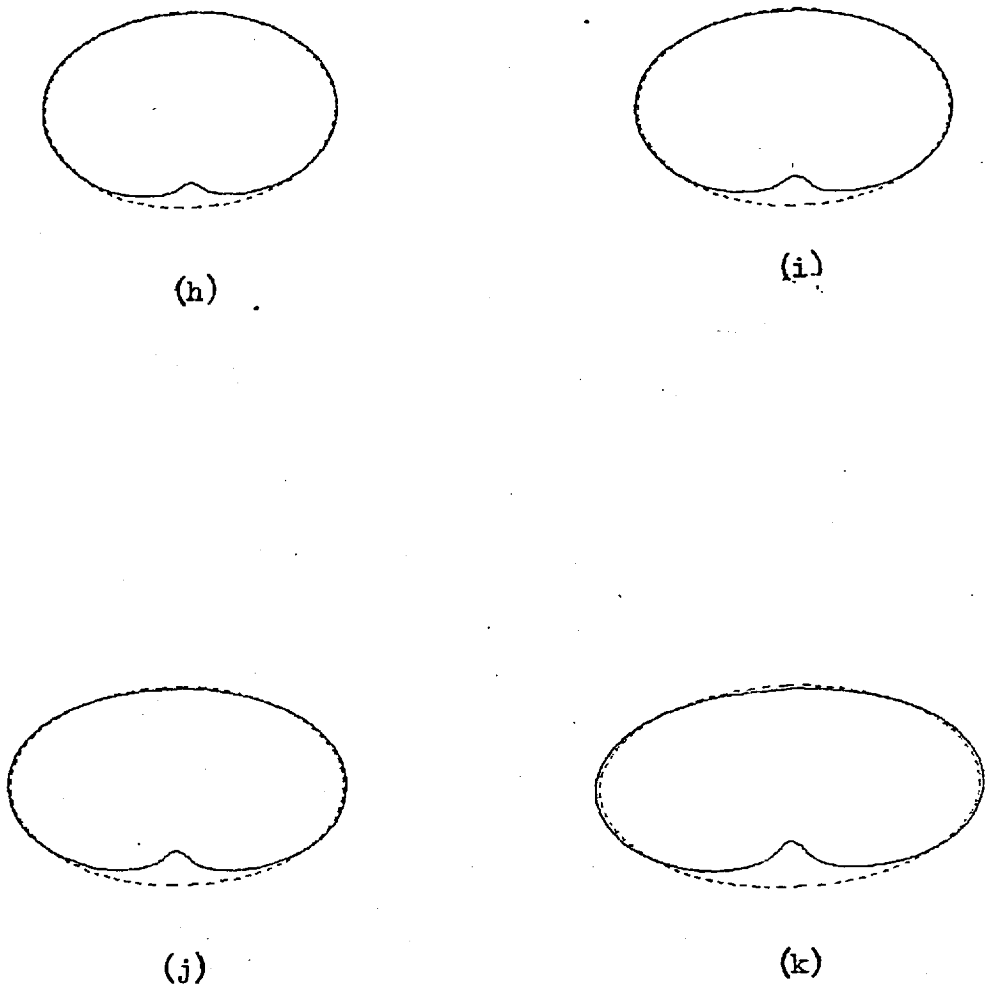


4.11. contd.

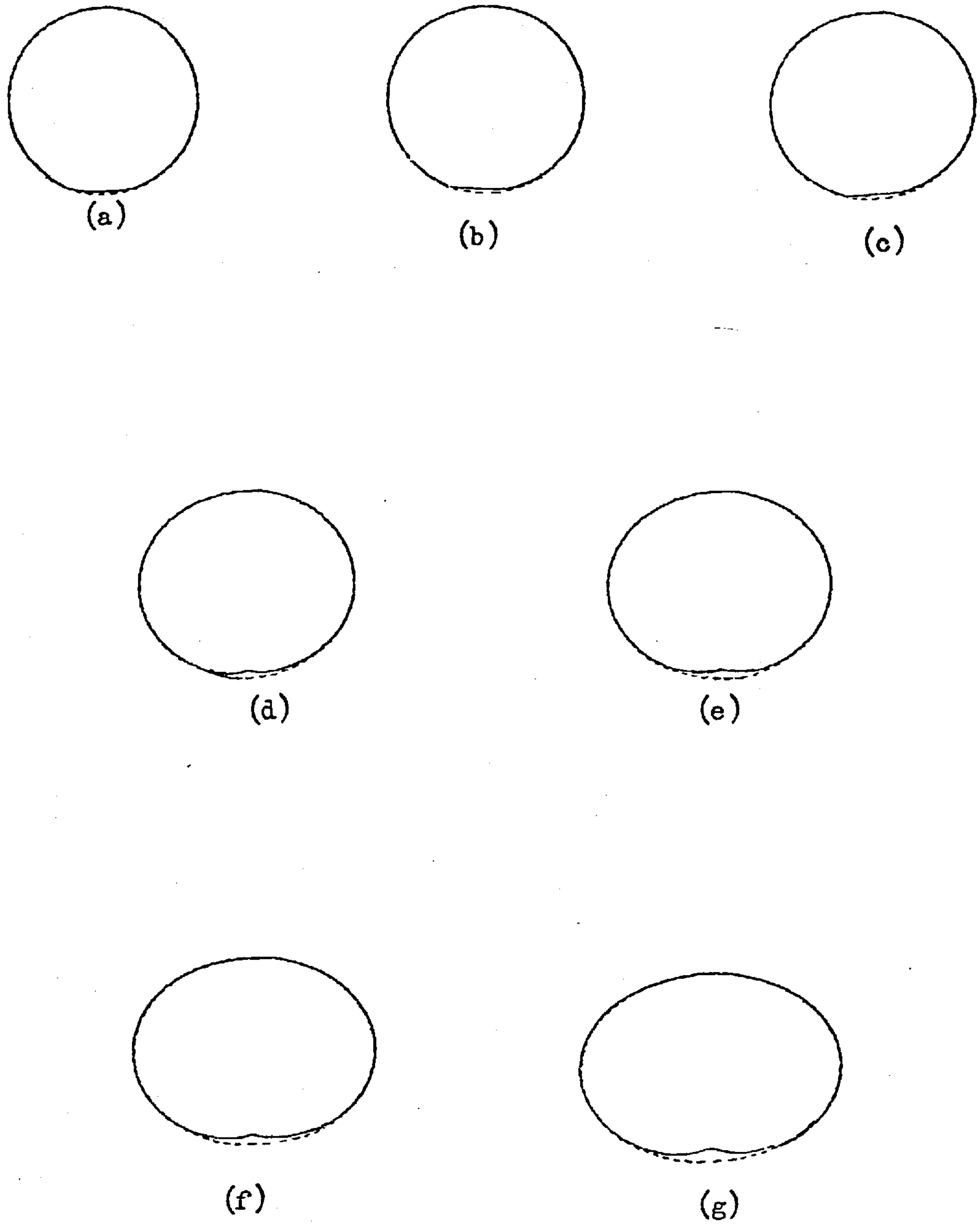


Fig. 4.12. Virial case $M=10^{-14}$.

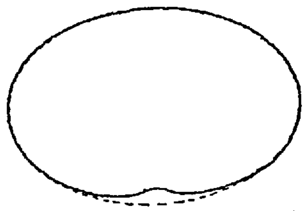

(h)

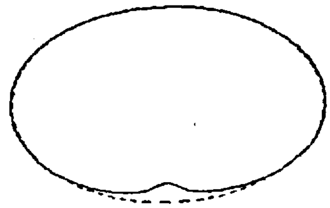

(i)

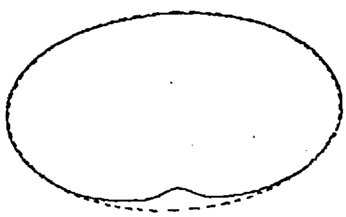

(j)

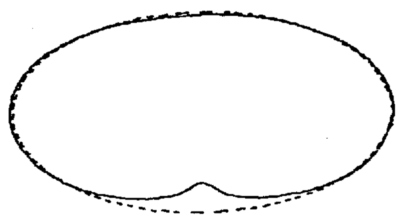

(k)

4.12. contd.

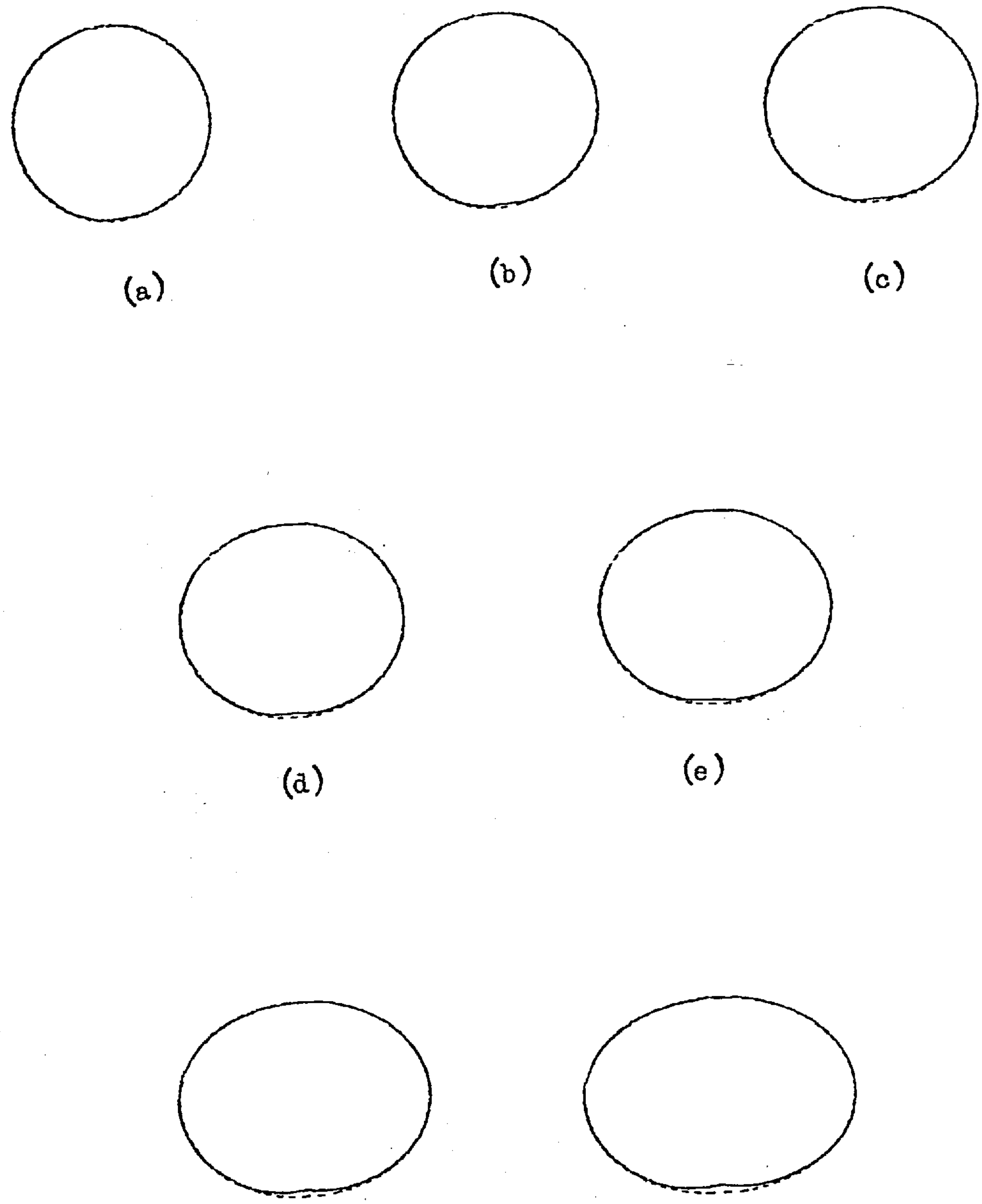

(a) (b) (c)

(d) (e)

(f) (g)

Fig. 4.13. Virial case $M=10^{-15}$.

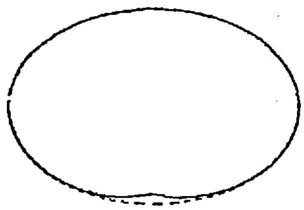

(h)

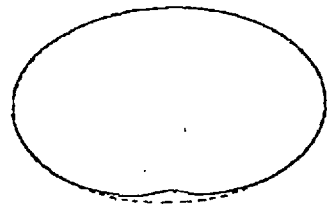

(i)

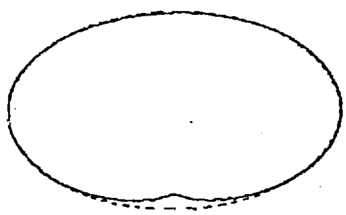

(j)

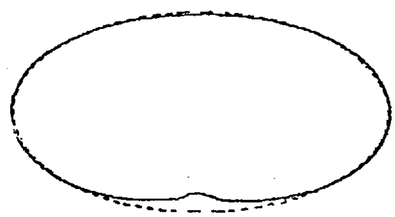

(k)

4.13. contd.

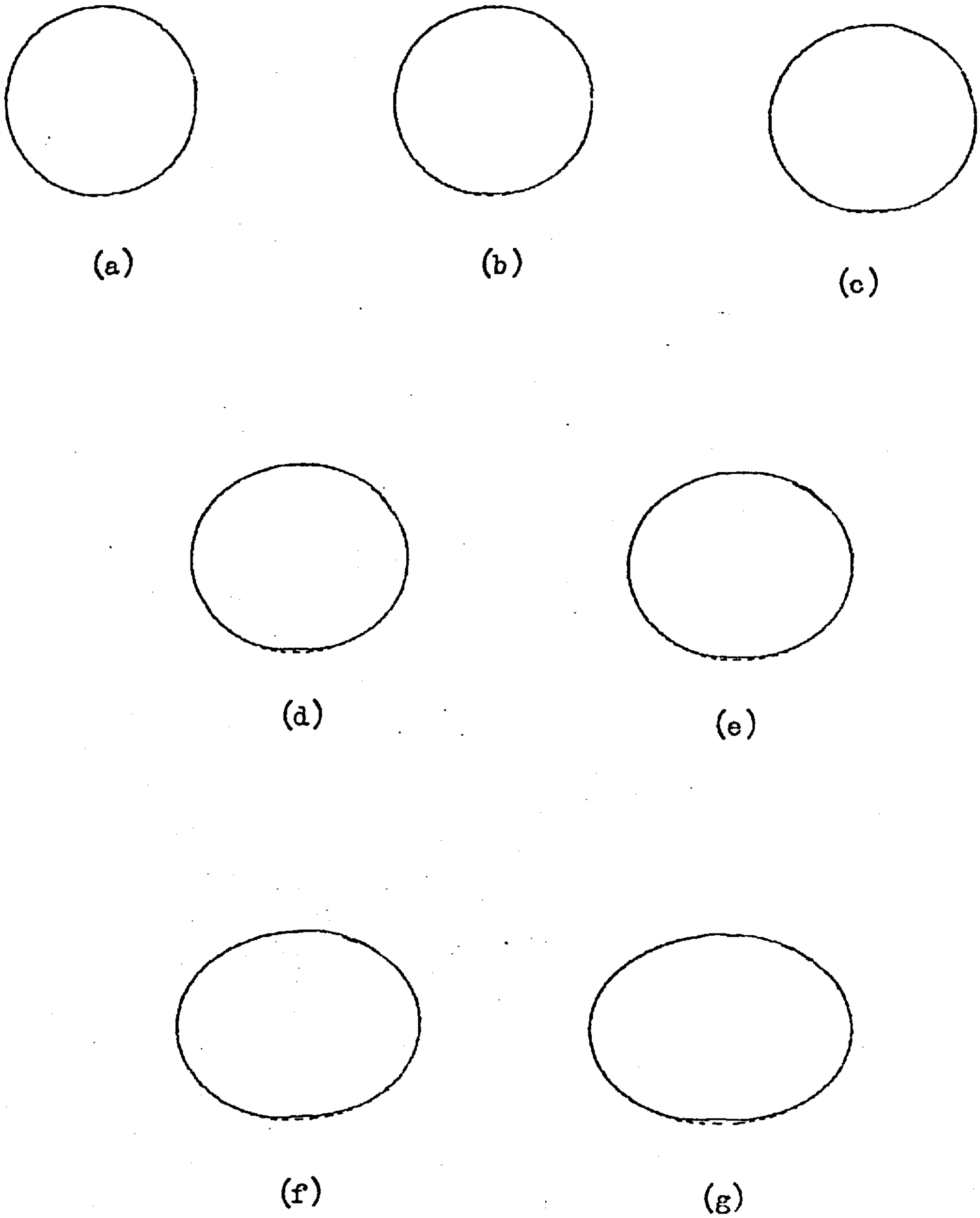

Fig. 4.14. Virial case $M=10^{-16}$.

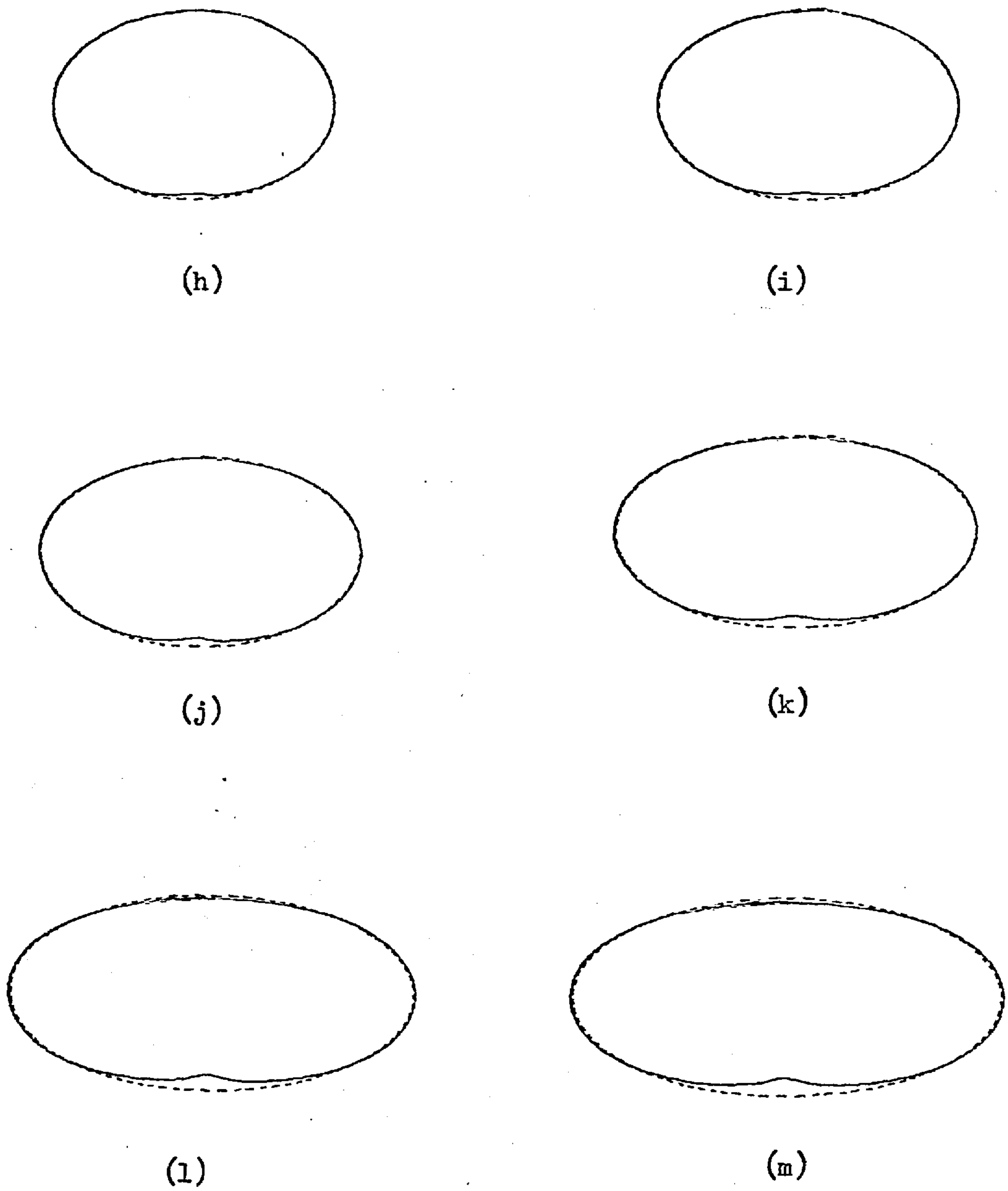


4.14. contd.

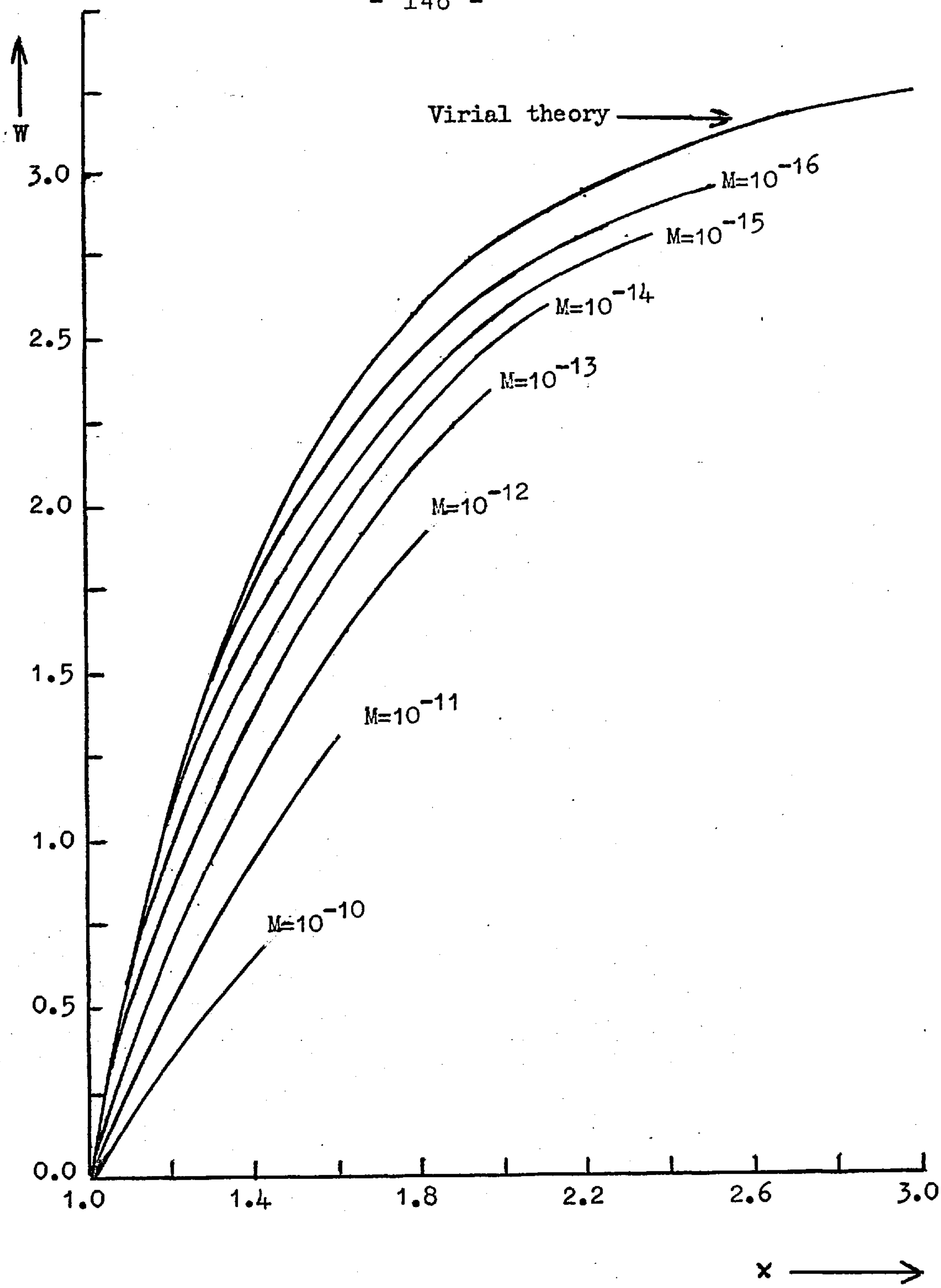


Fig. 4.15. Variation of the Weber number with the axis-ratio for different M-numbers.

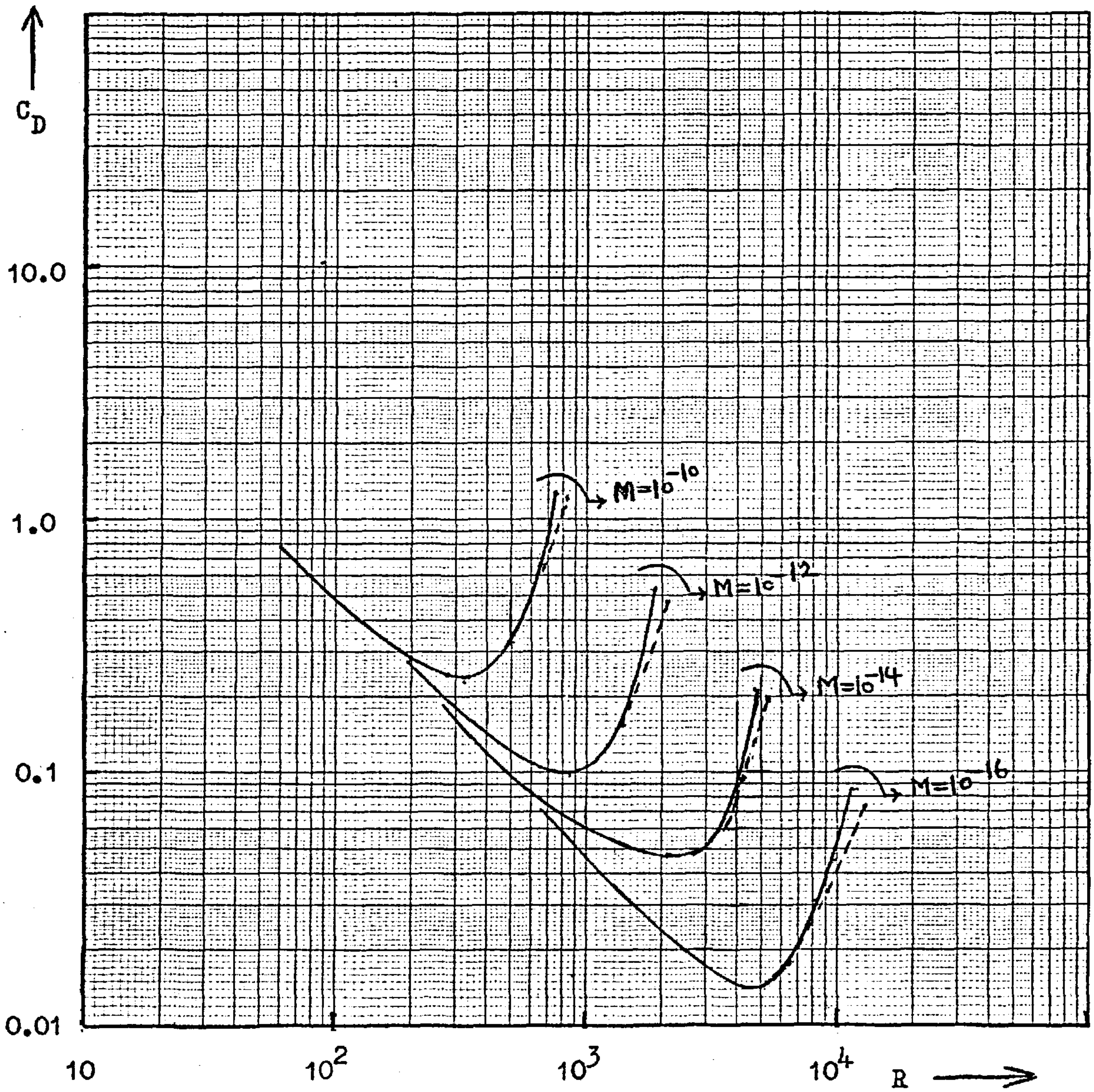


Fig. 4.16. The theoretical drag coefficient as a function of the Reynolds number. ——Virial theory. - - - - Two-point Theory. The right-hand end of the curves corresponds to an axis-ratio $\varkappa$ equal to 6.

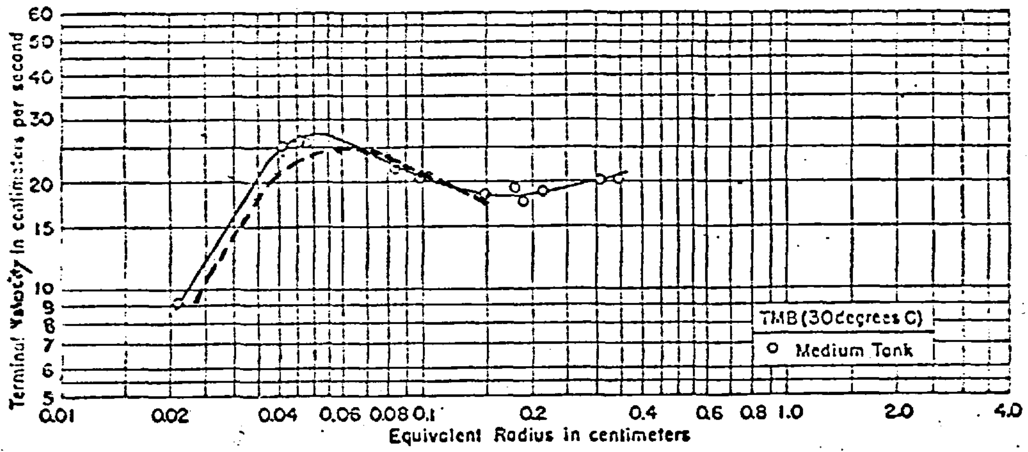


Fig. 4.17. Comparison of theory and experiment for air bubbles in methyl alcohol. ------ Virial theory; ______ Smoothed experimental curve (Haberman and Morton).

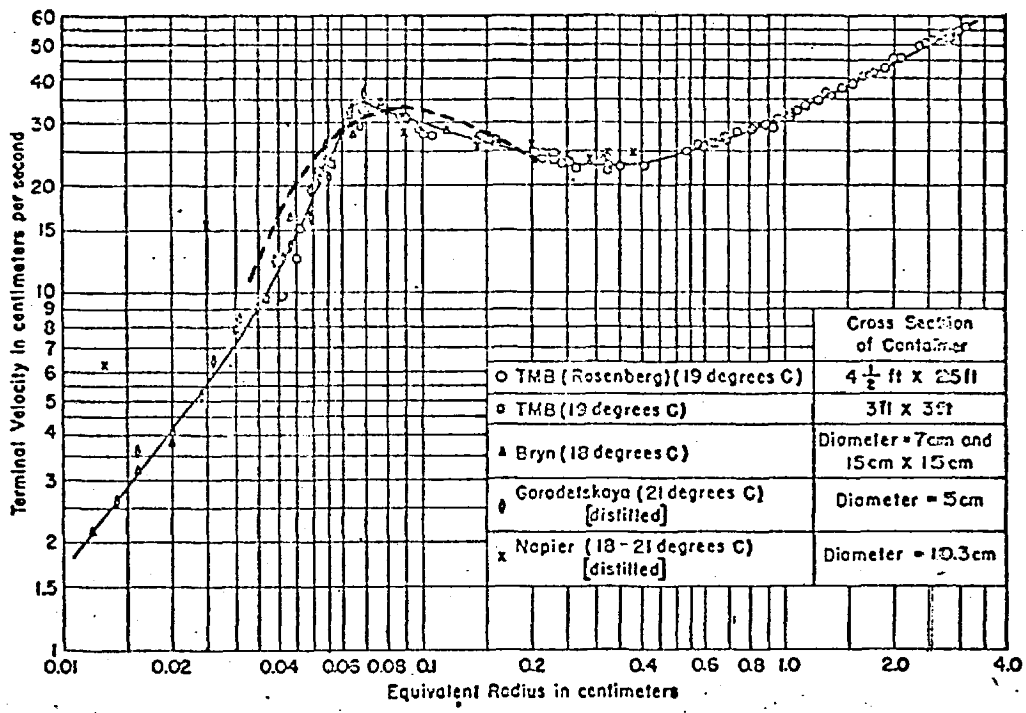


Fig. 4.18. Comparison of theory and experiment for air bubbles in distilled (or filtered) Water.------ Virial theory; _____ ,Smoothed experimental curve (Haberman and Morton).

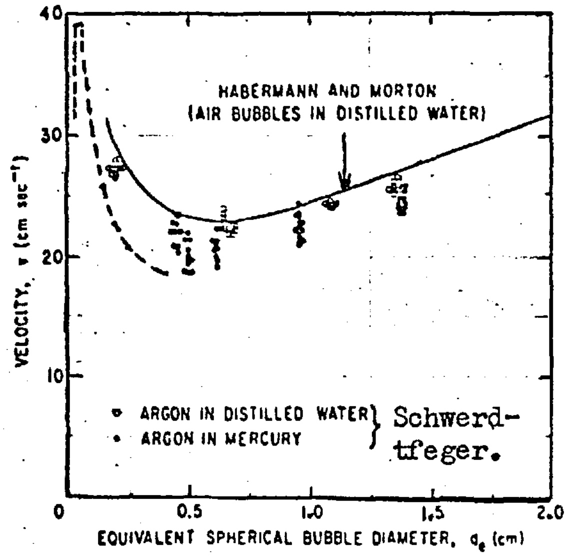


Fig. 4.19. Comparison of theory and experiment for argon bubbles in mercury.-----Virial theory.

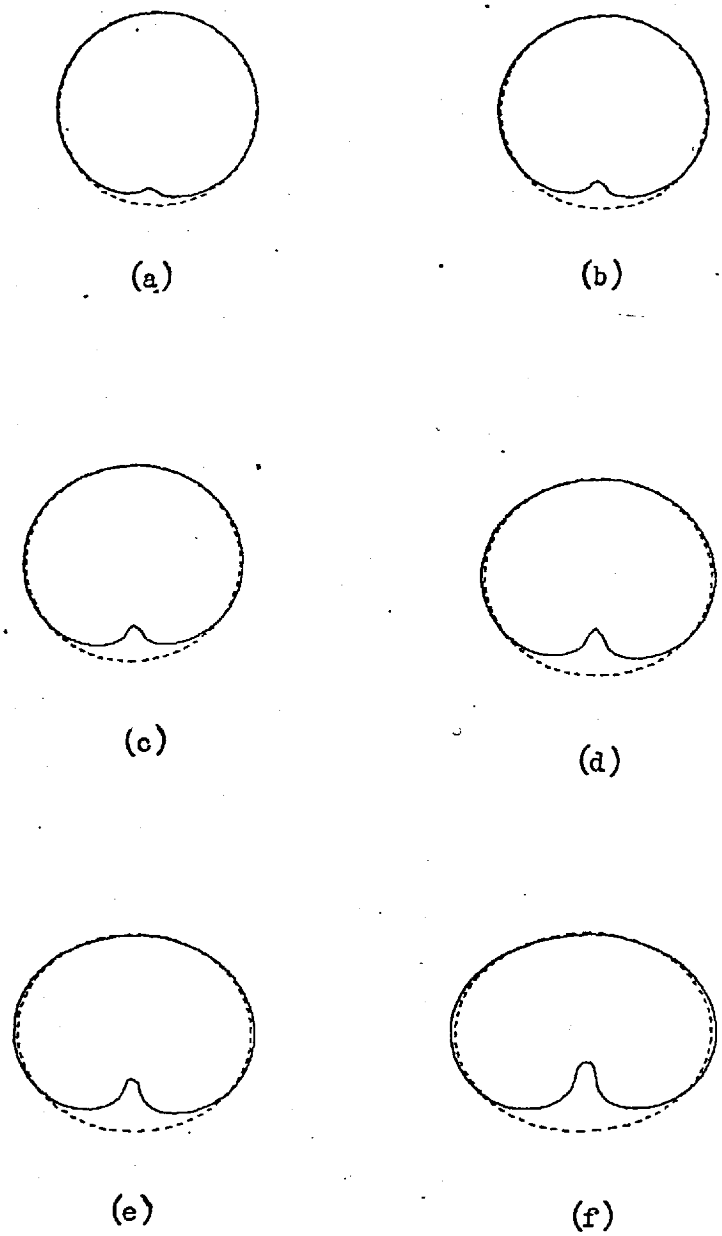

(a) (b) (c) (d) (e) (f)

Fig.4.20. Shapes predicted by the virial theory for air bubbles in methyl alcohol ($M=8.9\times10^{-11}$).

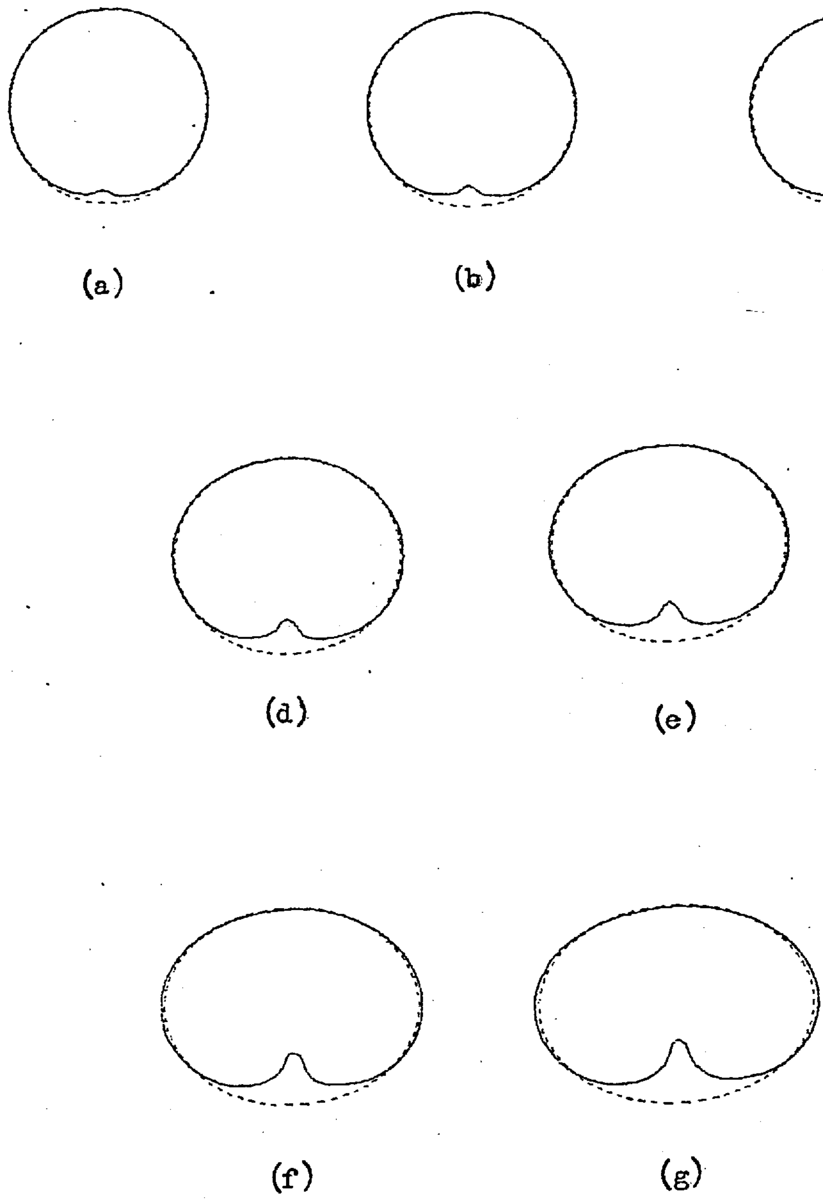


Fig. 4.21. Shapes predicted by the virial theory for air bubbles in distilled water ($M=2.4\times10^{-11}$).

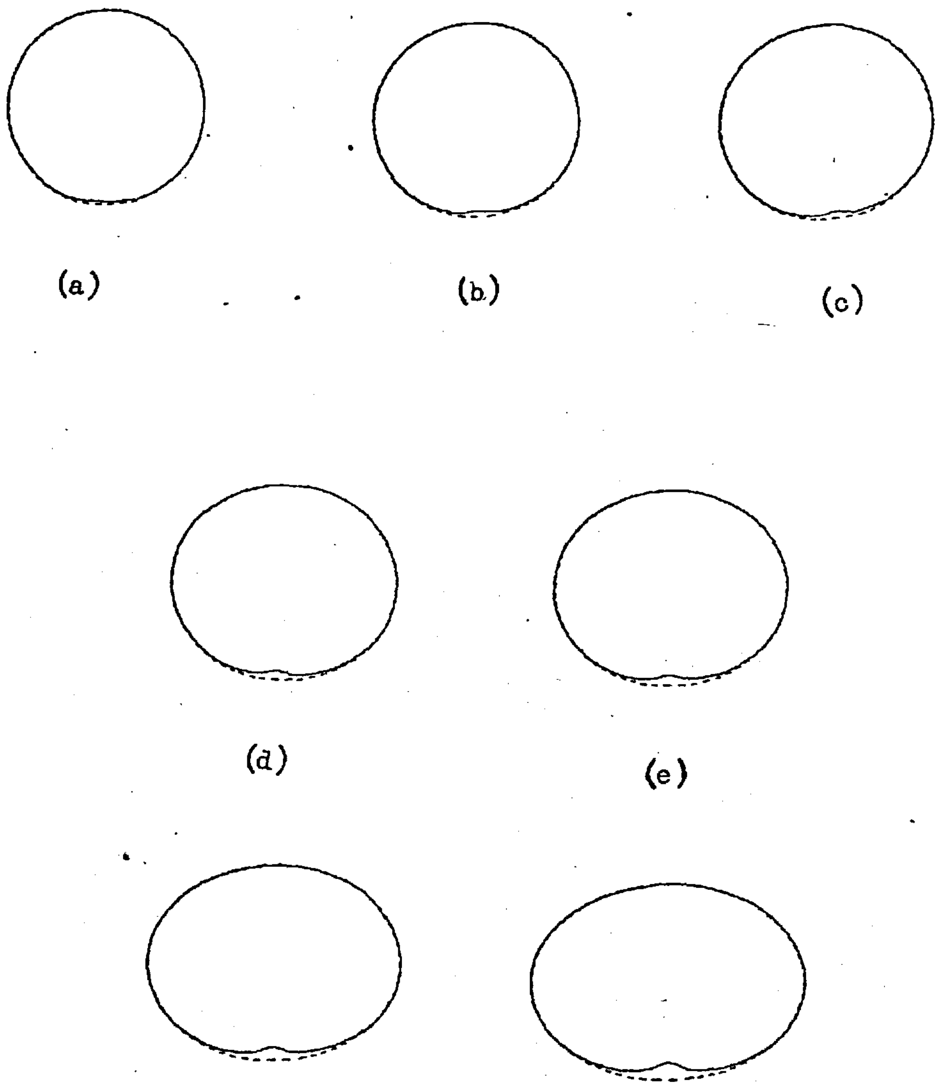

(a) (b) (c)

(d) (e)

(f) (g)

Fig.4.22. Shapes predicted by the virial theory for argon bubbles in mercury ($M=3.7\times10^{-14}$).

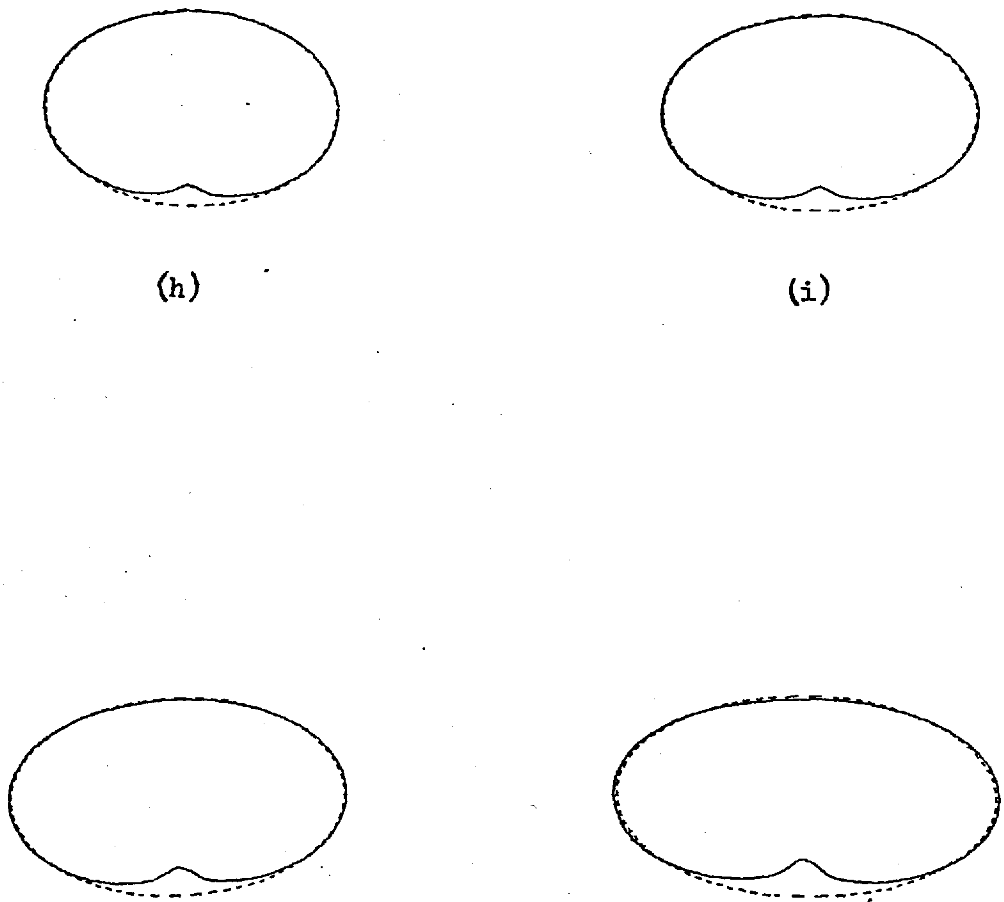

(h) (i)

(j) (k)

4.22. contd.

# C O R R I G E N D A